Exploring the climate change refugia potential of equatorial Pacific coral reefs

by

Elizabeth Joan Drenkard
B.A., Cornell University, 2009

Submitted in partial fulfillment of the requirements for the degree of
Doctor of Philosophy

at the

MASSACHUSETTS INSTITUTE OF TECHNOLOGY

and the

WOODS HOLE OCEANOGRAPHIC INSTITUTION

February 2015

© Elizabeth Joan Drenkard, 2015. All rights reserved.

The author hereby grants to MIT and to WHOI permission to reproduce and distribute publicly paper and electronic copies of this thesis document in whole or in part in any medium now known or hereafter created.

Author .....
Joint Program in Oceanography/ Applied Ocean Science and Engineering
Massachusetts Institute of Technology and Woods Hole Oceanographic Institution
October 3, 2014

Certified by .....
Anne L. Cohen
Associate Scientist, Department of Geology and Geophysics, WHOI
Thesis Co-Supervisor

Certified by .....
Daniel C. McCorkle
Senior Scientist, Department of Geology and Geophysics, WHOI
Thesis Co-Supervisor

Certified by .....
Kristopher B. Karnauskas
Associate Scientist, Department of Geology and Geophysics, WHOI
Thesis Co-Supervisor

Accepted by .....
Timothy L. Grove
Professor of Earth, Atmospheric, and Planetary Sciences, MIT
Chairman, Joint Committee for Marine Geology and Geophysics

Exploring the climate change refugia potential of equatorial Pacific coral reefs

by

Elizabeth Joan Drenkard

Submitted to the Joint Program in Oceanography/Applied Ocean Science and Engineering
Massachusetts Institute of Technology/Woods Hole Oceanographic Institution
on October 3, 2014, in partial fulfillment of the requirements for the degree of
Doctor of Philosophy

Abstract

Global climate models project a 21st century strengthening of the Pacific Equatorial Undercurrent (EUC). The consequent increase in topographic upwelling of cool waters onto equatorial coral reef islands would mitigate warming locally and modulate the intensity of coral bleaching. However, EUC water is potentially more acidic and richer in dissolved inorganic nutrients (DIN), both widely considered detrimental to coral reef health.

My analysis of the Simple Ocean Data Assimilation product indicates that the EUC has indeed strengthened over the past 130 years. This result provides an historical baseline and dynamical reference for future intensification. Additionally, I reared corals in laboratory experiments, co-manipulating food, light and CO_2 (acidity) to test the role of nutrition in coral response to elevate CO_2 conditions. Heterotrophy yields larger corals but CO_2 sensitivity is independent of feeding. Conversely, factors that enhance zooxanthellate photosynthesis (light and DIN) reduce CO_2 sensitivity. Corals under higher light also store more lipid but these reserves are not utilized to maintain calcification under elevated CO_2. My results suggest that while mitigation of CO_2 effects on calcification is not linked to energetic reserve, EUC fueled increases in DIN and productivity could reduce effects of elevated CO_2 on coral calcification.

Thesis Co-Supervisor: Anne L. Cohen
Title: Associate Scientist, Department of Geology and Geophysics, WHOI

Thesis Co-Supervisor: Daniel C. McCorkle
Title: Senior Scientist, Department of Geology and Geophysics, WHOI

Thesis Co-Supervisor: Kristopher B. Karnauskas
Title: Associate Scientist, Department of Geology and Geophysics, WHOI

Acknowledgments

I thank my advisors Drs. Anne Cohen, Daniel McCorkle, and Kristopher Karnauskas for their support and guidance throughout my graduate studies and for the opportunity to pursue such an interdisciplinary and fascinating research topic. Their mentorship, tutelage, and passion for oceanography have molded and inspired the direction of my scientific career.

I am also grateful to my thesis committee members, Drs. Janelle Thompson, Russell Brainard, committee chair, Dr. Delia Oppo and Generals advisor Dr. Sarah Cooley for their time and insights; their diverse perspectives and backgrounds have enriched my dissertation research. The contributions of my coauthors and collaborators Drs. Samantha dePutron, Vicke Starczak, Dan Repeta, and Ms. Alice Zicht have been essential to my experimental studies

The scientific and technical assistance of Ed O'Brien, Rebecca Belastock, Elizabeth Bonk, Paul Henderson, Dave Wellwood and Julie Arruda have been invaluable to my field-work preparations, and data generation and analyses. I greatly appreciated the WHOI Academic Programs Office and the MIT Academics Office for their endless help and support. Thanks also to the Geology and Geophysics department administrators, WHOI facilities staff, and the staff and interns at the Bermuda Institute of Ocean Sciences, especially Kascia White, who helped make my ocean acidification experiments a success.

Many thanks to the crew of the Sea Dragon, Captain Dale Selvam, Emily Penn, Ryan McInerney, and Alec Nordschow for a safe and successful expedition through the central Pacific and to Chip Young and Kelsie Ernsberger for sharing their knowledge of and respect for the exquisite ecosystems found on remote equatorial Pacific islands.

To the Cohen Lab family: Pat Lohmann, Kathryn Rose Pietro, Neal Cantin, Katie and One Shamberger, Michael Holcomb, Casey Saenger, Sara Bosshart, Hannah Barkley, Alice Alpert, Tom DeCarlo, Hanny Rivera, and Angela Helbling. Thank you for the scientific (and non-scientific) discussions, research assistance and camaraderie; it has always been an adventure.

I am grateful to my friends and fellow JP students for being at the core of my life on the Cape, especially Britta for enduring my antics and idiosyncrasies over the past four years. Also, many thanks to Alec, Elise, Mary, Kalina and Meagan for being amazing friends, especially during these last few months. Thanks also to Captain John Cartner for teaching me how to catch a lobster and the Friends of Falmouth Dogs for being a regular source of humanity; both have helped me maintain perspective and a positive attitude.

My family has been a perpetual source of encouragement and inspiration, in particular my grandmothers, Joan and Margot - two of the strongest, most stubborn and courageous women I have even known and from whom I have clearly inherited a passion for the ocean, music and chocolate. Finally, my parents, Hans and Diane, have been my rock these past five years and beyond. Their moral support, good humor, and sound advice have helped me navigate even the most difficult times and it is to them I dedicate this thesis.

Funding for this research was provided by NSF grants OCE-1220529, OCE-1041106, OCE-1031971, OCE-1233282, and OCE-1041052; the MIT Bermuda Biological Research Station Fund, the WHOI Oceans Venture Fund, and the EAPS Student Research Fund. Travel to meetings and conferences to present these results, was supported by grants from WHOI, MIT, and the MIT Graduate Student Council.

Contents

Chapter 1

Introduction

1.1 Climate Change Overview

Anthropogenic climate change and associated ocean impacts jeopardize marine species and ecosystems, including important living marine resources. Of these resources, coral reefs, which provide billions of dollars in ecosystem services annually to hundreds of millions of people worldwide (Moberg & Folke 1999, Cesar *et al.* 2003), are often considered the proverbial "canary in the coal mine" for climate change, due to their sensitivity to CO_2-driven changes in ocean temperature and pH (acidification; Hughes *et al.* 2003). The goal of my research is to investigate how these changes affect oceanic and environmental conditions on specific reef ecosystems, and explore the response of reef-building corals to resultant co-varying factors in order to better anticipate their viability under projected climate and ocean change.

Since the industrial revolution (mid-18^{th} century), human combustion of fossil fuels (i.e., coal, oil, and natural gas) and deforestation have accelerated the flux of carbon dioxide (CO_2) to the atmosphere (Keeling 1973, van der Werf *et al.* 2009). This shift in global carbon cycling has caused a dramatic and measurable increase in atmospheric CO_2 concentration ($> 43\%$ as of August 2014, relative to ~278 ppm in 1750; e.g., Keeling *et al.* 1976, Neftel *et al.* 1985, Friedli *et al.* 1986, Etheridge *et al.* 1996, Tans & Keeling 2014).

Anthropogenic CO_2 emissions and the warming of Earth's surface are linked. Earth's surface absorbs incoming shortwave radiation from the sun and reemits it as outgoing longwave radiation toward space. Greenhouse gases (GHGs), including CO_2, are not transparent to longwave radiation and absorb and reemit a large proportion (approximately 90%) of the energy radiated from Earth's surface in approximate proportion to their temperature (i.e., Stefan-Boltzmann law; Trenberth *et al.* 2009). Since the temperature of the atmosphere is lower than at the surface, the energy reemitted by CO_2 is less than the energy absorbed and, by conservation of energy, leads to an increase in atmospheric temperature. As the concentration of GHGs in the atmosphere increases, the overall emission temperature (and

thus the amount of energy emitted to space) decreases. This net radiative imbalance determines the rate at which the temperature of the surface and atmosphere rise. The transfer of heat between the atmosphere and ocean is determined in part by the thermal gradient across the air-sea interface. Warming of the lower atmosphere results in an increased heat flux into the surface ocean and thus contributes to ocean warming.

Global warming is expected to influence the circulation of the atmosphere and the ocean, the water cycle, and to stimulate complex feedbacks (e.g., reduced ice cover and planetary albedo, increased release of GHG due to permafrost thawing; Collins *et al.* 2013). In order to understand and anticipate such repercussions, considerable effort has been dedicated to the development of global coupled general circulation models (GCMs) and Earth System Models (ESMs). Such models numerically simulate the thermodynamics, fluid dynamics and in some cases the interactive chemical and biogeochemical processes occurring within and across all realms of the Earth system under prescribed scenarios of atmospheric GHG concentrations. The Climate Model Intercomparison Project (CMIP) was established in 1995 to evaluate and compare results from similarly-forced simulations from models that were developed by different international organizations, and to facilitate data availability to the scientific community (Covey *et al.* 2003). CMIP is currently in its fifth phase (CMIP5) and uses "representative concentration pathway" (RCPs) that describe specific CO_2 forcing trajectories that are numerically identified by end-of-century level of radiative forcing (e.g., under the high emission scenario RPC 8.5, radiative forcing in 2100 reaches 8.5 W m^{-2}; Taylor *et al.* 2012). CMIP5 models predict an increase of as much 4.8°C in global average temperature by the end of this century (upper RCP 8.5 projections for 2081-2100 relative to 1986-2005 mean; synthesized in Collins *et al.* 2013).

Thermal and chemical CO_2-forcing also impact ocean biogeochemistry. Increased water column stratification (as a result of higher sea surface temperatures; SST) and consequently, reduced upwelling of dissolved inorganic nutrients (DIN) from depth, is expected to impact surface ocean phytoplankton productivity (Behrenfeld *et al.* 2006). Additionally, ocean absorption of CO_2 has increased proportionally with atmospheric concentration (summarized in Doney *et al.* 2009, Fig. 1). Upon entering the ocean, CO_2 reacts with water to form carbonic acid, which in turn dissociates to bicarbonate and hydrogen ions, resulting in an overall reduction in ocean pH or ocean acidification (OA). This process shifts the balance

of dissolved inorganic carbon (DIC) species, thus reducing the concentration of carbonate ions. These carbonate ions are a fundamental component of the calcium carbonate ($CaCO_3$) structures of marine calcifying organisms. Already, average ocean pH has declined ~0.1 pH units (relative to preindustrial conditions, The Royal Society 2005) and is anticipated to drop up an additional ~0.3 pH units by the end of this century (RPC 8.5; Collins *et al.* 2013).

1.2 Impacts of CO_2-driven Ocean Change on Coral Reef Ecosystems

Coral reef communities can be acutely sensitive to environmental perturbations outside of the range to which they are accustomed. For example, reef-building corals bleach when SSTs exceed their thermal-tolerance thresholds. Coral bleaching often occurs when SST rises approximately 1°C above average summer maximum temperature (Hoegh-Guldberg 1999) although thresholds vary widely amongst species and reefs. Bleaching is a stress response whereby corals expel their algal endosymbionts (zooxanthellae) and, in doing so, lose most of their tissue pigmentation. The coral's white calcium carbonate skeleton is then clearly visible through its tissue, giving the coral a "bleached" appearance (Hoegh-Guldberg & Smith 1989, Hoegh-Guldberg 1999). Loss of zooxanthellae also means loss of a major source of coral nutrition. If corals do not recover their symbionts, they starve and eventually die. When corals die from bleaching, irreparable damage to reef systems can occur (Pandolfi *et al.* 2003, Donner *et al.* 2005). Large-scale bleaching events are expected to occur more frequently in the future as more corals and reef systems reach their thermal thresholds.

Corals also rely on heterotrophic feeding as a source of nutrition (e.g., reviewed in Ferrier-Pagès *et al.* 2011) and projected reductions in surface ocean nutrient concentrations and ocean productivity will affect coral food resources and as a consequence, coral growth and resilience to stress. Additionally, reduced carbonate ion availability due to OA impedes calcification by reef-building species (Kleypas *et al.* 1999). Numerous studies demonstrate that coral calcification declines under elevated CO_2 conditions (reviewed in Doney *et al.* 2009, Kroeker *et al.* 2010, Pandolfi *et al.* 2011) with one even predicting that coral reefs globally will transition from net accreting to net-eroding structures when atmospheric CO_2 concentrations double relative to pre-industrial levels (Silverman *et al.* 2009).

Ocean warming, acidification and loss of nutrients and productivity that occur on a global scale are considered global stressors. Today, and over the course of the 21st century, these global stressors will interact with acute, more localized pressures (e.g. overfishing, destructive fishing practices, coastal development and pollution), and together pose serious threats to the future existence of coral reefs ecosystems. Critically however, some reef systems may be naturally more resistant or resilient than others to these stressors (e.g., Glynn 1996, Riegl & Piller 2003). Recently, it has been proposed that coral reef islands and atolls in the equatorial Pacific Ocean may act as climate change refugia for coral communities. This is due to a projected strengthening of the Pacific Equatorial Undercurrent (EUC), caused by relaxation of the trade winds in response to global warming. Such a strengthening would increase the amount of cool water that is topographically upwelled onto equatorial islands, creating a localized cooling that would reduce the large-scale, radiatively-driven warming for a subset of Pacific reef systems (Karnauskas & Cohen 2012).

However, this specific refugia hypothesis does not yet account for the biogeochemical effects of upwelled EUC water, which is rich in dissolved inorganic nutrients (DIN) and CO_2 (e.g., Knauss 1960). Although increased nutrient delivery may counter declining productivity in the vicinity of the islands, high DIN concentrations are generally considered detrimental to coral (e.g., Fabricius 2005). Further, elevated CO_2 conditions generally reduce coral calcification rates and, may therefore, impact larval recruitment and shift the calcium carbonate budget of the reef system.

1.3 Thesis Objectives

My thesis adopts a two-pronged approach to investigate the potential for, and impacts of EUC strengthening on coral reef health through:

1. Analysis of an ocean circulation dataset for historical changes in EUC intensity. Given the ongoing increase in atmospheric CO_2 and global temperatures, it is hypothesized here that EUC intensification is already occurring. GCMs generally do a poor job of capturing EUC strength (Karnauskas *et al.* 2012) and additional evidence for EUC intensification would further support the viability of hypothesized refugia. These analyses assess the presence and robustness of EUC strengthening in the past with an

emphasis on physical mechanisms.

2. Experimental investigation of the coral calcification response to the combination of nutritional enhancement (via light and feeding) and elevated CO_2 conditions. CO_2-rich water normally reduces coral calcification, but it is possible that nutritional enhancement could mitigate, compound or have no effect on this response.

Chapter 2 assesses changes in equatorial Pacific circulation since the mid-19th century using the Simple Ocean Data Assimilation (SODA) reanalysis. This reanalysis product is an ocean circulation model that is constrained by atmospheric and ocean observations. In this data set, the EUC has strengthened significantly since the mid-1800s. Fig. 1-1 shows a relative comparison of historical and future (Karnauskas & Cohen 2012) percent change in EUC velocity. Although Fig. 1-1a describes change in maximum EUC velocity regardless of location, while Fig. 1-1b shows the future change at a single mid-Pacific location, both indicate similar and significant increases in EUC strength. Calculation of the momentum budget of the EUC indicates that the strengthening in SODA appears to be due to two distinct seasonal mechanisms

Chapters 3 and 4 describe laboratory manipulation experiments designed to investigate the impact of heterotrophic feeding and light, on the coral calcification response to ocean acidification. Light enhances nutritional status indirectly, by stimulating symbiont photosynthesis and increasing the production of photosynthate that is transferred to the coral. These experiments quantify the coral calcification response to the nutritionally replete but relatively acidic (elevated CO_2) conditions projected for the equatorial Pacific islands as the EUC strengthens over this century.

Several factors led us to use recently settled juveniles of the Bermudan Atlantic golf ball coral, *Favia fragum* as our test organism in these experiments. *F. fragum* are hermatypic, zooxanthellate, brooding scleractinians. Gamete fertilization and larval development occur within the mother coral polyp prior to their lunar-synchronized release as metamorphically competent larvae (Goodbody-Gringley & de Putron 2009). The timing of larval release on Bermuda is fairly well constrained, which assists in the planning of the experiments. Newly settled juvenile corals accrete their entire $CaCO_3$ skeleton under known experimental conditions, which facilitates interpretation of cross-treatment differences in skeletal and

organic parameters (Cohen *et al.* 2009). These larvae also exhibit high percent recruitment success and survival under laboratory conditions thus ensuring sufficient sample size for experimentation. Like many scleractinians (i.e., reef-building corals), *F. fragum* contribute to the $CaCO_3$ structure of the reef system and are zooxanthellate (i.e., harbor algal symbionts within their tissue). Although *F. fragum* are primarily found in the Atlantic, members of the *Favia* taxonomic family are also found throughout the Pacific (Veron 2000). We note that Bermudan *Favia* may be adapted to a relatively broad seasonal range of environmental conditions (e.g., temperature), that *F. fragum* tend to have smaller colony size relative to massive coral species, and that responses observed in juvenile corals, as studied here, might not be identical to those exhibited by adult colonies. For these reasons (i.e., variability among coral species, and the presence of confounding factors such as adaptation to environmental conditions and life history stage), caution is needed when extrapolating experimental results to broader reef systems. At the same time, controlled experimental studies with single model species provide a powerful tool for understanding coral calcification and its response to single and multiple stressors.

In Chapter 3, juvenile *F. fragum* were reared in either high or ambient CO_2 conditions for three weeks; half of these corals were regularly fed *Artemia* brine shrimp. Using skeletal size (i.e., septa diameter), weight and corallite (septal cycle) development to assess coral response, we found that fed corals were significantly larger and more developmentally advanced than their unfed counterparts, regardless of CO_2 level. Critically, fed corals reared under high CO_2 conditions produced as much $CaCO_3$ as unfed corals under ambient CO_2 conditions. This suggests that corals in nutritionally replete systems will continue to calcify at higher rates than corals in oligotrophic, low productivity habitats as CO_2 levels increase (Drenkard *et al.* 2013). Nevertheless, fed corals maintained the same degree of sensitivity to elevated CO_2 conditions, exhibiting a similar decline in bulk calcium carbonate production with declines in saturation state as unfed corals. This suggests that, while feeding increases coral tissue biomass and the area over which $CaCO_3$ is accreted (resulting in higher net $CaCO_3$ production) it does not eliminate the effect of OA. Thus, feeding does not appear to the coral calcification mechanism (i.e., the effort per calcifying epithelial cell is not increased).

In Chapter 4, juvenile *F. fragum* were again subjected to high and ambient CO_2 conditions (this time for two weeks and without feeding) under either elevated or low light conditions. Unlike the effect due to feeding in Chapter 3, corals under elevated light conditions did not exhibit a significant increase in total $CaCO_3$ production relative to corals under low light conditions, and in these experiments, we did not observe a significant effect of CO_2 on coral skeletal weight. However, in a broader multi-year comparison including unfed treatment data from all three experiments, we observe a significant effect of CO_2 under low light but not high light conditions. Unlike nutritional enhancement by heterotrophic feeding (which did not reduce coral calcification sensitivity to OA), elevated light conditions (which stimulate photosynthesis of the corals' algal endosymbionts) did reduce coral calcification sensitivity to OA. The mechanism for this reduced sensitivity is unclear. Calcification is an energetically costly process, suggesting that this mitigation could be due to the additional photosynthate (i.e., food) provided to the coral by the symbionts. However, while analysis of the coral tissue lipid content shows that corals grown under high light have significantly higher lipid contents than low-light light corals, there is no significant effect of CO_2 on lipid content at a given light level. This implies that corals reared under high light are preferentially storing excess nutrition from their endosymbionts regardless of CO_2 stress, and that a different mechanism must account for the lack of calcification sensitivity to OA.

These studies further our understanding of both the climate dynamics that may dictate EUC strengthening as well as the biological response of the coral organism to multiple stressors associated with increased EUC upwelling on equatorial Pacific reefs. Together, these results assist our efforts to quantitatively assess the climate change refugia potential of these ecosystems.

1.4 References

Behrenfeld MJ, O/'Malley RT, Siegel DA, McClain CR, Sarmiento JL, Feldman GC, Milligan AJ, Falkowski PG, Letelier RM, Boss ES (2006) Climate-driven trends in contemporary ocean productivity. *Nature* 444: 752–755

Cesar H, Burke L, Pet-Soede L (2003) The Economics of Worldwide Coral Reef Degradation. Cesar Environmental Economics Consulting, Arnhem, and WWF-Netherlands, Zeist, The Netherland

Cohen AL, McCorkle DC, de Putron S, Gaetani GA, Rose KA (2009) Morphological and compositional changes in the skeletons of new coral recruits reared in acidified seawater: Insights into the biomineralization response to ocean acidification. *Geochemistry, Geophysics, Geosystems* 10: Q07 005

Collins M, Knutti R, Arblaster J, Dufresne JL, Fichefet T, Friedlingstein P, Gao X, Gutowski W, Johns T, Krinner G, Shongwe M, Tebaldi C, Weaver A, Wehner M (2013) Long-term Climate Change: Projections, Commitments and Irreversibility. In: Stocker T, Qin D, Plattner GK, Tignor M, Allen S, Boschung J, Nauels A, Xia Y, Bex V, Midgley P (eds.) *Climate Change 2013: The Physical Science Basis. Contribution of Working Group I to the Fifth Assessment Report of the Intergovernmental Panel on Climate Change*, Cambridge University Press, Cambridge, United Kingdom and New York, NY, USA.

Covey C, AchutaRao KM, Cubasch U, Jones P, Lambert SJ, Mann ME, Phillips TJ, Taylor KE (2003) An overview of results from the Coupled Model Intercomparison Project. *Global and Planetary Change* 37: 103–133

Doney SC, Fabry VJ, Feely RA, Kleypas JA (2009) Ocean Acidification: The Other CO_2 Problem. *Annual Review of Marine Science* 1: 169–192, pMID: 21141034

Donner SD, Skirving WJ, , Little CM, Oppenheimer M, Hoegh-Guldberg O (2005) Global assessment of coral bleaching and required rates of adaptation under climate change. *Global Change Biology* 11: 2251–2265

Drenkard E, Cohen A, McCorkle D, de Putron S, Starczak V, Zicht A (2013) Calcification by juvenile corals under heterotrophy and elevated CO_2. *Coral Reefs* 32: 727–735

Etheridge DM, Steele LP, Langenfelds RL, Francey RJ, Barnola JM, Morgan VI (1996) Natural and anthropogenic changes in atmospheric CO2 over the last 1000 years from air in Antarctic ice and firn. *Journal of Geophysical Research: Atmospheres* 101: 4115–4128

Fabricius KE (2005) Effects of terrestrial runoff on the ecology of corals and coral reefs: review and synthesis. *Marine Pollution Bulletin* 50: 125–146

Ferrier-Pagès C, Hoogenboom M, Houlbrèque F (2011) The Role of Plankton in Coral Trophodynamics. In: Dubinsky Z, Stambler N (eds.) *Coral Reefs: An Ecosystem in Transition*, 215–229, Springer Netherlands

Friedli H, Lotscher H, Oeschger H, Siegenthaler U, Stauffer B (1986) Ice core record of the 13C/12C ratio of atmospheric CO_2 in the past two centuries. *Nature* 324: 237–238

Glynn PW (1996) Coral reef bleaching: facts, hypotheses and implications. *Global Change Biology* 2: 495–509

Goodbody-Gringley G, de Putron SJ (2009) Planulation patterns of the brooding coral Favia fragum (Esper) in Bermuda. *Coral Reefs* 28: 959–963

Hoegh-Guldberg O (1999) Climate change, coral bleaching and the future of the world's coral reefs. *Marine and Freshwater Research* 50: 839–866

Hoegh-Guldberg O, Smith G (1989) The effect of sudden changes in temperature, light and salinity on the population density and export of zooxanthellae from the reef corals Stylophora pistillata Esper and Seriatopora hystrix Dana. *Journal of Experimental Marine Biology and Ecology* 129: 279–303

Hughes TP, Baird AH, Bellwood DR, Card M, Connolly SR, Folke C, Grosberg R, Hoegh-Guldberg O, Jackson JBC, Kleypas J, Lough JM, Marshall P, Nyström M, Palumbi SR, Pandolfi JM, Rosen B, Roughgarden J (2003) Climate Change, Human Impacts, and the Resilience of Coral Reefs. *Science* 301: 929–933

Karnauskas KB, Cohen AL (2012) Equatorial refuge amid tropical warming. *Nature Climate Change* 2: 530–534

Karnauskas KB, Johnson GC, Murtugudde R (2012) An Equatorial Ocean Bottleneck in Global Climate Models. *Journal of Climate* 25: 343–349

Keeling CD (1973) Industrial production of carbon dioxide from fossil fuels and limestone. *Tellus* 25: 174–198

Keeling CD, Bacastow RB, Bainbridge AE, Ekdahl CA, Guenther PR, Waterman LS, Chin JFS (1976) Atmospheric carbon dioxide variations at Mauna Loa Observatory, Hawaii. *Tellus* 28: 538–551

Kleypas JA, Buddemeier RW, Archer D, Gattuso JP, Langdon C, Opdyke BN (1999) Geochemical Consequences of Increased Atmospheric Carbon Dioxide on Coral Reefs. *Science* 284: 118–120

Knauss A John (1960) Measurements of the Cromwell current. *Deep Sea Research* 6: 256–286

Kroeker KJ, Kordas RL, Crim RN, Singh GG (2010) Meta-analysis reveals negative yet variable effects of ocean acidification on marine organisms. *Ecology Letters* 13: 1419–1434

Moberg F, Folke C (1999) Ecological Goods and Services of Coral Reef Ecosystems. *Ecological Economics* 29: 215–233

Neftel A, Moor E, Oeschger H, Stauffer B (1985) Evidence from polar ice cores for the increase in atmospheric CO_2 in the past two centuries. *Nature* 315: 45–47

Pandolfi JM, Bradbury RH, Sala E, Hughes TP, Bjorndal KA, Cooke RG, McArdle D, McClenachan L, Newman MJH, Paredes G, Warner RR, Jackson JBC (2003) Global Trajectories of the Long-Term Decline of Coral Reef Ecosystems. *Science* 301: 955–958

Pandolfi JM, Connolly SR, Marshall DJ, Cohen AL (2011) Projecting Coral Reef Futures Under Global Warming and Ocean Acidification. *Science* 333: 418–422

Riegl B, Piller W (2003) Possible refugia for reefs in times of environmental stress. *International Journal of Earth Sciences* 92: 520–531

Silverman J, Lazar B, Cao L, Caldeira K, Erez J (2009) Coral reefs may start dissolving when atmospheric CO_2 doubles. *Geophysical Research Letters* 36: L05 606

Tans P, Keeling R (2014) NOAA Earth System Reasearch Laboratory, Global Monitoring Division: Trends in Atmospheric Carbon Dioxide. *http://www.esrl.noaa.gov/gmd/ccgg/trends/index.html*

Taylor KE, Stouffer RJ, Meehl GA (2012) An Overview of CMIP5 and the Experiment Design. *Bulletin of the American Meteorological Society* 93: 485–498

The Royal Society (2005) Ocean acidification due to increasing atmospheric carbon dioxide. The Royal Society, London

Trenberth KE, Fasullo JT, Kiehl J (2009) Earth's Global Energy Budget. *Bulletin of the American Meteorological Society* 90: 311–323

Veron J (2000) *Corals of the World*, vol. 1-3. Australian Institute of Marine Science, Townsville, Australia

van der Werf GR, Morton DC, DeFries RS, Olivier JGJ, Kasibhatla PS, Jackson RB, Collatz GJ, Randerson JT (2009) CO_2 emissions from forest loss. *Nature Geoscience* 2: 737–738

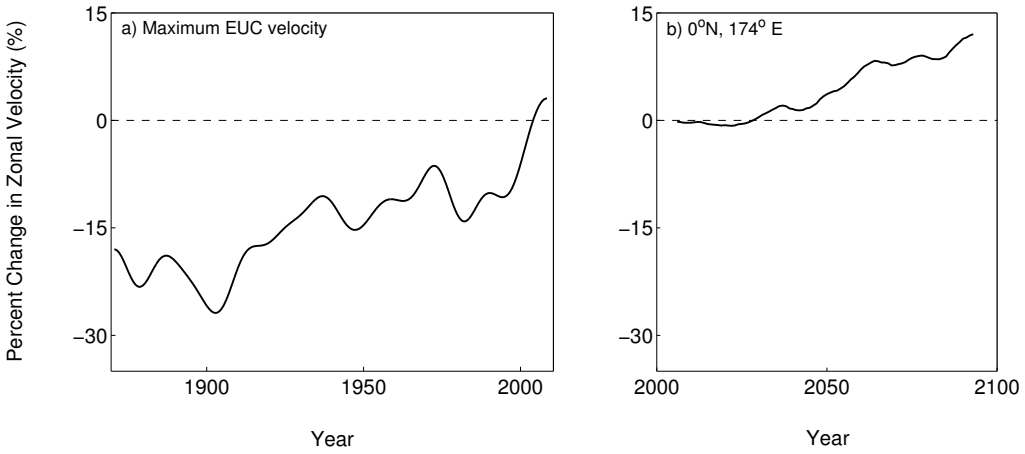

Figure 1-1: Comparison of a) historical and b) projected percent changes in EUC strength. a) is a time series of percent change in maximum zonal velocity from the SODA reanalysis that has been smoothed with a low-pass fllter (adapted from Chapter 2) while b) shows percent change in zonal velocity projected by CMIP3 models at 0° N, 174° E (i.e., near the Gilbert Islands; adapted from Karnauskas & Cohen 2012)

Chapter 2

Strengthening of the Pacific Equatorial Undercurrent in the SODA Reanalysis: Mechanisms, Ocean Dynamics, and Implications

2.1 Abstract

Several recent studies utilizing global climate models predict that the Pacific Equatorial Undercurrent (EUC) will strengthen over the twenty-first century. Here, historical changes in the tropical Pacific are investigated using the Simple Ocean Data Assimilation (SODA) reanalysis toward understanding the dynamics and mechanisms that may dictate such a change. Although SODA does not assimilate velocity observations, the seasonal-to-interannual variability of the EUC estimated by SODA corresponds well with moored observations over a ~20-yr common period. Long-term trends in SODA indicate that the EUC core velocity has increased by 16% century^{-1} and as much as 47% century^{-1} at fixed locations since the mid-1800s. Diagnosis of the zonal momentum budget in the equatorial Pacific reveals two distinct seasonal mechanisms that explain the EUC strengthening. The first is characterized by strengthening of the western Pacific trade winds and hence oceanic zonal pressure gradient during boreal spring. The second entails weakening of eastern Pacific trade winds during boreal summer, which weakens the surface current and reduces EUC deceleration through vertical friction. EUC strengthening has important ecological implications as upwelling affects the thermal and biogeochemical environment. Furthermore, given the potential large-scale influence of EUC strength and depth on the heat budget in the eastern Pacific, the seasonal strengthening of the EUC may help reconcile paradoxical observations of Walker circulation slowdown and zonal SST gradient strengthening. Such a process would represent a new dynamical "thermostat" on CO_2-forced warming of the tropical Pacific Ocean, emphasizing the importance of ocean dynamics and seasonality in understanding climate change projections.

Drenkard EJ, Karnauskas KB (2014) Strengthening of the Pacific equatorial undercurrent in the SODA reanalysis: Mechanisms, ocean dynamics, and implications. *Journal of Climate* 27: 2405-2416 © 2014 American Meteorological Society

2.2 Introduction

The Equatorial Undercurrent (EUC) is the swiftest, most coherent eastward-moving flow in the tropical Pacific Ocean (e.g., Philander 1973; Wyrtki & Kilonsky 1984; Philander *et al.* 1987). The EUC slopes upward from 200±100m at 156°E to 100±100m at 95°W and is confined to within ~2° latitude of the equator (summarized in Arthur 1960; Johnson *et al.* 2002). The zonal pressure gradient force, related to the zonal sea level slope, is maintained by the easterly trade winds and the westward surface current and constitutes a dominant acceleration term in the momentum budget of the EUC (Knauss 1960, Knauss 1966). The balance between the eastward zonal pressure gradient force and westward surface stress determines the strength as well as zonal and vertical structure of the EUC (philander1973; McPhaden & Taft 1988).

The EUC plays a crucial role in Pacific and global climate processes and biogeochemical cycles; it delivers cold, CO_2- and nutrient-rich water to the eastern Pacific, where it feeds the cold tongue. Here, EUC water contributes to the largest oceanic source of atmospheric CO_2 (e.g., Feely *et al.* 2006) and to maintaining the zonal sea surface temperature (SST) gradient across the Pacific (Bjerknes 1966). This thermal gradient is one of the primary controls on tropical Pacific atmospheric circulation, which affects weather patterns and climate worldwide (e.g., Bjerknes 1969; Julian & Chervin 1978). Additionally, upwelling of EUC water provides thermal balance and nutrients to valuable fisheries (e.g., Ganachaud *et al.* 2013) and equatorial island ecosystems (e.g., Houvenaghel 1978; Gove *et al.* 2006; Karnauskas & Cohen 2012). Therefore, changes in EUC intensity will likely have important climatic and ecological repercussions.

Studies predicting future EUC strengthening (e.g., Luo *et al.* 2009; Karnauskas & Cohen 2012; Sen Gupta *et al.* 2012) have attributed this change to rising concentrations of atmospheric CO_2. Anthropogenic CO_2 emissions have unequivocally affected atmospheric composition over the past century (Mann *et al.* 1999; Keeling *et al.* 1976). Thus it begs the question: Has the EUC already responded to historical CO_2 forcing? If so, is it consistent with the future change predicted by global coupled models, is it significant, and can it be explained in a robust dynamical framework? In this study, we used the most recent version of a widely accepted ocean data assimilation product to analyze past trends in EUC

strength and to diagnose the oceanic and atmospheric mechanisms driving these changes. The following sections describe the reanalysis dataset we analyzed and methods we followed to determine the historical trends and evaluate the equatorial Pacific zonal momentum budget. The results of these analyses are reported in section 4 and discussed within the context of their potential climatological and ecological significance in section 5.

2.3 Data

We analyzed the most recent version of the Simple Ocean Data Assimilation (SODA) reanalysis (version 2.2.6; Yang & Giese 2013) to characterize and understand historical changes in EUC strength. This version of SODA and its predecessors (Carton & Giese 2008) are data assimilation products: ocean general circulation models constrained by quality-controlled observations. Monthly SODA fields extend from 1871 to 2008 and are the ensemble mean of eight model runs, each driven by a different realization of wind stress and variables needed for the calculation of heat and freshwater fluxes from the National Oceanic and Atmospheric Administration (NOAA) twentieth-century atmospheric reanalysis (Compo *et al.* 2011; Yang & Giese 2013), thus ensuring that the statistics of weather noise do not change over time. Furthermore, version 2.2.6 assimilates observations of SST only, which prevents the appearance of spurious trends and shifts due to the rise of hydrographic measurements starting in the late 1960s. The spatial and temporal completeness of SODA allows for rigorous assessment of EUC structure and dynamics over long periods of time; such assessments are not typically possible with in situ observations alone. Throughout this paper, we frequently refer to "observed" phenomena; it should be understood that we are referring to results derived from the SODA reanalysis.

The sources of observational data assimilated vary by reanalysis product and even by version within families of reanalyses, but in no case are in situ ocean subsurface velocities assimilated. Figure 2-1 compares acoustic Doppler current profiler (ADCP) measurements of the EUC from equatorial Tropical Atmosphere Ocean (TAO; McPhaden *et al.* 1998) moorings with coinciding SODA estimates. We include comparison of both monthly (Figs. 2-1a,c,e,g) and normalized filtered (13-month running mean) time series (Figs. 2-1b,d,f,h) to assess correspondence between reanalysis and TAO variability at both annual and lower than annual frequencies. With the exception of 0°, 170°W, where there is not a significant

difference between SODA and TAO records (Table 2.1), the SODA reanalysis tends to underestimate the EUC's maximum zonal velocity by 10 cm s^{-1}; this may be related to the reanalysis's relatively coarse spatial resolution (Karnauskas *et al.* 2012). However, as evidenced by the correlation coefficients for each comparison (reported in Table 2.1) and similar comparisons in the literature (Seidel & Giese 1999), SODA captures the seasonal-to-interannual variability of the EUC quite well.

2.4 Results

2.4.1 Observed trends in the EUC and other basin-scale fields

The linear trends in the short, coinciding SODA and TAO time series are also reported in Table 2.1. With the exception of the filtered time series at 165°E (where proximity to land/basin edge may complicate modeled ocean dynamics), none of the SODA trends at a given longitude and smoothing regime differ significantly from their TAO counterparts. Additionally, the majority of these trends are positive and, particularly among the filtered time series, significantly greater than zero.

We first investigated the trends in annual-mean zonal velocity at a fixed point within the mean-state core of the EUC (0°, 146°W, 112m depth; Fig. 2-2). Here we observe a trend of 0.43±0.10m s^{-1} per century (equivalent to 47% $century^{-1}$ of the annual mean) increase in zonal velocity since 1871. However, the position and structure of the EUC are not fixed in time (e.g., Philander 1973; Johnson *et al.* 2002) and, therefore, evaluating temporal trends in zonal velocity at a single depth and geographic location could potentially exaggerate or underrepresent comprehensive changes in the undercurrent. To account for this, we compiled and evaluated a monthly time series (Fig. 2-2) of the maximum zonal velocity found in the spatial domain: 2°N-2°S, 150°-90°W and 10-300m depth. This time series effectively tracks the velocity at the center of the EUC core over the course of the SODA record. The 0.17±0.03m s^{-1} $century^{-1}$ trend in maximum zonal velocity indicates that the core of the EUC has sped up significantly over 1871-2008 (Fig. 2-2). This observed trend, equivalent to roughly 16% of the twentieth-century mean, is in excellent agreement with the 14.4% EUC strengthening that phase 3 of the Coupled Model Intercomparison Project (CMIP3)/ International Panel on Climate Change Fourth Assessment Report (IPCC AR4) global climate

models predict for the twenty-first century in response to increasing atmospheric greenhouse gases (Karnauskas & Cohen 2012).

To analyze large-scale trends in EUC velocity including their spatial variation, we repeated the analysis for Fig. 2-2 at 0°, 146°W, and 112m depth for all depths and longitudes along the equator. With this, we produced a depth-longitude cross section showing the long-term trends in zonal velocity (colored contours in Fig. 2-3a) set in the context of the mean-state zonal velocity (black contours in Fig. 2-3a). Because the EUC flows along the pycnocline and is sensitive to stratification (Philander 1973), we also include a complementary depth profile (Fig. 2-3b) of the vertical density gradient in order to provide additional context for the structural changes we observe in the EUC.

The longitude versus depth section of the observed trends in zonal velocity (Fig. 2-3a) illustrates the structure and nature of the observed strengthening which entails a westward translation and shoaling of the time-mean EUC core and weakening of the South Equatorial Current (SEC). The observation that the region below the EUC core also exhibits a significant trend toward a stronger, eastward velocity confirms that this is not simply a longterm translation but a significant intensification of the EUC. In the density gradient profile, the stratification increase and reduction that occurs above and below the thermocline, respectively, indicates a shoaling of the mean-state thermocline, west of 130°W (Fig. 2-3b). However, the regions of maximum gradient intensification and weakening do not occur at the same longitude. East of 150°W, the shallower increase in stratification exceeds the magnitude of the deeper decrease in stratification, which suggests a sharpening of the thermocline similar to the findings of DiNezio *et al.* (2009). The opposite is found between 170°E and 150°W, indicating a diffusing of the thermocline that spatially corresponds with the region of maximum EUC strengthening (Fig. 2-3a).

We turn now toward potential dynamical mechanisms for the observed EUC intensification. Here, we consider the long-term trends in maximum EUC velocity in relation to potential drivers for these trends. We compared, by longitude, the trends in zonal wind stress, surface zonal velocity, and maximum zonal velocity (depth range: 10 - 300m) on the equator (Figs. 2-4a-c, respectively). Maximum zonal velocity trends (Fig. 2-4c) indicate a significant, nearly basinwide strengthening of the EUC in excess of 0.25m s^{-1} $century^{-1}$ at 150°W. The majority of EUC strengthening (i.e., above 0.1m s^{-1} $century^{-1}$) is accompanied

by significant slowing of the westward surface current between longitudes 180° and 115°W (Fig. 2-4b). This speaks to the mechanism speculated upon by Karnauskas & Cohen (2012) wherein a reduction in the friction or downward mixing of westward momentum imposed by the surface current would cause the EUC to locally accelerate. However, the long-term trend in zonal wind stress as a function of longitude (Fig. 2-4a) is at apparent odds with this mechanism: maximum EUC strengthening at 150°W does not coincide with the point of maximum wind stress weakening (~105°W). Two observations in particular prompted the remainder of our efforts to diagnose EUC intensification: The nonuniformity in zonal wind stress trends across the basin (i.e., weakening in the east versus strengthening in the west) likely affects the longitudinal gradient in sea surface height, which suggests that forces such as the zonal pressure gradient may also influence the observed trends in EUC strength. Additionally, the trends shown in Fig. 2-4 are annual mean perspectives; if the dynamics driving EUC acceleration are seasonally dependent, averaging over the annual cycle may obscure specific mechanisms.

Therefore, we also considered seasonal trends in zonal wind stress, surface ocean velocity, sea surface height, zonal transport, and maximum zonal velocity (colored contours in Figs. 2-5a-e, respectively). Each field is shown in the context of its climatology (black contours in Figs. 2-5a-e). We used a depth range of 0-640m (first 20 depth layers in SODA reanalysis) to calculate zonal transport, a depth range of 10-300m to determine maximum zonal velocity, and a horizontal dimension of 110.6 km between latitudes for calculating transport between 0.5°N and 0.5°S. Climatological Hövmoller diagrams (longitude versus time; Fig. 2-5) highlight two seasons within the annual cycle that clearly dominate the observed EUC intensification. These periods are March - May (MAM) and June - August (JJA); they are characterized by the largest positive trends in eastward volume transport (Fig. 2-5d) and maximum zonal velocity (Fig. 2-5e). The MAM intensification occurs approximately one month after maximum strengthening of the easterly trades and westward surface velocity in the western Pacific (Figs. 2-5a,b) and is concurrent with an increase in the zonal gradient of sea surface height (SSH; Fig. 2-5c). This suggests that the long-term acceleration of the EUC during MAM is related to the zonal pressure gradient rather than a reduction of vertical friction. In contrast, EUC core strengthening during JJA occurs when the weakening trend in both the eastern Pacific zonal wind stress (Fig. 2-5a) and, to a greater extent, the

westward surface current (Fig. 2-5b) is prominent. Therefore, it appears that the dynamical mechanisms driving the observed EUC intensification are caused by a seasonally dependent combination of both local (i.e., friction) and nonlocal (i.e., basin-scale pressure gradient) factors. Investigation into long-term changes in ocean kinematics from the view of the zonal momentum budget during both MAM and JJA is the subject of the following section.

2.4.2 Diagnosis of the zonal momentum equation

To formally elucidate the mechanism and drivers of historical changes in the EUC we performed a thorough analysis of the zonal momentum budget, which is similar to the approach of Brown *et al.* (2007) and Qiao & Weisberg (1997). We use the following rearrangement of the zonal momentum equation (ZME):

$$\frac{\partial u}{\partial t} = -u\frac{\partial u}{\partial x} - v\frac{\partial u}{\partial z} - w\frac{\partial u}{\partial z} - \frac{1}{\rho}\frac{\partial P}{\partial x} + 2\Omega v \sin\vartheta + A_H\nabla^2 u + \frac{\partial}{\partial z}\left[A_v\left(\frac{\partial u}{\partial z}\right)\right] \qquad (2.1)$$

where $\partial u/\partial t$ is the time rate of change in zonal velocity; $u\partial u/\partial x$, $v\partial u/\partial y$, and $w\partial u/\partial z$ represent the nonlinear advective terms; $-(1/\rho)(\partial P/\partial x)$ is the zonal pressure gradient force; and $2\Omega v \sin\vartheta$ is the Coriolis force where Ω is the rotation of Earth and ϑ is the latitude at which the ZME (2.1) is evaluated. Finally, $A_H\nabla^2 u$, or $(\partial/\partial x)[A_H(\partial u/\partial x)] + (\partial/\partial y)[A_H(\partial u/\partial y)]$, are the horizontal friction terms while $(\partial/\partial z)[A_V(\partial u/\partial z)]$ is the vertical friction term. All SODA fields were interpolated from their original depth divisions to regular, 5m intervals; partial derivatives were calculated via central finite differencing. Density was calculated based on the equation of state using salinity, temperature and depth (Fofonoff & Millard 1983); A_H and A_V are the horizontal and vertical coefficients of eddy viscosity, respectively. Because these coefficients were not retained following each model run of the SODA reanalysis (B. Giese 2013, personal communication), we estimated or calculated them in the following way: We assigned A_H a constant value of 1.5×10^{-3} m^2 s^{-1} (Wallcraft *et al.* 2005), while we varied the value of A_V with depth: 4.5×10^{-3} m^2 s^{-1} above the thermocline, 0.3×10^{-3} m^2 s^{-1} within the thermocline, 1.5×10^{-3} m^2 s^{-1} below the thermocline, and a smooth spline interpolation in between (Qiao & Weisberg 1997). These values are not well known and are, consequently, a primary source of uncertainty in our

calculations that leads to a nontrivial mean residual. However, we only invoke the temporal change in these terms to explain seasonal EUC intensification mechanisms (i.e., Fig. 2-7, described in greater detail below), which is not influenced by methodological uncertainties to the same extent. Friction terms were calculated on isopycnal layers and thus all terms are displayed in an isopycnic coordinate system.

For reference, shown in Fig. 2-6 are the SODA record mean longitudinal profiles of zonal wind stress τ_x and SSH (Fig.2-6a), vertical sections of zonal velocity u (Fig. 2-6b), and individual terms of the zonal momentum equation (Figs. 2-6c-h). Note that, because of the central differencing approach used for calculating the vertical friction term, we are unable to resolve the upper and lower two isopycnal layers. The zonal pressure gradient force, nonlinear vertical advection, and vertical friction terms are the most dominant terms balancing the time-mean state and play the largest role in distinguishing the two seasonal mechanisms of EUC strengthening.

We then evaluated the change in each of the ZME components in the equatorial Pacific by differencing terms that were calculated using the seasonal, time-mean fields for the fourth versus first quarters (i.e., each 35 yr) of the SODA reanalysis (Fig. 2-7). Other methods were checked to confirm the insensitivity of the salient results to such temporal choices. During MAM, the EUC strengthens at its core and in the western Pacific while a stronger surface current weakens the undercurrent and depresses the EUC core depth in the eastern Pacific (Fig. 2-7c). Stronger easterly trade winds coincide with stronger zonal SSH and pressure gradients (cf. Figs. 2-7a,g). The vertical nonlinear advective term ($w\partial u/\partial z$; Fig. 2-7e) exhibits a strong eastward acceleration within the upper layers of the EUC, while the vertical friction term $\{(\partial/\partial z)[A_V(\partial u/\partial z)]$; Fig. 2-7i$\}$ shows a westward surface acceleration, which is in opposition to the flow of the EUC.

Conversely, EUC intensification during JJA is concentrated at and near the surface of the eastern equatorial Pacific (Fig. 2-7d); this is zonally aligned with a pronounced weakening of the easterly trade winds (Fig. 2-7b) and the zonal pressure gradient force (Fig. 2-7h). Additionally, both the vertical nonlinear advective and friction terms (Figs. 2-7f & j, respectively) exhibit eastward acceleration within this region of maximum EUC strengthening (i.e., east of 160°W). EUC intensification in the west is associated with a less pronounced strengthening of the trade winds (Fig. 2-7b) and the zonal pressure gradient

force (Fig. 2-7h) between 170°E and 160°W.

2.5 Summary and Discussion

We have shown that the EUC has strengthened significantly in the SODA reanalysis since the mid nineteenth century, a signal that is even apparent in the short-term TAO in situ record (Table 2.1 and Fig. 2-1). Analyses of long-term trends in zonal velocity indicate that this intensification entails a shoaling, vertical broadening, and westward migration of the EUC core. These structural changes in the undercurrent are tightly coupled with stratification trends and, despite different mechanisms, are similar to those projected by Luo et al. (2009; cf. Fig. 3) and Sen Gupta et al. (2012; cf. Fig. 1b).

Further investigation into equatorial Pacific climatological trends and zonal momentum budget indicates that the majority of observed, historical EUC strengthening is explained by two seasonally and dynamically different mechanisms. The intensification observed during boreal spring locally appears to be caused by a strengthening of the easterly trade winds in the west. This increases the zonal SSH gradient and, consequently, the zonal pressure gradient, which accelerates the core of the EUC in the western Pacific. The shallow, eastward acceleration in the vertical nonlinear advective term is tightly linked to this process. This advective term is influenced by intensified equatorial upwelling (i.e., larger w) because of the faster westward surface current and by zonal momentum advected upward from the accelerated EUC core, which crosses a larger vertical gradient in zonal velocity (i.e., larger $\partial u/\partial z$). However, the westward wind stress, as well as subsequent vertical transmission of friction, resists this intensification and slows and depresses the core depth of the EUC in the east. This mechanism strongly resembles the mean state of the equatorial Pacific and thus operates within the canonical dynamics governing the mean EUC (e.g., Fofonoff & Montgomery 1955; Knauss 1960).

In light of historical observations of EUC weakening or even disappearance during strong El Niño events (e.g., Firing *et al.* 1983), it is at first counterintuitive to also observe a strengthening of the EUC during JJA when the weakening trend in both the easterly trade winds and the westward surface current is so prominent. In the SODA reanalysis, the long-term weakening of the eastern Pacific trade winds causes a local flattening of the zonal SSH and pressure gradients. If relying strictly on ENSO correlations, one might expect the EUC

to weaken. Instead, we observe a strong and shallow intensification of the EUC in close synchrony with the seasonal weakening of the easterly trades. This appears to be largely apparent in the eastward acceleration in the vertical friction term $(\partial/\partial z)[A_V(\partial u/\partial z)]$, which is influenced by both the change in the vertical gradient of zonal velocity ($\partial u/\partial z$; primarily determined here by zonal wind stress) as well as the increase in stratification (Fig. 2-3b). Finally, the nonlinear vertical advection term ($w\partial u/\partial z$) also contributes to shallow strengthening of the EUC. Apparently the magnitude of the change in the vertical gradient in zonal velocity ($\partial u/\partial z$) exceeds the reduction in upwelling (i.e., smaller w) that also is caused by slowing of the trades and surface current and increased stratification.

The underlying mechanism and EUC strengthening during boreal summer may be analogous to that projected by climate models, which exhibit a weakening Walker circulation (Vecchi & Soden 2007; Karnauskas & Cohen 2012). Additionally, it may be a key to reconciling historical observations of weakened Walker circulation with strengthening Pacific zonal SST gradient. Vecchi *et al.* (2006) report a 3.5% slowdown of Pacific Walker circulation since 1860 (and project a 10% decrease by 2100) based on CMIP3 simulations. As they point out, such a reduction in zonal wind stress would weaken equatorial upwelling and effectively reduce the amount of cold water brought up from depth, resulting in a warming of the eastern Pacific cold tongue. However, this is fundamentally at odds with the long line of studies reporting observations of a historical cooling trend in the eastern equatorial Pacific Ocean (Cane *et al.* 1997; Karnauskas *et al.* 2009; Compo & Sardeshmukh 2010; Kumar *et al.* 2010; Zhang *et al.* 2010; Solomon & Newman 2012; L'Heureux *et al.* 2013). The mechanism dominant in JJA exhibits both a weakening of the easterly trade winds, which would appear to be consistent with a weakening of the Walker circulation, and a means of increasing the zonal SST gradient: namely, a shoaling and robust strengthening of the thermocline and EUC. However, bulk measures of the Walker circulation such as SLP differences and basin-mean zonal winds, especially in an annual-mean-only basis, likely do not encapsulate the dynamics and time scales that the ocean actually responds to.

Both increased stratification and EUC intensification can be invoked as possible contributors to seasonal surface cooling. DiNezio *et al.* (2009) demonstrate that, despite reductions in upwelling, increased stratification (e.g., Fig. 2-3b) can lead to a net cooling in the eastern Pacific. Additionally, Moum *et al.* (2013) highlight the critical role of ocean mixing driving

sea surface cooling during boreal summer. Changing subsurface zonal velocity and vertical shear may further stimulate turbulent mixing and enhance this seasonal cooling. Certainly the efficacy of the coupling mechanism we propose here depends upon a number of factors: not least of which is the impact of climate change on the temperature of the water masses that feed the EUC (Cane *et al.* 1997). Further work focusing on the mixed-layer heat budget is necessary to confirm this speculation but may yield a mechanism parallel to that described by Sun & Liu (1996), Clement *et al.* (1996), and Seager & Murtugudde (1997) as an ocean dynamical thermostat.

It should be noted that this study does not directly address off-equatorial mechanisms for EUC trends, and recent studies such as those addressing the western boundary currents that feed the EUC as prominent drivers of intensification (Luo *et al.* 2009; Sen Gupta *et al.* 2012) are possibly complementary rather than mutually exclusive. Indeed, our momentum budget analyses focus on the two seasons that exhibit the largest increase in maximum zonal velocity and transport. However, these fields, particularly maximum velocity (Fig. 2-5e), show strengthening throughout most of the annual cycle. This may be driven by an increase in the zonal sea surface height gradient (and thus, pressure gradient force), which is characterized in part by a persistent, year-long elevation in the western Pacific (Fig. 2-3c). This signal is highly suggestive of off-equatorial drivers such as strengthening western boundary currents, for both their dynamical influence and the absence of a clear causative signal in seasonal wind stress (Fig. 2-5a), and further illustrates the potential for multiple oceanic-atmospheric drivers contributing to changing tropical circulation.

A strengthening of the EUC has important implications for affected equatorial Pacific island and oceanic ecosystems. Topographic upwelling of the EUC delivers cold, nutrient- and CO_2-rich water to the surface and plays a fundamental role in dictating the structure and evolution of exposed ecosystems (Houvenaghel 1978). Such regions have been proposed as potential priorities for enhanced conservation efforts because they may locally mitigate and are thus resilient to the rapidity of ocean surface warming that poses a serious threat to tropical coral reef ecosystems (West & Salm 2003). Karnauskas & Cohen (2012) specifically highlight the refugia potential of equatorial Pacific islands because of the modeled cooling influence of predicted EUC intensification. However, enhanced upwelling could also adversely impact exposed coral reefs because CO_2-rich EUC water may deter calcium car-

bonate and thus essential framework production on these ecosystems (Feely *et al.* 2008; Manzello *et al.* 2008). An historical precedence for EUC intensification is valuable because investigation into past reef response to EUC strengthening may enable fishery managers and marine conservation planners to better anticipate and plan for the inevitable ecological consequences of future changes in ocean temperatures, circulation, and nutrient supply.

2.6 Acknowledgments

The authors gratefully acknowledge Benjamin Giese for his tireless efforts to improve the SODA reanalysis product, for his assistance in procuring the version 2.2.6 fields, and for his insightful feedback on this manuscript. The authors also thank the three anonymous reviewers for their constructive suggestions. EJD is supported by NSF Grants OCE-1031971 and OCE-1233282. KBK is supported by NSF Grant OCE-1233282.

2.7 References

Arthur RS (1960) A review of the calculation of ocean currents at the equator. *Deep Sea Research* 6: 287–297

Bjerknes J (1966) A possible response of the atmospheric Hadley circulation to equatorial anomalies of ocean temperature. *Tellus* 18: 820–829

Bjerknes J (1969) Atomspheric teleconnections from the Equatorial Pacific. *Monthly Weather Review* 97: 163–172

Brown JN, Godfrey JS, Fiedler R (2007) A Zonal Momentum Balance on Density Layers for the Central and Eastern Equatorial Pacific. *Journal of Physical Oceanography* 37: 1939–1955

Cane MA, Clement AC, Kaplan A, Kushnir Y, Pozdnyakov D, Seager R, Zebiak SE, Murtugudde R (1997) Twentieth-Century Sea Surface Temperature Trends. *Science* 275: 957–960

Carton JA, Giese BS (2008) A Reanalysis of Ocean Climate Using Simple Ocean Data Assimilation (SODA). *Monthly Weather Review* 136: 2999–3017

Clement AC, Seager R, Cane MA, Zebiak SE (1996) An Ocean Dynamical Thermostat. *Journal of Climate* 9: 2190–2196

Compo GP, Sardeshmukh PD (2010) Removing ENSO-Related Variations from the Climate Record. *Journal of Climate* 23: 1957–1978

Compo GP, Whitaker JS, Sardeshmukh PD, Matsui N, Allan RJ, Yin X, Gleason BE, Vose RS, Rutledge G, Bessemoulin P, Brönnimann S, Brunet M, Crouthamel RI, Grant AN, Groisman PY, Jones PD, Kruk MC, Kruger AC, Marshall GJ, Maugeri M, Mok HY, Nordli Ø, Ross TF, Trigo RM, Wang XL, Woodruff SD, Worley SJ (2011) The Twentieth Century Reanalysis Project. *Quarterly Journal of the Royal Meteorological Society* 137: 1–28

DiNezio PN, Clement AC, Vecchi GA, Soden BJ, Kirtman BP, Lee SK (2009) Climate Response of the Equatorial Pacific to Global Warming. *Journal of Climate* 22: 4873–4892

Feely RA, Takahashi T, Wanninkhof R, McPhaden MJ, Cosca CE, Sutherland SC, Carr ME (2006) Decadal variability of the air-sea CO2 fluxes in the equatorial Pacific Ocean. *Journal of Geophysical Research: Oceans* 111: C08S90

Feely RA, Sabine CL, Hernandez-Ayon JM, Ianson D, Hales B (2008) Evidence for Upwelling of Corrosive "Acidified" Water onto the Continental Shelf. *Science* 320: 1490–1492

Firing E, Lukas R, Sadler J, Wyrtki K (1983) Equatorial Undercurrent Disappears During 1982-1983 El Niño. *Science* 222: 1121–1123

Fofonoff NP, Millard RC (1983) Algorithms for computation of fundamental properties of seawater. *UNESCO Technical Papers in Marine Science* 44: 53 pp

Fofonoff NP, Montgomery RB (1955) The Equatorial Undercurrent in the Light of the Vorticity Equation1. *Tellus* 7: 518–521

Ganachaud A, Sen Gupta A, Brown J, Evans K, Maes C, Muir L, Graham F (2013) Projected changes in the tropical Pacific Ocean of importance to tuna fisheries. *Climatic Change* 119: 163–179

Gove JM, Merrifield MA, Brainard RE (2006) Temporal variability of current-driven upwelling at Jarvis Island. *Journal of Geophysical Research: Oceans* 111: C12 011

Houvenaghel G (1978) Oceanographic conditions in the Galapagos Archipelago and their telationships with life on the islands. In: Boje R, Tomczak M (eds.) *Upwelling Ecosystems*, 181–200, Springer Berlin Heidelberg

Johnson GC, Sloyan BM, Kessler WS, McTaggart KE (2002) Direct measurements of upper ocean currents and water properties across the tropical Pacific during the 1990s. *Progress in Oceanography* 52: 31–61

Julian PR, Chervin RM (1978) A Study of the Southern Oscillation and Walker Circulation Phenomenon. *Monthly Weather Review* 106: 1433–1451

Karnauskas KB, Cohen AL (2012) Equatorial refuge amid tropical warming. *Nature Climate Change* 2: 530–534

Karnauskas KB, Seager R, Kaplan A, Kushnir Y, Cane MA (2009) Observed Strengthening of the Zonal Sea Surface Temperature Gradient across the Equatorial Pacific Ocean. *Journal of Climate* 22: 4316–4321

Karnauskas KB, Johnson GC, Murtugudde R (2012) An Equatorial Ocean Bottleneck in Global Climate Models. *Journal of Climate* 25: 343–349

Keeling CD, Bacastow RB, Bainbridge AE, Ekdahl CA, Guenther PR, Waterman LS, Chin JFS (1976) Atmospheric carbon dioxide variations at Mauna Loa Observatory, Hawaii. *Tellus* 28: 538–551

Knauss A John (1960) Measurements of the Cromwell current. *Deep Sea Research* 6: 256–286

Knauss A John (1966) Further measurements and observations on the Cromwell Current. *Journal of Marine Research* 24: 205–240

Kumar A, Jha B, L'Heureux M (2010) Are tropical SST trends changing the global teleconnection during La Niña? *Geophysical Research Letters* 37: L12 702

L'Heureux ML, Lee S, Lyon B (2013) Recent multidecadal strengthening of the Walker circulation across the tropical Pacific. *Nature Climate Change* 3: 571–576

Luo Y, Rothstein LM, Zhang RH (2009) Response of Pacific subtropical-tropical thermocline water pathways and transports to global warming. *Geophysical Research Letters* 36: L04 601

Mann ME, Bradley RS, Hughes MK (1999) Northern hemisphere temperatures during the past millennium: Inferences, uncertainties, and limitations. *Geophysical Research Letters* 26: 759–762

Manzello DP, Kleypas JA, Budd DA, Eakin CM, Glynn PW, Langdon C (2008) Poorly cemented coral reefs of the eastern tropical Pacific: Possible insights into reef development in a high-CO2 world. *Proceedings of the National Academy of Sciences* 105: 10 450–10 455

McPhaden MJ, Taft BA (1988) Dynamics of Seasonal and Intraseasonal Variability in the Eastern Equatorial Pacific. *Journal of Physical Oceanography* 18: 1713–1732

McPhaden MJ, Busalacchi AJ, Cheney R, Donguy JR, Gage KS, Halpern D, Ji M, Julian P, Meyers G, Mitchum GT, Niiler PP, Picaut J, Reynolds RW, Smith N, Takeuchi K (1998) The Tropical Ocean-Global Atmosphere observing system: A decade of progress. *Journal of Geophysical Research: Oceans* 103: 14 169–14 240

Moum JN, Perlin A, Nash JD, McPhaden MJ (2013) Seasonal sea surface cooling in the equatorial Pacific cold tongue controlled by ocean mixing. *Nature* 500: 64–67

Philander SGH (1973) equatorial undercurrent: Measurements and theories. *Reviews of Geophysics* 11: 513–570

Philander SGH, Hurlin WJ, Seigel AD (1987) Simulation of the Seasonal Cycle of the Tropical Pacific Ocean. *Journal of Physical Oceanography* 17: 1986–2002

Qiao L, Weisberg RH (1997) The Zonal Momentum Balance of the Equatorial Undercurrent in the Central Pacific. *Journal of Physical Oceanography* 27: 1094–1119

Seager R, Murtugudde R (1997) Ocean Dynamics, Thermocline Adjustment, and Regulation of Tropical SST. *Journal of Climate* 10: 521–534

Seidel HF, Giese BS (1999) Equatorial currents in the Pacific Ocean 1992–1997. *Journal of Geophysical Research: Oceans* 104: 7849–7863

Sen Gupta A, Ganachaud A, McGregor S, Brown JN, Muir L (2012) Drivers of the projected changes to the Pacific Ocean equatorial circulation. *Geophysical Research Letters* 39: L09 605

Solomon A, Newman M (2012) Reconciling disparate twentieth-century Indo-Pacific ocean temperature trends in the instrumental record. *Nature Clim Change* 2: 691–699

Sun DZ, Liu Z (1996) Dynamic Ocean-Atmosphere Coupling: A Thermostat for the Tropics. *Science* 272: 1148–1150

Vecchi GA, Soden BJ (2007) Global Warming and the Weakening of the Tropical Circulation. *Journal of Climate* 20: 4316–4340

Vecchi GA, Soden BJ, Wittenberg AT, Held IM, Leetmaa A, Harrison MJ (2006) Weakening of tropical Pacific atmospheric circulation due to anthropogenic forcing. *Nature* 441: 73–76

Wallcraft AJ, Kara AB, Hurlburt HE (2005) Convergence of Laplacian diffusion versus resolution of an ocean model. *Geophysical Research Letters* 32: L07 604

West JM, Salm RV (2003) Resistance and Resilience to Coral Bleaching: Implications for Coral Reef Conservation and Management. *Conservation Biology* 17: 956–967

Wyrtki K, Kilonsky B (1984) Mean Water and Current Structure during the Hawaii-to-Tahiti Shuttle Experiment. *Journal of Physical Oceanography* 14: 242–254

Yang C, Giese BS (2013) El Niño Southern Oscillation in an ensemble ocean reanalysis and coupled climate models. *Journal of Geophysical Research: Oceans* 118: 4052–4071

Zhang W, Li J, Zhao X (2010) Sea surface temperature cooling mode in the Pacific cold tongue. *Journal of Geophysical Research: Oceans* 115: C12 042

		Equatorial TAO locations (lon)			
		165°E	170°W	140°W	110°W
Monthly time Series	R	0.53	0.75	0.82	0.75
	Bias (ms^{-1})	−0.08	0.01	−0.14	−0.10
	ADCP trend	0.61 ± 0.63	0.44 ± 0.71	1.15 ± 0.94*	0.61 ± 1.18
	($ms^{-1}century^{-1}$)				
	SODA trend	−0.16 ± 0.58	0.71 ± 0.62*	2.10 ± 0.83*	0.82 ± 1.01
	($ms^{-1}century^{-1}$)				
Monthly time Series	R	0.60	0.84	0.91	0.93
(13-month smoothing filter)	Bias (ms^{-1})	−0.09	0.01	−0.14	−0.10
	ADCP trend	0.70 ± 0.44*	0.64 ± 0.47*	1.31 ± 0.43*	0.70 ± 0.39*
	($ms^{-1}century^{-1}$)				
	SODA trend	−0.17 ± 0.31	0.73 ± 0.40*	2.20 ± 0.44*	0.91 ± 0.51*
	($ms^{-1}century^{-1}$)				

*Statistically significant trend (α=0.01).

Table 2.1: Correlation coefficients R, average SODA-ADCP bias, and linear trends for both monthly and filtered time series. All correlation and bias values (with the exception of biases reported at 170°W) are significant ($\alpha = 0.01$; $p < 0.001$).

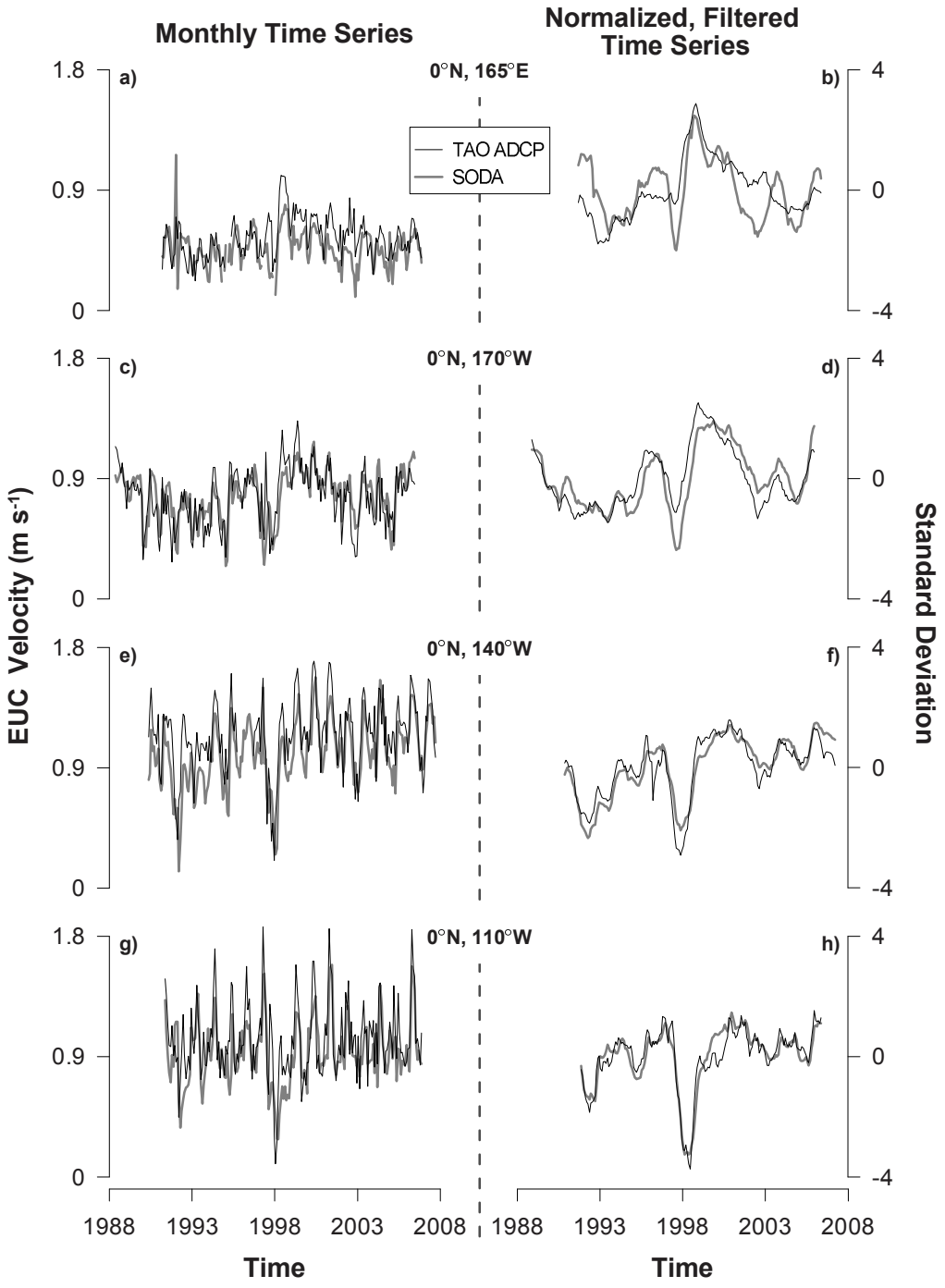

Figure 2-1: Comparison of maximum EUC zonal velocity estimated by SODA (grey) and Acoustic Doppler Current Profiler (ADCP) measurements by equatorial TAO moorings (black) at 0°N and (a, b) 165°E (c, d) 170°W (e, f) 140°W and (g, h) 110°W. The ADCP data were regridded via linear interpolation to depth intervals that match the vertical resolution of SODA; maximum velocities located below 300 meters were masked out. The plots on the left (a, c, e, g) compare the monthly time series of maximum zonal velocity while the plots on the right (b, d, f, h) compare these time series after filtering (13-month running mean) and normalization.

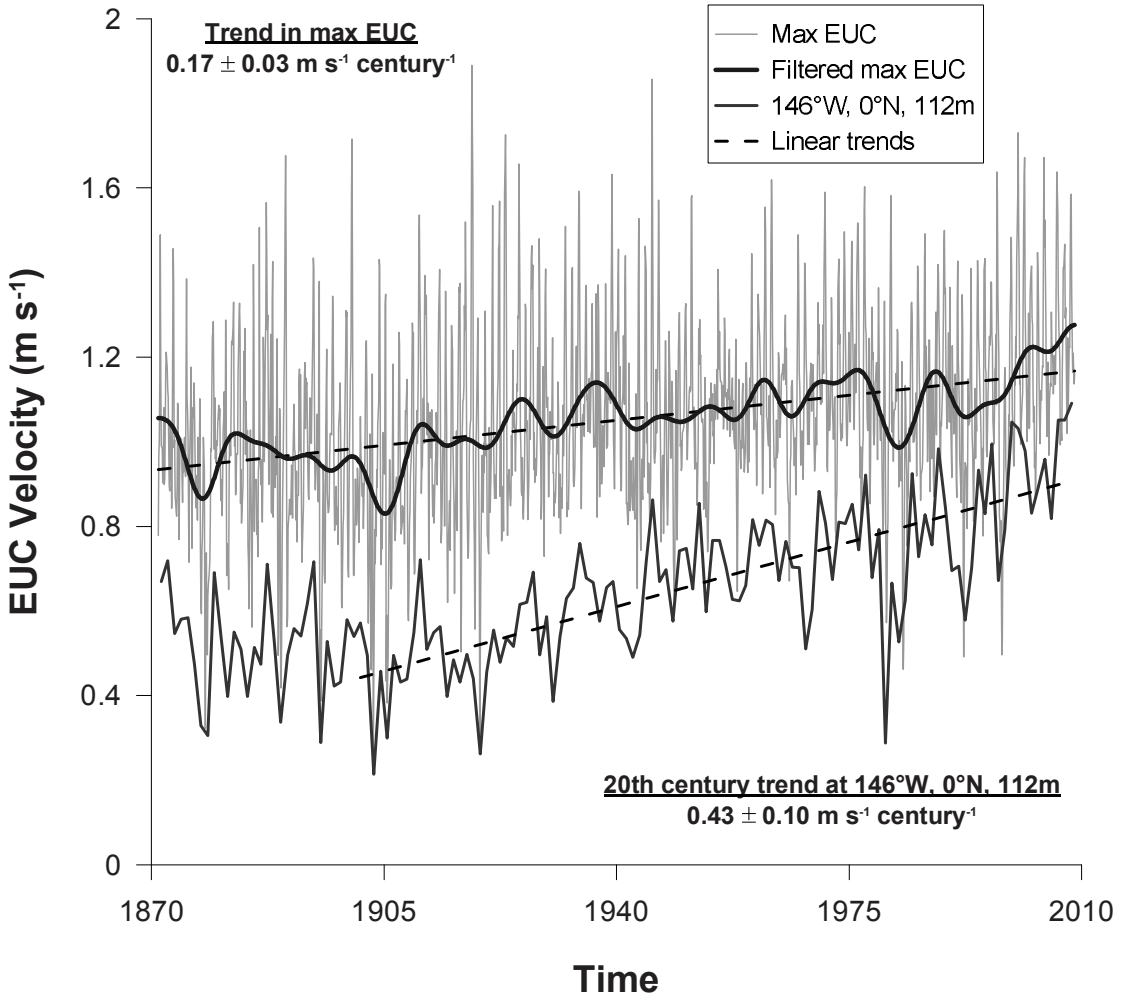

Figure 2-2: Time series of maximum EUC strength and zonal velocity at 146°W, 0°N, 112m. The solid, pale grey line depicts the monthly maximum velocity from SODA within the domain of the EUC core (i.e. latitude: 2°N-2°S; longitude: 150°W-90°W; depth: 10-300 meters), while the thick black line is a 7-year filtering of this time series. The solid, dark grey line indicates the annual mean zonal velocity at the fixed location: 146°W, 0°N, 112m. Lastly, we report two linear trends (i.e. regression slopes; dashed lines) for the annual and monthly time series, both of which are significant at the 99% confidence interval.

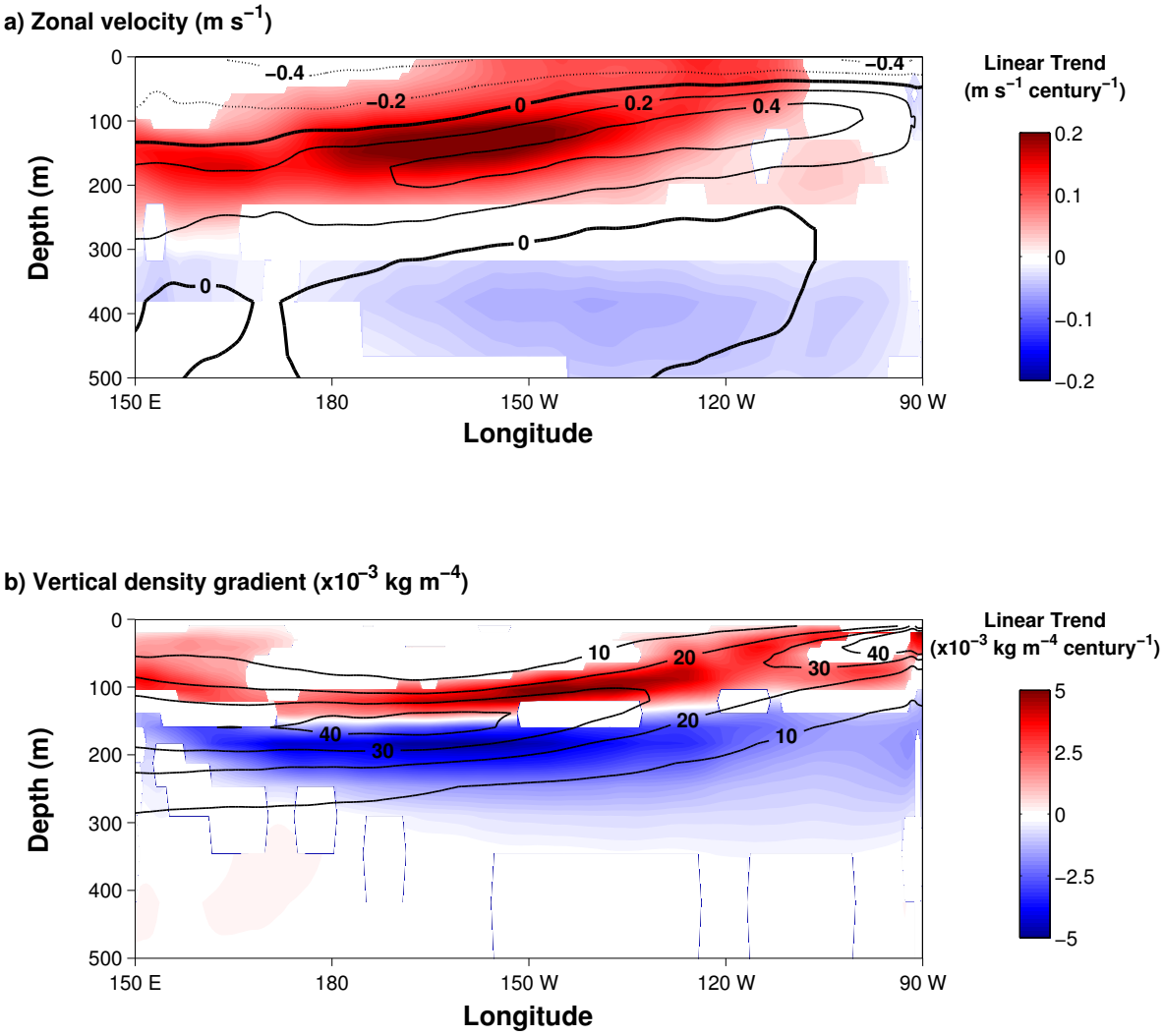

Figure 2-3: Depth-longitude profiles of both average, and long-term trends in a) zonal velocity and b) density gradient along the equatorial Pacific. In a) the solid and dashed black contours indicate the mean state of the EUC and overlying SEC, respectively: zonal velocity (in units: m s^{-1}). Note the sign convention: positive (negative) contours indicate eastward (westward) average or trending movement. In b) the solid black contours indicate the mean state of the vertical density gradient with positive (negative) contours indicating strengthening (weakening) stratification. Velocity and density values were averaged from 2°N-2°S prior to calculating trends and the means state over the time span of the SODA record. Regions where the long-term trends were not significant at the 99% confidence interval were masked out.

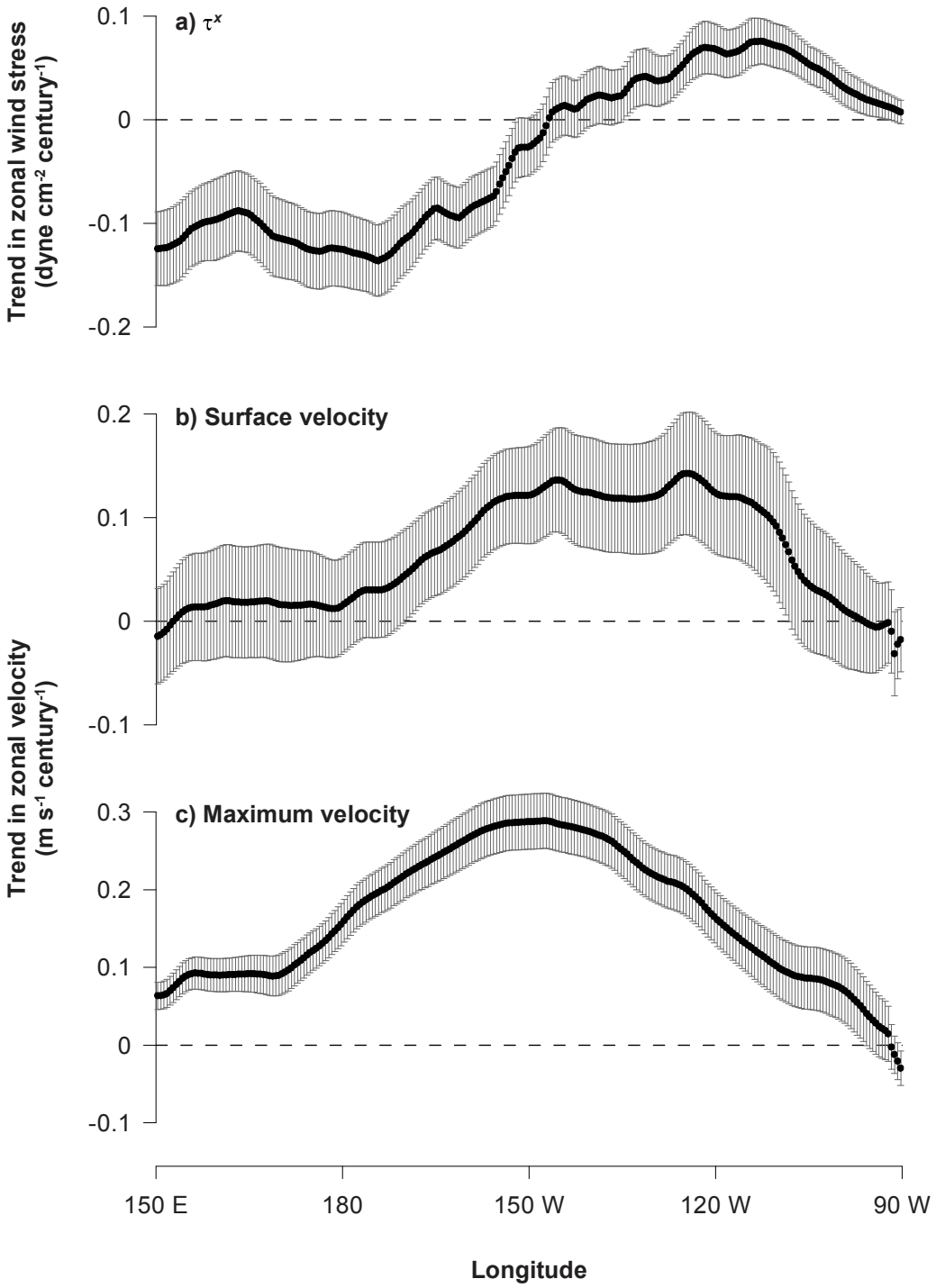

Figure 2-4: Long-term trends by longitude along the equator in a) zonal wind stress, and b) surface and c) maximum (i.e. EUC) zonal velocity. Error bars indicate the 99% confidence interval of the reported trend. The surface b) is defined as SODA's top depth layer (~10 meter), while the EUC domain c) extends through SODA's first 15 sub-surface depth layers (~10-300 meters). Note the sign convention: positive (i.e. above the '0' line) values indicate eastward trending movement.

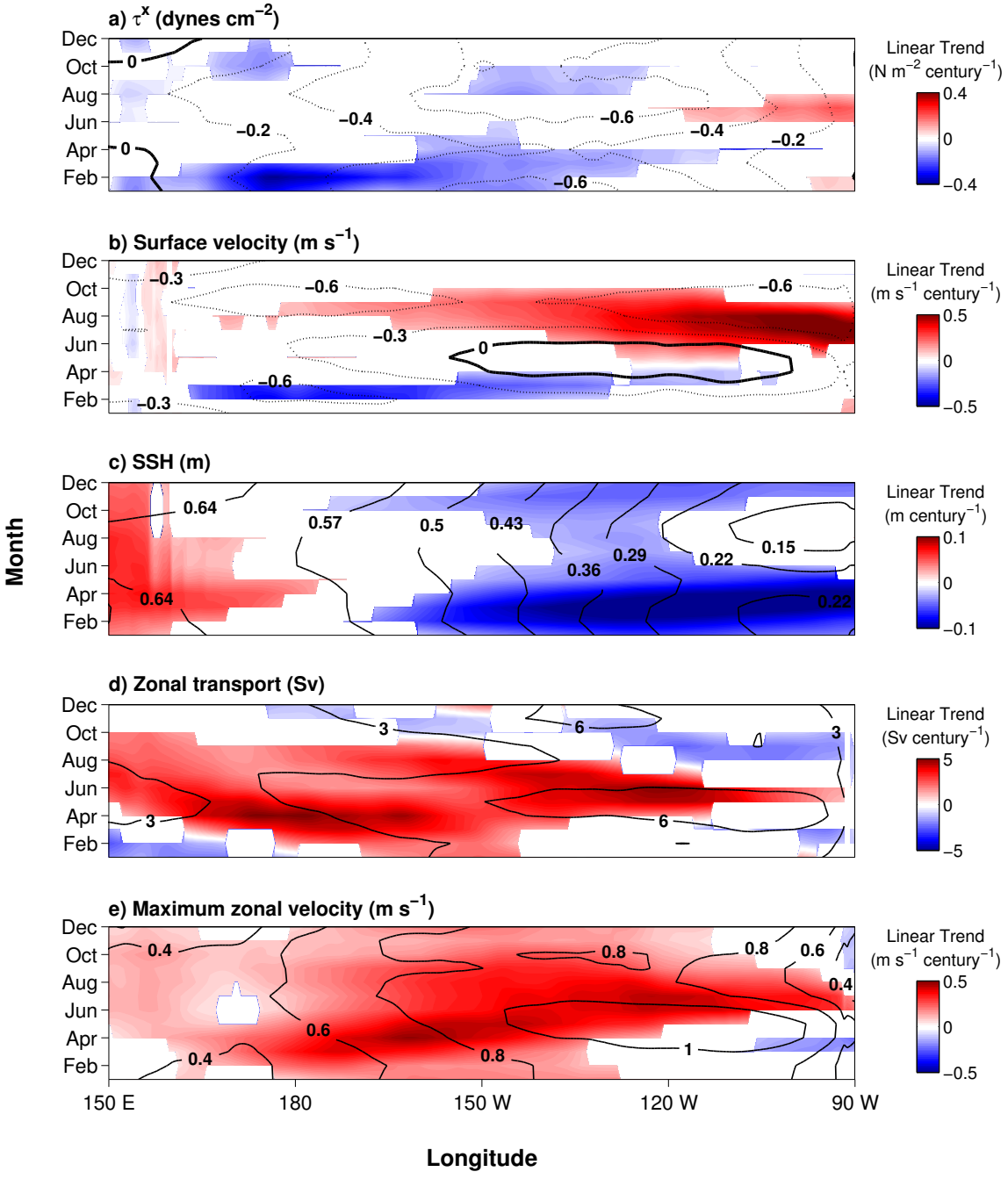

Figure 2-5: Hovmöller diagrams of significant (95% confidence interval) long-term trends (filled contours) and climatologies (black contours) for a) zonal wind stress, b) surface velocity, c) sea surface height, d) zonal transport and e) maximum zonal (i.e. EUC) velocity on the equator. The surface b) is defined as the top depth layer (~10 meter), while the transport c) domain extends through the top 20 depth layers in the SODA record (surface to ~640 meters) and maximum velocity e) is evaluated between 10 and 300 meters depth. Note the sign convention: positive (negative) contours indicate eastward/upward (westward/downward) average or trending movement. All long-term trends were calculated via linear regression with significance determined at the 95% confidence interval; regions where the long-term trends were not significant were masked out.

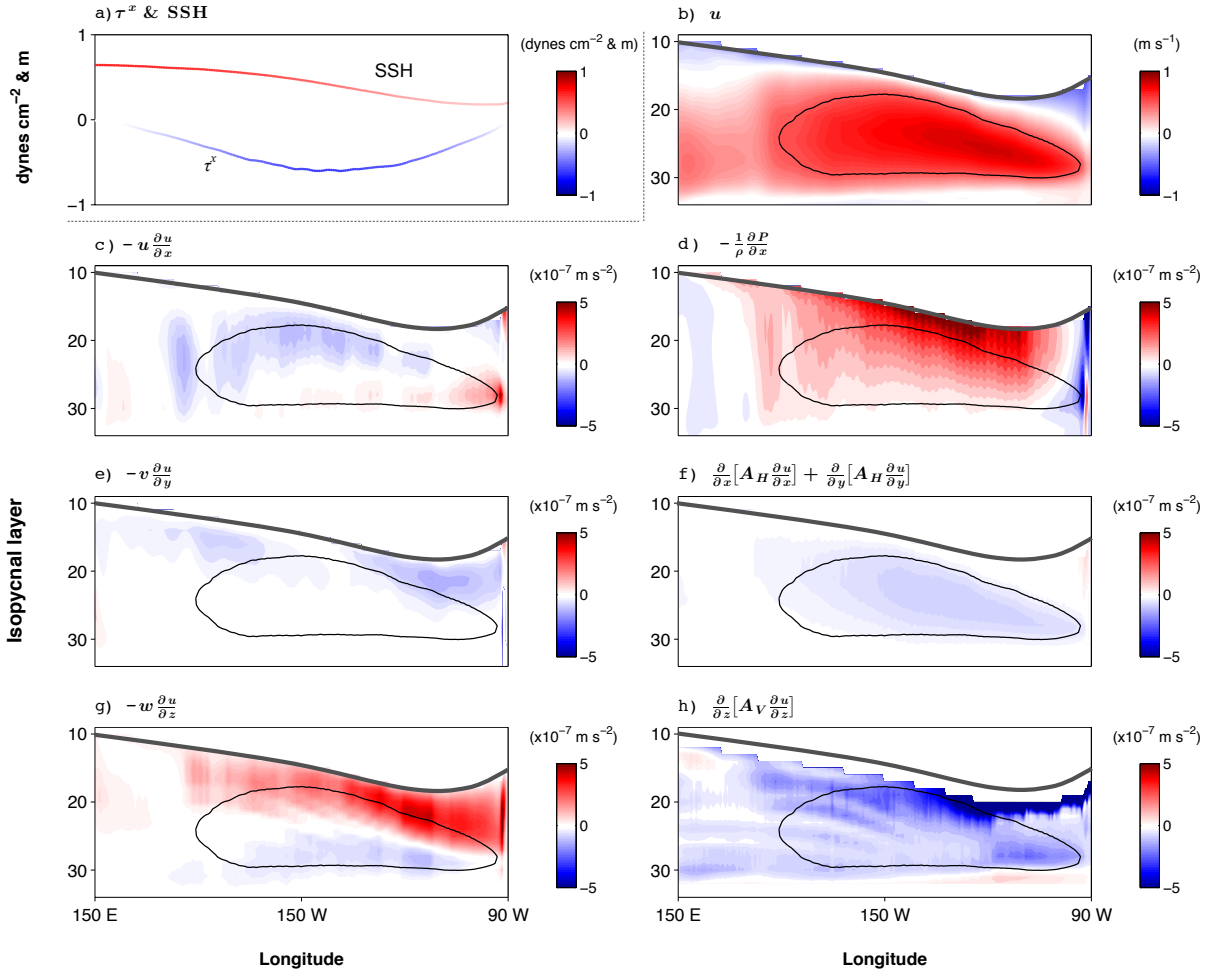

Figure 2-6: Diagrams of the equatorial mean state of a) zonal wind stress and sea surface height, b) zonal velocity and c-h) momentum budget terms. The line color in a) reiterates the y-axis and reflects the magnitude of the wind stress or sea surface height at a given longitude. b-h) are plotted on isopycnals where the solid gray line indicates the surface. The solid black contours are for spatial reference and indicate the region of .5 m s^{-1} zonal velocity in the SODA time-mean. Note the sign convention: positive (negative) contours indicate eastward (westward) movement or acceleration.

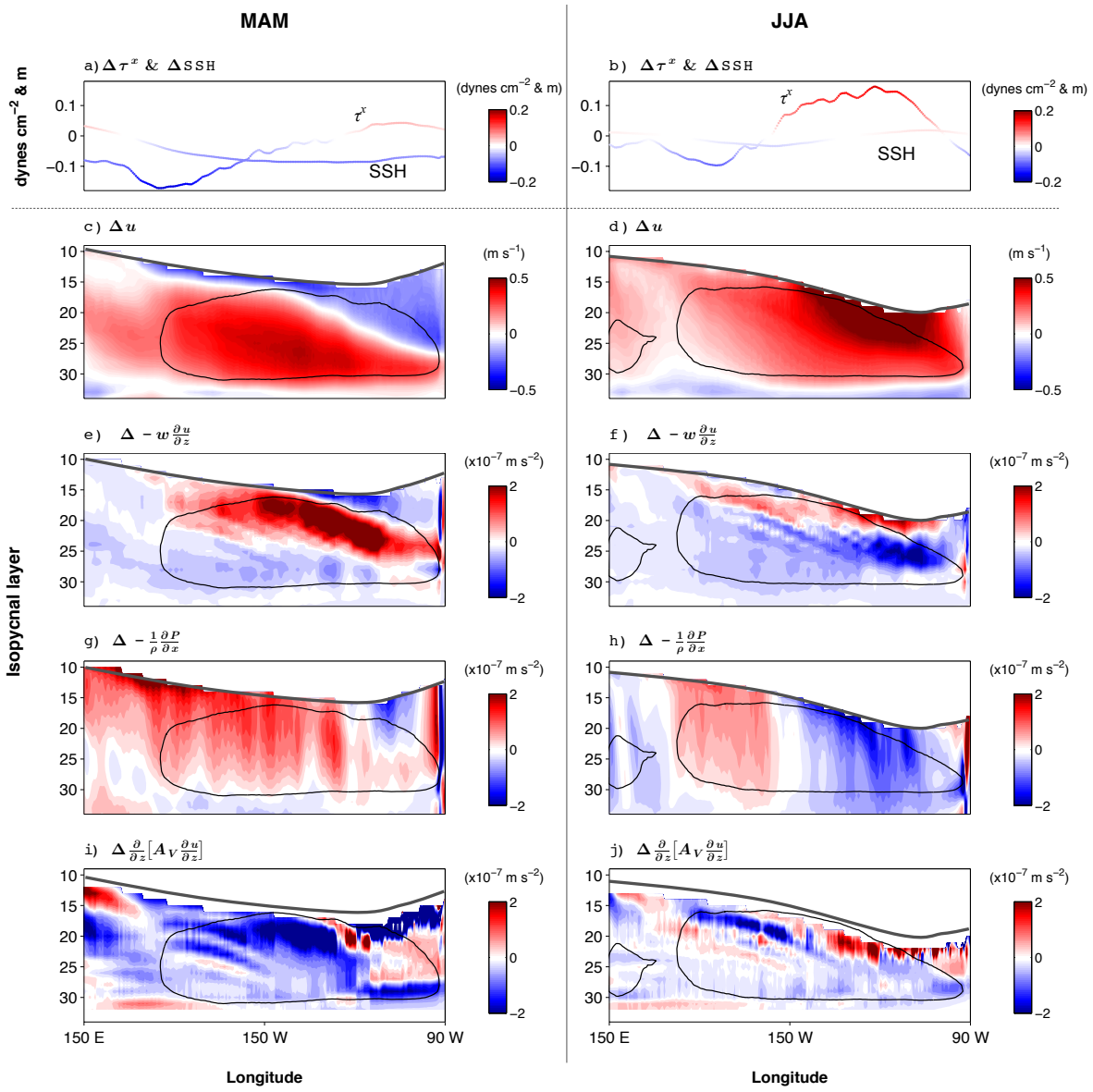

Figure 2-7: Differences between the 4th and 1st quarter of the SODA reanalysis, by season, for: a & b) zonal wind stress and sea surface height, c & d) zonal velocity and c-h) select momentum budget terms. The line color in a & b reflects the magnitude of the wind stress or sea surface height at a given longitude. c-h are plotted on isopycnals where the solid gray line indicates the surface. The solid black contours spatially reference the 4th quarter, time-mean region of 0.5 m s^{-1} zonal velocity during the respective seasonal subset (i.e. MAM or JJA). Note the sign convention: positive (negative) contours indicate eastward (westward) movement or acceleration.

Chapter 3

Calcification by juvenile corals under heterotrophy and elevated CO_2

3.1 Abstract

Ocean acidification (OA) threatens the existence of coral reefs by slowing the rate of calcium carbonate ($CaCO_3$) production of framework-building corals thus reducing the amount of $CaCO_3$ the reef can produce to counteract natural dissolution. Some evidence exists to suggest that elevated levels of dissolved inorganic nutrients can reduce the impact of OA on coral calcification. Here, we investigated the potential for enhanced energetic status of juvenile corals, achieved via heterotrophic feeding, to modulate the negative impact of OA on calcification. Larvae of the common Atlantic golf ball coral, *Favia fragum*, were collected and reared for 3 weeks under ambient (421 μatm) or significantly elevated (1,311 μatm) CO_2 conditions. The metamorphosed, zooxanthellate spat were either fed brine shrimp (i.e., received nutrition from photosynthesis plus heterotrophy) or not fed (i.e., primarily autotrophic). Regardless of CO_2 condition, the skeletons of fed corals exhibited accelerated development of septal cycles and were larger than those of unfed corals. At each CO_2 level, fed corals accreted more $CaCO_3$ than unfed corals, and fed corals reared under 1,311 μatm CO_2 accreted as much $CaCO_3$ as unfed corals reared under ambient CO_2. However, feeding did not alter the sensitivity of calcification to increased CO_2; Δcalcification/$\Delta\Omega$ was comparable for fed and unfed corals. Our results suggest that calcification rates of nutritionally replete juvenile corals will decline as OA intensifies over the course of this century. Critically, however, such corals could maintain higher rates of skeletal growth and $CaCO_3$ production under OA than those in nutritionally limited environments.

Drenkard EJ, Cohen AL, McCorkle DC, de Putron SJ, Starczak VR, Zicht AE. Calcification by juvenile corals under heterotrophy and elevated CO_2. *Coral Reefs* 32: 727-735 © 2013 Springer; Permissions License: 3475791406564

3.2 Introduction

The ocean has absorbed 25-30% of the CO_2 emitted by human activities, driving a 0.1 unit decline in surface ocean pH and a 30% decrease in carbonate ion concentration ($[CO_3^{2-}]$), a process known as ocean acidification (OA) (Caldeira & Wickett 2003; Feely *et al.* 2004). Scleractinian corals build skeletons of aragonite, a polymorph of calcium carbonate ($CaCO_3$), and rely on carbonate ions for calcification (Marubini & Atkinson 1999; Silverman et al. 2007; dePutron2011). The aragonite saturation state (Ωar, $[Ca^{2+}][CO_3^{2-}]/K_{sp(arag)}$) of seawater reflects the thermodynamic tendency for $CaCO_3$ to form (Ω >1) or dissolve (Ω <1). Although the tropical oceans where most coral reefs are located are not likely to become under saturated with respect to aragonite (Ωar <1) during this century, most experimental studies show that skeletal growth and $CaCO_3$ production by corals are negatively impacted by OA long before aragonite under saturation is reached. On the ecosystem scale, the relative rates of $CaCO_3$ production versus dissolution are critical for coral reefs. If rates of production fall below natural rates of erosion and dissolution, reefs will shift from net accreting to net dissolving structures (Orr *et al.* 2005; Silverman *et al.* 2009), diminishing their capacity to provide habitats for marine organisms and to function as effective barriers against waves and tsunamis. Using coral reef community calcification data from the Gulf of Aqaba, Silverman *et al.* (2009) predicted a global-scale shift from net accreting to net dissolving reefs within the next 60 yrs.

The impact of Ωar on calcification by reef organisms has been explored largely in laboratory manipulation experiments, although a handful of in situ datasets provide key insights into the sensitivity of ecosystem-scale calcification to rising CO_2 levels (e.g., silverman2007; Shamberger *et al.* 2011). In general, these studies have shown that both coral and coral reef calcification decline with decreasing Ωar (reviewed in Langdon *et al.* 2000; Hoegh-Guldberg *et al.* 2007; Fabry *et al.* 2008; Doney *et al.* 2009; Pandolfi *et al.* 2011), but there is considerable variability among populations, species, and studies in the calcification response or sensitivity at a given Ωar (summarized in Pandolfi *et al.* 2011). There is also variability in the absolute rates of calcification among different corals and coral reefs at the same Ωar (Shamberger *et al.* 2011). For example, flume incubations of Hawaiian *Porites compressa* and *Montipora verucosa* show a positive, linear relationship between Ωar and calcification

rate (mmol $CaCO_3$ m^{-2} h^{-1}) (Langdon and Atkinson 2005). However, de Putron et al. (2011) reported a nonlinear relationship between Ωar and calcification by Bermudan *Favia fragum* and *Porites asteroides* over a similar range of Ωar while Ries *et al.* (2010) found that *Oculina sp.* responded only at a treatment pCO_2 of 2,800 ppm (Ωar <1) and not at values of 900 ppm and below. On the scale of coral reef communities, different reef ecosystems at the same Ωar exhibit significant differences in the rate of net reef calcification. For example, the average net calcification rate of a Red Sea reef was reported as 54.5 mmol $CaCO_3$ m^{-2} h^{-1} at an average Ωar of 3.9 (Silverman *et al.* 2007), whereas average net calcification rate of the Kaneohe Bay barrier reef on Hawaii was significantly higher (264.2 mmol $CaCO_3$ m^{-2} h^{-1}) despite a significantly lower average Ωar (2.9) (Shamberger *et al.* 2011). Multiple environmental and biological factors that influence biogenic calcification on a coral reef could be invoked to explain the variability, but few have been directly tested.

Here, we conducted an experiment in which the nutritional status of zooxanthellate (photosynthesizing) juvenile corals, that were reared under very high and ambient pCO_2 was enhanced via heterotrophic feeding. A number of experimental and field studies have demonstrated (Langdon & Atkinson 2005; Holcomb *et al.* 2010) or suggested (Atkinson *et al.* 1995; (Atkinson & Cuet 2008; Cohen *et al.* 2009; Shamberger *et al.* 2011; Edmunds 2011) that elevated dissolved inorganic nutrients (DIN) and/or nutrition via heterotrophic feeding could reduce the impact of elevated CO_2 on calcification. We chose to manipulate heterotrophic feeding conditions because the addition of DIN to coral cultures under ambient CO_2 can lead to decreased calcification due to a proposed disruption in the coral-zooxanthellae symbiosis (Muscatine *et al.* 1989; Falkowski *et al.* 1993; Marubini & Davies 1996), whereas heterotrophic feeding tends to enhance calcification under ambient CO_2 conditions (Houlbrèque & Ferrier-Pagès 2009).

3.3 Materials and Methods

3.3.1 Experimental setup and conditions

This experiment was conducted at the Bermuda Institute of Ocean Sciences (BIOS) in St. George's, Bermuda. The experimental treatments were two CO_2 levels (high and ambient) and two feeding conditions (fed and unfed). The two pCO_2 levels were established

in static 5.5 gallon aquaria filled with serially filtered (50, 5 μm) seawater prior to the addition of metamorphosed larvae. These conditions were achieved and maintained by directly bubbling air (in the ambient condition) or CO_2-enriched air (high CO_2 treatment) through micropore bubble "wands" fixed horizontally approximately 5 cm from the base of each aquarium. A pair of Aalborg mass flow controllers maintained the CO_2 concentration of the enriched treatment. The resultant average calculated pCO_2 for ambient and high CO_2 conditions were 421 $\pm$ 35 and 1,311 $\pm$ 76 μatm (mean $\pm$ SD), respectively, with corresponding average Ωar of 3.66 $\pm$ 0.15 and 1.63 $\pm$ 0.08 (mean $\pm$ SD), respectively (Table 1). Ωar of our high CO_2 treatments is within range of average global surface ocean Ωar predicted by global climate models for the end of this century under the IPCC SRES A2 (Steinacher *et al.* 2009). Corals in fed treatments were isolated (every night for 2 weeks, every other night for the third week) for 3 h in 12.5 cm $\times$ 12.5 cm $\times$ 3 cm plastic containers filled with seawater from their respective treatment tanks and provided with 24-h-old Artemia nauplii (brine shrimp). Feeding took place at night, shortly after lights were switched off to mimic crepuscular feeding and temporal zooplankton abundance observed in local coral reef environments (Lewis & Price 1975). Unfed corals were not provided nauplii during the 3-week experiment and were not isolated in empty feeding containers.

Each CO_2-feeding treatment was conducted in triplicate for a total of twelve aquaria, and all treatments were kept on a 12/12 h light-dark cycle. Fluorescent aquarium lamps maintained maximum light levels of 62 $\pm$ 8 μmol quanta m^{-2} s^{-1} (mean $\pm$ SD), which were monitored using a LI-COR probe/meter assemblage. The compensation range for *F. fragum* spat on Bermuda is not yet known. We used the low end of known compensation ranges for corals (e.g. 3-233 μmol quanta m^{-2} s^{-1} as reported by Mass *et al.* 2007) for two reasons. The first was to ensure that corals under elevated CO_2 did not bleach (as experienced by Anthony *et al.* 2009, and the second was to minimize the potential for enhanced photosynthesis to overwhelm or inhibit the feeding-modulated calcification response to elevated CO_2. Aquarium temperatures were maintained by in-line chiller/heater systems and monitored every 15 min (Hobo temperature loggers, Onset Corp.). Average temperature for all treatments over the course of the experiment was 27.6 $\pm$ 0.1 °C ($\pm$ SD).

Aquarium water was replaced with filtered seawater every week to prevent the build-up of dissolved inorganic nitrogen and other wastes. Prior to removing water from the aquaria,

we collected discrete water samples for salinity, alkalinity (Alk), and dissolved inorganic carbon (DIC) from every aquarium. Salinity was measured at BIOS with an Autosal salinometer. The Alk/DIC samples were poisoned with mercuric chloride immediately after collection and analyzed using a Marianda VINDTA-3C analysis system at WHOI. Alkalinity was determined by nonlinear curve fitting of data obtained by open-cell titrations, and DIC concentrations were determined by coulometric analysis. Both measurements were standardized using certified reference materials obtained from Dr. A. Dickson (Scripps IO). The pH (NBS) of each tank was measured every 3-4 d (Orion pH meter and temperature-compensated electrode) to provide a real-time assessment of tank chemistry. Short-term variations in NBS pH were also assessed on a higher-resolution time scale: for one, 24-h period, by measuring pH in each aquarium at 3-h time intervals. The pH within each tank was maintained within a few hundredths of a pH unit on both sub-weekly and sub-daily time scales. The carbonate system parameters used to compare treatments (pCO_2, $[HCO_3^-]$, $[CO_3^{2-}]$, and Ωar) were calculated from the average temperature and discretely sampled salinity, Alk, and DIC data using the CO2SYS program (Lewis & Wallace 1998; Pelletier *et al.* 2007) with the constants of Mehrbach *et al.* (1973) as refit by Dickson & Millero (1987) (Table 1).

3.3.2 Coral collection, spawning, and larval settlement

In July 2010, approximately 1 week prior to anticipated peak larval release date (Goodbody-Gringley & de Putron 2009), we collected 30 mature colonies of the brooding coral, *F. fragum*, from the Bailey's Bay patch reefs off the northwest Bermudan coast at approximately three to seven meters water depth. Adult colonies were maintained in outdoor flow-through seawater aquaria at BIOS under ambient light and temperature conditions. Parent colonies were kept isolated in glass jars during planula release, which occurred over the course of 6 nights. The live zooxanthellate planulae were collected from all parents and pooled together. Ceramic tiles, approximately 9 cm^2, were left out on the reef for 2 months prior to the start of the experiment and further conditioned for larval settlement by scattering bits of freshly collected crustose coralline algae on the tiles. Immediately after collection, actively swimming larvae were transferred to small plastic tubs each containing ceramic tiles and filled with seawater preset to targeted CO_2 levels. The tubs had mesh

lids, allowing for water exchange, while they are submerged in the treatment aquaria. After 48 h, larvae had settled and metamorphosed into primary polyps (at this stage, larvae are "spat"). Spat on tiles were quickly counted, and tiles were pseudo-randomly distributed among the experimental aquaria so that each aquarium had approximately the same number of juvenile corals. Calcification was visible approximately 3 d after settlement. At the end of 3 weeks (±1 d), 20-50 primary polyps (including their primary corallite) per treatment were removed from the tiles and frozen at -80 °C for analysis of total lipid. Tiles were then removed from treatments and submerged in a 10% bleach solution for 1 h, which removed the polyp tissue from all of the remaining juvenile corals and exposed the calcified skeleton or primary corallite.

3.3.3 Quantification of skeletal development, size, and weight

Each bleached skeleton was digitally photographed, removed from the tile, and weighed using a Metro-Toledo micro-balance (Cohen *et al.* 2009; de Putron *et al.* 2011). Images of the spat were examined for skeletal development and size using Spot Imaging software. Length of the primary septa (present in all samples) was used to estimate corallite diameter (i.e., size). The septa are lateral $CaCO_3$ plates that corals accrete in cycles (Fig. 3-1). In our experiment, most spat accreted both primary and secondary septa; the tertiary septa were the last septal cycle accreted by any of the juvenile corals. Rate of skeletal development was defined as percent spat exhibiting tertiary septa, and a two-way ANOVA was used to test for differences in the mean proportion of spat with tertiary septa between the treatments. Feeding treatment and CO_2 level were fixed effects (Table A.5.1). Data were arc sin square root transformed to homogenize variances prior to analyses.

To test for differences in mean spat weight and diameter among treatments, a two-way, nested multivariate analysis of variance (MANOVA) was performed on natural log transformed weight data and square root transformed diameter data. Feeding treatment and CO_2 levels were fixed main effects, while tank effect was the random factor nested within feeding and CO_2 levels (Table A.5.2). Eight univariate F tests were conducted to test each of the dependent variables. A Bonferonni corrected alpha value of 0.0062 was used to declare significance of F statistics (Table A.5.3). It should be noted that the MANOVA only considers corals that have data for both diameter and weight. If part of a corallite is lost during

weighing or was attached to coralline algae, both coral size and weight were excluded from the MANOVA analyses. Likewise, if the skeleton was irregularly shaped (i.e., primary septa did not lie in a straight line), the data for those corals were not included. In order to account for any bias that may have resulted from corallite exclusion in the MANOVA, ANOVAs for the dependent variables, weight, and diameter were conducted. These tests considered all data for a given dependent variable to compare with the MANOVA's univariate results.

3.3.4 Quantification of total lipid and symbiont density

Ten individual spat from each aquarium were pooled per tissue lipid sample for quantification of total lipid by gravimetric analysis. Pooling was necessary due to the small size of the spat at 3 weeks. Extraction methods follow that of Folch *et al.* (1957) and Cantin *et al.* (2007).

Five individual spat from each aquarium were pooled per sample for quantification of symbiont density. Spat were homogenized, centrifuged and the resultant pellet was re-suspended in 250 μL filtered seawater. Symbionts from multiple (6-9) aliquot sub-samples of the slurry were counted on a known volume hemocytometer grid. Both total tissue lipid and symbiont counts were normalized to the circular area described by the average primary septa length (diameter) for a respective tank and then divided by the number of corals pooled in the sample (i.e., 10 or 5).

Both area-normalized lipid content and symbiont density were compared among levels of CO_2 and feeding conditions using two-way ANOVAs with tank as a random factor nested within the CO_2 and feeding combinations. Total lipid concentration was transformed to -1/x in order to homogenize the variances. All statistical analyses were conducted on SYSTAT.

3.4 Results

3.4.1 Skeletal development

A significantly higher mean percentage of fed spat accreted tertiary septa (i.e., exhibited a faster rate of development) than did unfed spat (two-way ANOVA $p < 0.001$; Table A.5.1), but the percentage with tertiary septa did not differ between ambient and high CO_2 nor was there a significant interaction between CO_2 and feeding (Fig. 3-2a; Table A.5.1).

3.4.2 Skeletal size and weight

Multivariate analysis (MANOVA) of both skeletal weight and diameter indicated that the effect due to CO_2 (ambient vs. high) and feeding treatments (fed vs. unfed) were both significant ($p < 0.001$; Table A.5.2), but the interaction between feeding and CO_2 was not significant. Univariate analyses of the effect of feeding indicate a significant impact on both corallite diameter and weight ($p < 0.001$; Table A.5.3): fed spat accreted larger and heavier skeletons. Likewise, CO_2 level significantly impacted corallite weight ($p < 0.001$; Table A.5.3): Skeletons accreted at ambient CO_2 were heavier than those raised under high CO_2 conditions for a given feeding regime. In contrast, the impact of CO_2 on skeletal diameter was not significant (Table A.5.3). The follow-up, independent ANOVAs for weight and diameter, conducted to account for potential bias due to corallite exclusion from the MANOVA, were consistent with the MANOVA's univariate results: Elevated CO_2 did not significantly impact the diameter (size) of the skeletons (Figs. 3-2a, 3-3a) but did impact skeletal weight (Figs. 3-2b, 3-3b).

3.4.3 Lipid and symbiont density

We did not detect statistically significant differences in area-normalized zooxanthellae density and total tissue lipid content between fed and unfed spat or between CO_2 treatments (Fig. 3-4a, b; Table A.5.4). There was significant variability among tanks, which reduced the power to detect differences between CO_2 and feeding treatments.

3.5 Discussion

Skeletal size and development, rate of $CaCO_3$ production, and energetic status (e.g., total lipid stores and metabolic performance) are key physiological indices of coral health and fitness. High growth rate contributes to juvenile coral survival and successful reef recruitment (Rylaarsdam 1983; Hughes & Jackson 1985; Vermeij & Sandin 2008). Linear extension affects a colony's ability to compete for space with algae and reduced skeletal density may affect the structural integrity of the coral holobiont (Hoegh-Guldberg *et al.* 2007). Further, energetic reserves have been used to model and predict coral colony mortality risk (Anthony *et al.* 2009). These parameters are sensitive to a number of environmental

stressors. For example, skeletal growth and calcification tend to decline in corals stressed by elevated temperatures (e.g., Rodrigues & Grottoli 2006; Cooper *et al.* 2008; Cantin *et al.* 2010) or eutrophication (Marubini & Atkinson 1999), and bleaching can result in rapid depletion of energetic reserves (e.g., Grottoli *et al.* 2004; Rodrigues & Grottoli 2007). Given anticipated (Kleypas *et al.* 1999) and experimentally observed (e.g., Langdon & Atkinson 2005) declines in coral calcification due to acidification, it has been suggested that OA may increase the energetic demands of $CaCO_3$ production (Cohen *et al.* 2009; Holcomb *et al.* 2010; Ries 2011).

In this study, OA induced by significantly elevated levels of CO_2 had no effect on the rate of development of septal cycles and skeletal diameter (size) nor could we detect a significant effect on area-normalized total tissue lipid content and symbiont density of juvenile corals reared from planulae larvae (Figs. 3-2, 3-4). Conversely, fed juveniles reared under elevated CO_2 conditions (~5 times preindustrial) exhibited faster tertiary septa development and had larger skeletons than unfed juveniles reared under ambient CO_2 levels (~1.5 times preindustrial). Thus, for newly settled corals of this species, OA may have little, if any, impact on lateral size and septal development, whereas factors that impact food availability or a coral's ability to acquire food could affect these aspects of postsettlement growth.

Heterotrophic feeding also significantly impacted the rate of $CaCO_3$ production (as measured by total corallite weight). Under both ambient and elevated CO_2 conditions, fed corals produced significantly more $CaCO_3$ over the 3-week experimental period than unfed corals (Fig. 3-2c). At 421 μatm CO_2 fed corals produced 55% more $CaCO_3$ than unfed corals; at 1,311 μatm CO_2 the difference was 68%. Thus, under significantly elevated CO_2 conditions, fed spat develop faster, grow bigger, and weigh more than unfed spat. This suggests that, to the extent that young corals affect the reef $CaCO_3$ budget, nutritionally enhanced juveniles contribute more $CaCO_3$ than those that are nutritionally restricted and subjected to the same CO_2 conditions. Remarkably, fed juveniles subjected to significantly elevated CO_2 also develop faster and grow larger than unfed corals reared under ambient CO_2 conditions, and their rate of $CaCO_3$ production are comparable. Therefore, by implication, nutritionally replete corals could perform better under OA than corals that are nutritionally restricted.

Nevertheless, our results indicate that feeding does not mitigate the impact of OA on

calcification by juvenile corals. In both fed and unfed groups, skeletal weight decreased, by 23.0 ± 2.9 and 28.9 ± 0.1%, respectively (~8-14% per unit drop in omega), under elevated CO_2. This change is equivalent to that observed by dePutron2011 for both acid addition and CO_2 manipulation experiments with the same *Favia* species, although it is significantly less than the 80% drop predicted by the Langdon and Atkinson model (2005).

A number of studies report increased calcification by corals under heterotrophic feeding (e.g., Houlbrèque & Ferrier-Pagès 2009), which is consistent with the observations in this study. However, our data show that the negative effect of OA on calcification persists under conditions of heterotrophic feeding. In our study, feeding did not change the sensitivity of calcification to OA. This suggests that nutritional enhancement via heterotrophic feeding did not change the mechanics of the calcification response to OA in our corals. Although Edmunds (2011) concluded that heterotrophic feeding does mitigate the impact of elevated CO_2 on juvenile *Porites* calcification, both the fed and unfed *Porites* corals in his experiment exhibited reduced biomass-corrected calcification under elevated CO_2, which is consistent with our result for *Favia*. Indeed, Edmunds' (2011) result lends support to our observation that the sensitivity of calcification response to elevated CO_2 is consistent between fed and unfed corals. In other words, heterotrophic feeding does not mitigate the effect of OA on coral calcification.

That heterotrophic feeding does not mitigate the impact of OA on juvenile coral differs from the results of Langdon & Atkinson (2005) and Holcomb *et al.* (2010) who reported significant modulation of the CO_2 effect with inorganic nutrient enrichment. In these studies, addition of ammonium, and of nitrates, phosphates, and iron, respectively, did reduce calcification sensitivity to OA. In the experiments of Langdon & Atkinson (2005), nutrient addition enhanced symbiont photosynthesis (photosynthesis was not measured in Holcomb *et al.* (2010). We were not able to detect a significant impact on area-normalized symbiont densities due to feeding in our experiments (Fig. 3-4b). This observation is different from that reported by a number of previous studies (Muscatine *et al.* 1989; Titlyanov *et al.* 2000a; Titlyanov *et al.* 2000b; Titlyanov *et al.* 2001; Houlbrèque *et al.* 2003; Houlbrèque *et al.* 2004) and may be due to our lack of statistical power to detect a significant feeding effect. Alternatively, although our corals were fully zooxanthellate at the time of settlement, the impact of feeding on symbiont densities might differ between young corals and

the mature colonies used in other experiments. Endosymbiont density is only one component of the coral holobiont's photosynthetic capacity and is not a substitute for direct measurements of photosynthesis (e.g., Langdon & Atkinson 2005) because the performance of individual symbionts is still unknown. Therefore, we can only speculate that the difference between our result (i.e., no significant difference detected in symbiont density or reduction in sensitivity to CO_2 due to feeding) and that of Langdon & Atkinson (2005), that is, DIN enrichment resulting in enhanced photosynthesis and reduced sensitivity to CO_2, suggest a role for symbiont photosynthesis in the coral calcification response to OA. From our data, it does not appear that simply enhancing coral energetic status (in this case, via feeding) alters calcification sensitivity to OA. However, photosynthesis and heterotrophy may impact coral calcification via different mechanisms. If this is the case, then the impact of OA on calcification when photosynthesis is enhanced might differ from the impact of OA on calcification when feeding is enhanced. Incidentally, it should be noted that the degree to which feeding impacted calcification rates in this study may be specific to our relatively low-light regime and test species and could therefore differ among organisms subjected to higher light environments.

Additionally, fast-growing, prereproductive juvenile corals might respond to feeding differently from adults, which were used in both the Langdon & Atkinson (2005) and Holcomb *et al.* (2010) experiments. Adult corals may allocate the extra energy from heterotrophic feeding differently from juveniles. To investigate whether our juvenile corals were storing the extra energy from heterotrophic feeding as lipid reserve, or using it to build new tissue or skeleton, we averaged total tissue lipid content over circular surface area (Fig. 3-4b). We could not detect a significant difference in the amount of lipid accumulated by the corals in the different feeding regimes. This suggests that, in this particular experiment, the fed coral spat did not store the extra energy acquired from feeding but rather used it for growth. Whether or not mature colonies in experimental conditions and on actual reefs respond to food availability the same way, that is, by investing in tissue growth rather than lipid storage, is yet to be tested.

Our results show that healthy, nutritionally replete spat of the Atlantic coral, *F. fragum*, can sustain high rates of calcification under significantly elevated CO_2. However, enhanced nutritional status does not render these corals immune to OA. This has important impli-

cations for the ability of corals and coral reefs to maintain levels of growth and $CaCO_3$ production required to sustain reef ecosystems through increasingly hostile conditions over the twentyfirst century.

3.6 Acknowledgements

The authors are grateful to Rebecca Belastock (WHOI) for DIC/Alk analyses. We also thank Ms. Hannah Barkley (WHOI), Ms. Kascia White (BIOS) and Mr. Mark Dowar (BIOS) for assistance with fieldwork and experiment maintenance, and Dr Neal Cantin (WHOI) for assistance with laboratory procedures. This project was funded by NSF OCE-1041106 and NSF OCE-1041052, a WHOI winter intern fellowship to A. Zicht made possible by the A. V. Davis Foundation and support from the MIT/WHOI Bermuda Biological Station for Research Fund. We thank the three anonymous reviewers and the editor for suggestions that greatly improved the manuscript.

3.7 References

Anthony KRN, Hoogenboom MO, Maynard JA, Grottoli AG, Middlebrook R (2009) Energetics approach to predicting mortality risk from environmental stress: a case study of coral bleaching. *Functional Ecology* 23: 539–550

Atkinson M, Carlson B, Crow G (1995) Coral growth in high-nutrient, low-pH seawater: a case study of corals cultured at the Waikiki Aquarium, Honolulu, Hawaii. *Coral Reefs* 14: 215–223

Atkinson MJ, Cuet P (2008) Possible effects of ocean acidification on coral reef biogeochemistry: topics for research. *Marine Ecology Progress Series* 373: 249–256

Caldeira K, Wickett ME (2003) Oceanography: Anthropogenic carbon and ocean pH. *Nature* 425: 365–365

Cantin NE, Negri AP, Willis BL (2007) Photoinhibition from chronic herbicide exposure reduces reproductive output of reef-building corals. *Marine Ecology Progress Series* 344: 81–93

Cantin NE, Cohen AL, Karnauskas KB, Tarrant AM, McCorkle DC (2010) Ocean Warming Slows Coral Growth in the Central Red Sea. *Science* 329: 322–325

Cohen AL, McCorkle DC, de Putron S, Gaetani GA, Rose KA (2009) Morphological and compositional changes in the skeletons of new coral recruits reared in acidified seawater: Insights into the biomineralization response to ocean acidification. *Geochemistry, Geophysics, Geosystems* 10: Q07 005

Cooper TF, De'ath G, Fabricius KE, Lough JM (2008) Declining coral calcification in massive Porites in two nearshore regions of the northern Great Barrier Reef. *Global Change Biology* 14: 529–538

Dickson A, Millero F (1987) A comparison of the equilibrium constants for the dissociation of carbonic acid in seawater media. *Deep Sea Research Part A Oceanographic Research Papers* 34: 1733 – 1743

Doney SC, Fabry VJ, Feely RA, Kleypas JA (2009) Ocean Acidification: The Other CO_2 Problem. *Annual Review of Marine Science* 1: 169–192, pMID: 21141034

Edmunds J Peter (2011) Zooplanktivory ameliorates the effects of ocean acidification on the reef coral *Porites spp. Limnology and Oceanography* 56: 2402–2410

Fabry VJ, Seibel BA, Feely RA, Orr JC (2008) Impacts of ocean acidification on marine fauna and ecosystem processes. *ICES Journal of Marine Science: Journal du Conseil* 65: 414–432

Falkowski PG, Dubinsky Z, Muscatine L, McCloskey L (1993) Population Control in Symbiotic Corals: Ammonium ions and organic materials maintain the density of zooxanthellae. *BioScience* 43: 606–611

Feely RA, Sabine CL, Lee K, Berelson W, Kleypas J, Fabry VJ, Millero FJ (2004) Impact of Anthropogenic CO_2 on the $CaCO_3$ System in the Oceans. *Science* 305: 362–366

Folch J, Lees M, Sloane Stanley GH (1957) A simple method for the isolation and purification of total lipides from animal tissues. *Journal of Biological Chemistry* 226: 497–509

Goodbody-Gringley G, de Putron SJ (2009) Planulation patterns of the brooding coral Favia fragum (Esper) in Bermuda. *Coral Reefs* 28: 959–963

Grottoli A, Rodrigues L, Juarez C (2004) Lipids and stable carbon isotopes in two species of Hawaiian corals, Porites compressa and Montipora verrucosa, following a bleaching event. *Marine Biology* 145: 621–631

Hoegh-Guldberg O, Mumby PJ, Hooten AJ, Steneck RS, Greenfield P, Gomez E, Harvell CD, Sale PF, Edwards AJ, Caldeira K, Knowlton N, Eakin CM, Iglesias-Prieto R, Muthiga N, Bradbury RH, Dubi A, Hatziolos ME (2007) Coral Reefs Under Rapid Climate Change and Ocean Acidification. *Science* 318: 1737–1742

Holcomb M, McCorkle DC, Cohen AL (2010) Long-term effects of nutrient and CO_2 enrichment on the temperate coral Astrangia poculata (Ellis and Solander, 1786). *Journal of Experimental Marine Biology and Ecology* 386: 27–33

Houlbrèque F, Ferrier-Pagès C (2009) Heterotrophy in Tropical Scleractinian Corals. *Biological Reviews* 84: 1–17

Houlbrèque F, Tambutté E, Ferrier-Pagès C (2003) Effect of zooplankton availability on the rates of photosynthesis, and tissue and skeletal growth in the scleractinian coral Stylophora pistillata. *Journal of Experimental Marine Biology and Ecology* 145–166

Houlbrèque F, Tambutté E, Allemand D, Ferrier-Pagès C (2004) Interactions between zooplankton feeding, photosynthesis and skeletal growth in the scleractinian coral *Stylophora pistillata*. *Journal of Experimental Biology* 207: 1461–1469

Hughes TP, Jackson JBC (1985) Population Dynamics and Life Histories of Foliaceous Corals. *Ecological Monographs* 55: 141–166

Kleypas JA, Buddemeier RW, Archer D, Gattuso JP, Langdon C, Opdyke BN (1999) Geochemical Consequences of Increased Atmospheric Carbon Dioxide on Coral Reefs. *Science* 284: 118–120

Langdon C, Atkinson MJ (2005) Effect of elevated pCO_2 on photosynthesis and calcification of corals and interactions with seasonal change in temperature/irradiance and nutrient enrichment. *Journal of Geophysical Research: Oceans* 110: C09S07

Langdon C, Takahashi T, Sweeney C, Chipman D, Goddard J, Marubini F, Aceves H, Barnett H, Atkinson MJ (2000) Effect of calcium carbonate saturation state on the calcification rate of an experimental coral reef. *Global Biogeochemical Cycles* 14: 639–654

Lewis E, Wallace DWR (1998) Program Developed for CO_2 System Calculations. ORNL/CDIAC-105, Carbon Dioxide Information Analysis Center Oak Ridge Natl Lab, US Dept of Energy, Oak Ridge, TN

Lewis JB, Price WS (1975) Feeding mechanisms and feeding strategies of Atlantic reef corals. *Journal of Zoology* 176: 527–544

Marubini F, Atkinson MJ (1999) Effects of lowered pH and elevated nitrate on coral calcification. *Marine Ecology Progress Series* 188: 117–121

Marubini F, Davies P (1996) Nitrate increases zooxanthellae population density and reduces skeletogenesis in corals. *Marine Biology* 127: 319–328

Mass T, Einbinder S, Brokovich E, Shashar N, Vago R, Erez J, Dubinsky Z (2007) Photoacclimation of Stylophora pistillata to light extremes: metabolism and calcification. *Marine Ecology Progress Series* 334: 93–102

Mehrbach C, Culberson CH, Haeley JE, Pytkowicz RM (1973) Measurement of apparent dissociation constants of carbonic acid in seawater at atmospheric pressure. *Limnology and Oceanography* 18: 897–907

Mucci A (1983) The solubility of calcite and aragonite in seawater at various salinities, temperatures, and one atmosphere total pressure. *American Journal of Science* 283: 780–799

Muscatine L, Falkowski PG, Dubinsky Z, Cook PA, McCloskey LR (1989) The Effect of External Nutrient Resources on the Population Dynamics of Zooxanthellae in a Reef Coral. *Proceedings of the Royal Society of London B Biological Sciences* 236: 311–324

Orr JC, Fabry VJ, Aumont O, Bopp L, Doney SC, Feely RA, Gnanadesikan A, Gruber N, Ishida A, Joos F, Key RM, Lindsay K, Maier-Reimer E, Matear R, Monfray P, Mouchet A, Najjar RG, Plattner GK, Rodgers KB, Sabine CL, Sarmiento JL, Schlitzer R, Slater RD, Totterdell IJ, Weirig MF, Yamanaka Y, Yool A (2005) Anthropogenic ocean acidification over the twenty-first century and its impact on calcifying organisms. *Nature* 437: 681–686

Pandolfi JM, Connolly SR, Marshall DJ, Cohen AL (2011) Projecting Coral Reef Futures Under Global Warming and Ocean Acidification. *Science* 333: 418–422

Pelletier G, Lewis E, Wallace DWR (2007) CO2sys.xls: A Calculator for the CO_2 System in Seawater for Microsoft Excel/VBA. Washington State Department of Ecology, Olympia, WA/ Brookhaven National Laboratory, Upton, NY, USA

de Putron S, McCorkle D, Cohen A, Dillon A (2011) The impact of seawater saturation state and bicarbonate ion concentration on calcification by new recruits of two Atlantic corals. *Coral Reefs* 30: 321–328

Ries J, Cohen A, McCorkle D (2010) A nonlinear calcification response to CO_2-induced ocean acidification by the coral Oculina arbuscula. *Coral Reefs* 29: 661–674

Ries JB (2011) A physicochemical framework for interpreting the biological calcification response to CO_2-induced ocean acidification. *Geochimica et Cosmochimica Acta* 75: 4053 – 4064

Rodrigues LJ, Grottoli A (2007) Energy reserves and metabolism as indicators of coral recovery from bleaching. *Limnology and Oceanography* 52: 1874–1882

Rodrigues LJ, Grottoli AG (2006) Calcification rate and the stable carbon, oxygen, and nitrogen isotopes in the skeleton, host tissue, and zooxanthellae of bleached and recovering Hawaiian corals. *Geochimica et Cosmochimica Acta* 70: 2781–2789

Rylaarsdam KW (1983) Life histories and abundance patterns of colonial corals on Jamaican reefs. *Marine Ecology Progress Series* 13: 249–260

Shamberger K, Feely R, Sabine C, Atkinson M, DeCarlo E, Mackenzie F, Drupp P, Butterfield D (2011) Calcification and organic production on a Hawaiian coral reef. *Marine Chemistry* 127: 64–75

Silverman J, Lazar B, Erez J (2007) Community metabolism of a coral reef exposed to naturally varying dissolved inorganic nutrient loads. *Biogeochemistry* 84: 67–82

Silverman J, Lazar B, Cao L, Caldeira K, Erez J (2009) Coral reefs may start dissolving when atmospheric CO_2 doubles. *Geophysical Research Letters* 36: L05 606

Steinacher M, Joos F, Frölicher TL, Plattner GK, Doney SC (2009) Imminent ocean acidification in the Arctic projected with the NCAR global coupled carbon cycle-climate model. *Biogeosciences* 6: 515–533

Titlyanov EA, Bil' K, Fomina I, Titlyanova TV, Leletkin VA, Eden N, Malkin A, Dubinsky Z (2000a) Effects of dissolved ammonium addition and host feeding with Artemia salina on photoacclimation of the hermatypic coral *Stylophora pistillata*. *Marine Biology* 137: 463–472

Titlyanov EA, Tsukahara J, Titlyanova TV, Leletkin VA, van Woesik R, Yamazato K (2000b) Zooxanthellae population density and physiological state of the coral *Stylophora pistillata* during starvation and osmotic shock. *Symbiosis* 303–322

Titlyanov EA, Titlyanova TV, Yamazato K, van Woesik R (2001) Photo-acclimation of the hermatypic coral *Stylophora pistillata* while subjected to either starvation or food provisioning. *Journal of Experimental Marine Biology and Ecology* 257: 163–181

Vermeij MJA, Sandin SA (2008) Density-dependent settlement and mortality structure the earliest life phases of a coral population. *Ecology* 89: 1994–2004

Treatment	Salinity (psu ± SD)	Alkalinity (μeq kg^{-1} ± SD)	DIC (μmol kg^{-1} ± SD)	pCO_2 (μatm ± SD)	pH (total ± SD)	$[HCO_3^-]$ (μmol kg^{-1} ± SD)	$[CO_3^{2-}]$ (μmol kg^{-1} ± SD)	Ωar (± SD)
Ambient CO_2, Fed	37.6 ± 0.3	2,332 ± 22	2,012 ± 33	443 ± 40	8.00 ± 0.03	1,775 ± 40	225 ± 9	3.55 ± 0.16
Ambient CO_2, Unfed	37.4 ± 0.3	2,325 ± 20	1,984 ± 16	398 ± 4	8.04 ± 0.00	1,735 ± 13	239 ± 3	3.77 ± 0.03
High CO_2, Fed	37.0 ± 0.2	2,324 ± 9	2,213 ± 16	1,344 ± 78	7.59 ± 0.02	2,077 ± 17	100 ± 4	1.59 ± 0.06
High CO_2, Unfed	37.0 ± 0.2	2,326 ± 23	2,207 ± 21	1,278 ± 70	7.61 ± 0.02	2,069 ± 20	105 ± 5	1.66 ± 0.08

Table 3.1: Average (± SD) seawater chemistry for given experimental treatment conditions. Average temperature (27.6 °C) and measured salinity, alkalinity, and DIC were used to calculate pCO_2, pH, $[HCO_3^-]$, $[CO_3^{2-}]$, and aragonite saturation state (Ωar) for each aquarium using CO2SYS (Lewis & Wallace 1998). We used Dickson & Millero (1987)'s dissociation constants from the refit of Mehrbach *et al.* (1973) and the aragonite solubility of Mucci (1983). We computed mean treatment condition from the average values of each treatment's three replicate tanks. One anomalous pair of alkalinity/DIC values from one aquarium was omitted from the calculations for the ambient, fed aquaria

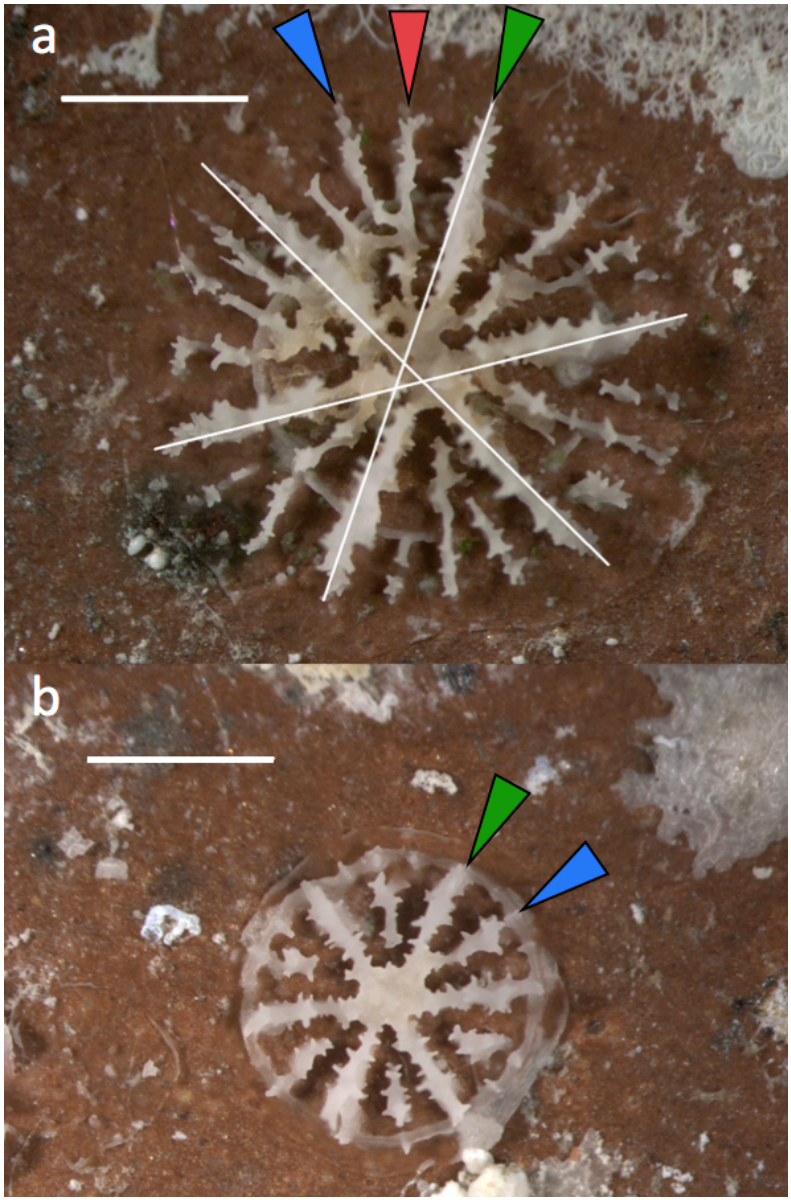

Figure 3-1: Three-week-old *F. fragum* corallites from (a) fed corals and (b) unfed corals in this study. In both images, the different septal stages are identified. Primary septa are indicated with green arrows, secondary with blue, and tertiary with red. White lines along the primary septa in (a) indicate corallite diameter used to determine lateral size. Scale bars are 1 mm

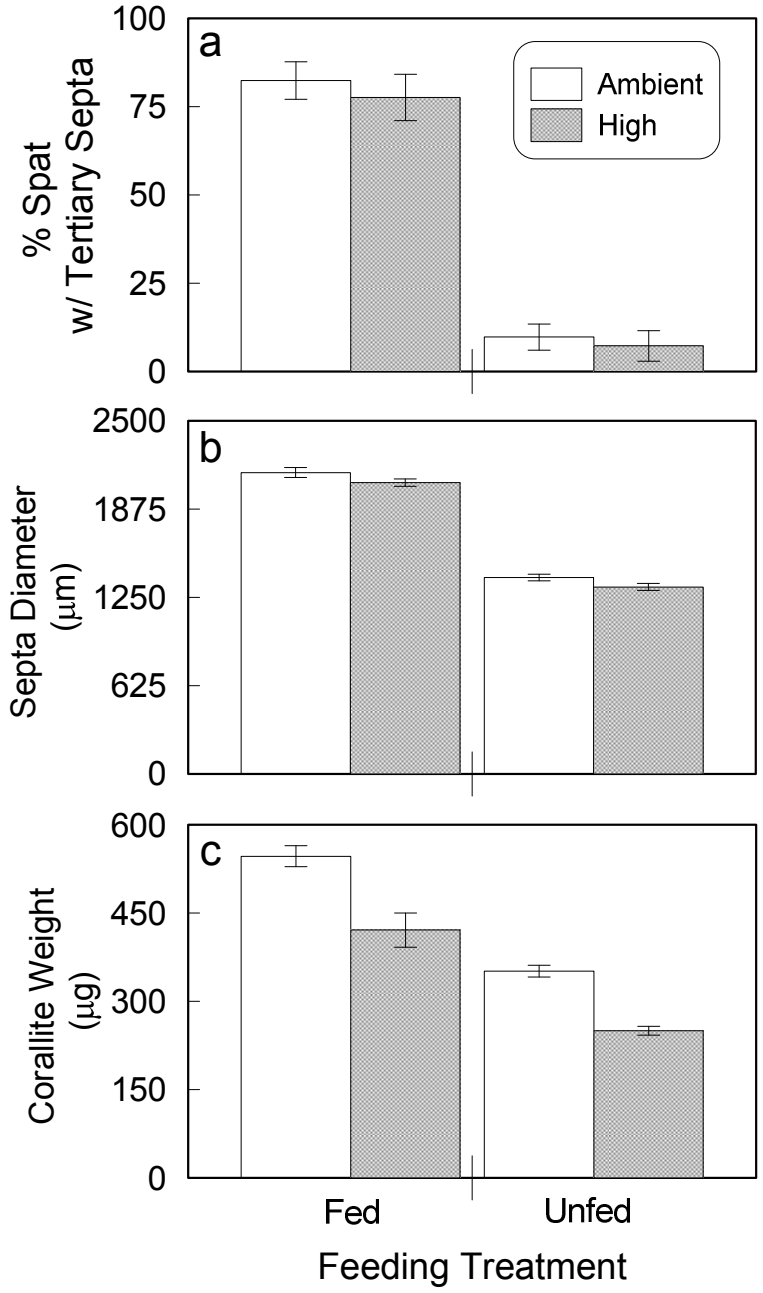

Figure 3-2: The percent of spat in a given treatment exhibiting tertiary septa (a), the diameter of primary septa (b), and the corallite weight (c) of fed and unfed spat. Bars indicate the average across three replicate tanks, which are themselves averaged across the number of samples for a given tank. Gray bars indicate high CO_2 and white bars indicate ambient CO_2 conditions. Error bars represent ± one standard error among replicate tanks

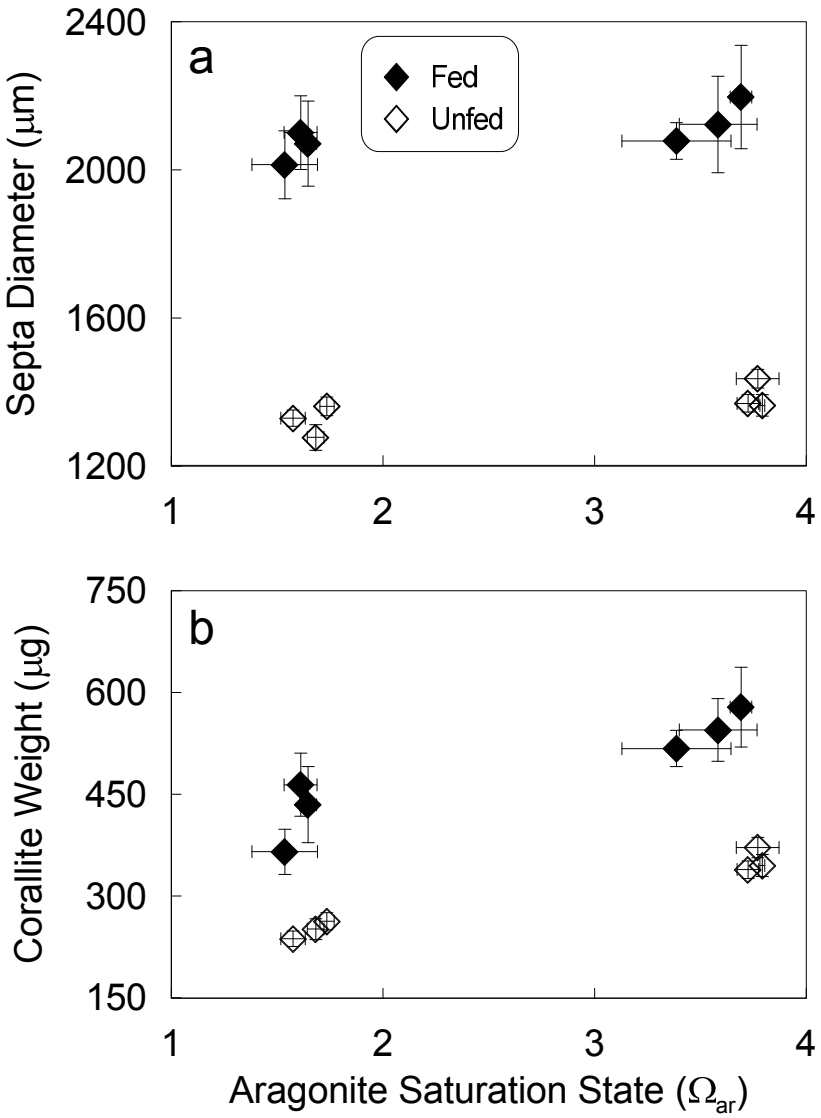

Figure 3-3: Corallite diameter (a) and total corallite weight (b) versus Ωar observed in fed (filled diamonds) and unfed (empty diamonds) corals. Error bars represent ± one standard error for replicate analyses of each tank

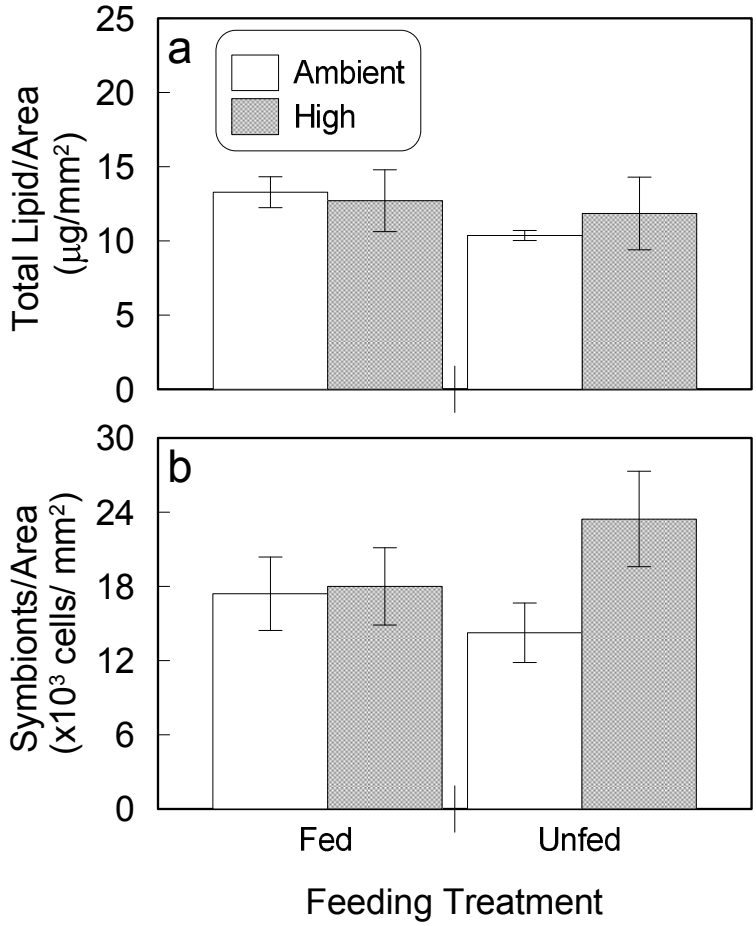

Figure 3-4: Area-normalized total tissue lipid weight per spat in fed and unfed corals. Bars indicate the average across three replicate tanks, which are themselves averaged across the number of samples for a given tank. Gray bars indicate high CO_2 and white bars indicate ambient CO_2 conditions. Error bars represent $\pm$ one standard error among replicate tanks. Although these plots depict the raw data from the experiment, the ANOVA was performed on the transformed data, which met the criteria for homogeneity of variance

Chapter 4

Calcification by juvenile corals under varied light and elevated CO_2

4.1 Abstract

Ocean acidification (OA) caused by rising levels of atmospheric carbon dioxide (CO_2) reduces the concentration of carbonate ions ($[CO_3{}^{2-}]$) in seawater. Multiple laboratory and field studies have shown that rates of calcification by reef-building corals decline when seawater $[CO_3{}^{2-}]$ decreases, raising concerns about the impact of OA on the future survival of coral reef ecosystems. Nevertheless, other studies show that the sensitivity of coral calcification to OA can be modulated by other factors. Specifically, elevated concentrations of dissolved inorganic nutrients (DIN) have been shown to reduce (Holcomb *et al.* 2010) or eliminate entirely (Langdon & Atkinson 2005) the impact of OA on calcification. Further, zooxanthellate corals receiving additional nourishment via heterotrophy can grow larger and produce as much $CaCO_3$ under significantly elevated CO_2 as conspecifics relying solely on autotrophy and reared under ambient CO_2 conditions (Drenkard *et al.* 2013).

Building on these results, we investigated the impact of light on coral calcification under OA conditions. In two separate experiments conducted over two consecutive years, we quantified total calcification, lipid content, zooxanthellate densities and photosynthetic pigments in juveniles of the Atlantic golf ball coral *Favia fragum*, reared under a range of CO_2 and light levels.

Experiment 1 was conducted in 2011 under higher light conditions (220 μmol quanta m^{-2} s^{-1}) across four levels of CO_2: ambient (420 ppm) and 1060, 1720, and 2660 ppm corresponding to Ωarvalues of 3.5, 2, 1.5 and 1.1 respectively. Corals were reared for 3 weeks post-recruitment and either fed with *Artemia* brine shrimp, or unfed. We found no statistically significant effect of CO_2 on calcification. Conversely, feeding had a significant effect on calcification with fed corals producing significantly more $CaCO_3$than unfed corals regardless of CO_2 treatment.

Experiment 2 was conducted in 2012 under higher (220 μmol quanta m^{-2} s^{-1}) and

lower (60 μmol quanta m^{-2} s^{-1}) light conditions and two CO_2 levels: ambient (430 ppm) and 1920 ppm, corresponding to Ωar values of 3.7 and 1.5 respectively. Corals were reared for two weeks postrecruitment and not fed. We found no effect of CO_2 or light level on calcification.

We combined these data with those generated in our previous (2010) experiment (Drenkard *et al.* 2013, Chapter 2) to compare daily calcification rates, total lipid content, zooxanthellate densities and photosynthetic pigments (chlorophyll *a* density) of unfed juveniles only, reared under ambient versus elevated CO_2 and light. This cross-year comparison revealed that corals reared under higher light levels had consistently lower chlorophyll a densities, higher total lipid content and reduced calcification sensitivity to elevated CO_2 compared with corals raised under lower light levels. That corals in higher light conditions have higher total lipid content is consistent with higher rates of zooxanthellate photosynthesis, and implies that the reduction in CO_2 sensitivity of corals under higher light conditions is linked to photosynthesis.

Our interpretation is consistent with previous studies that show enhancement of photosynthesis by elevated DIN reduces sensitivity of coral calcification to OA. Lack of sensitivity of total lipid to elevated CO_2 argues against a simple energetics explanation. Conversely, heterotrophic feeding produces larger, heavier corallites (this study), but does not reduce sensitivity to OA (Drenkard *et al.* 2013). That fed corals are as sensitive to OA as unfed corals also argues against a simple energetics explanation. While the mechanism(s) by which enhanced heterotrophy and enhanced autotrophy modulate the impact of OA on coral calcification remain unclear, our results indicate that corals in nutritionally replete and/or optimal light environments will likely fare better under 21^{st} century ocean acidification than those in oligotrophic and/or low light environments.

4.2 Introduction

Ocean acidification (OA), caused by ocean absorption of atmospheric CO_2, shifts the balance of dissolved inorganic carbon (DIC) species in seawater, resulting in a reduction in the concentration of carbonate ions. Scleractinian corals utilize carbonate ions to produce aragonite (a polymorph of calcium carbonate; $CaCO_3$) skeletons that serve as both the structural scaffolding and an important source of $CaCO_3$ for coral reef ecosystems. The thermodynamic tendency for spontaneous nucleation and growth of aragonite is described by the saturation state (Ωar, $[Ca^{2+}][{CO_3}^{2-}]/K_{sp(arag)}$), with net $CaCO_3$ dissolution occurring when seawater is under saturated (i.e., $\Omega < 1$). However, overwhelming experimental and field evidence indicate that coral calcification is adversely affected by declining Ωar well before seawater conditions reach undersaturation (e.g., Gattuso *et al.* 1998, reviewed in Langdon *et al.* 2000, Hoegh-Guldberg *et al.* 2007, Fabry *et al.* 2008, Doney *et al.* 2009, Pandolfi *et al.* 2011). Nevertheless, there is considerable variability among experiments regarding the level of CO_2 at which Ωar begins to affect calcification (summarized in Pandolfi et al. 2011), the degree of calcification sensitivity to OA (e.g., Langdon & Atkinson 2005), and, among field studies, differences in calcification rates among organisms and ecosystems under similar Ωar conditions as well as differences in the extrapolated/ projected Ωar at which these systems will transition to states of net $CaCO_3$ dissolution (e.g., Silverman *et al.* 2007 vs. Shamberger *et al.* 2011; Fabricius *et al.* 2011 vs. Shamberger *et al.* 2014).

Recent studies suggest that coral nutrition and energetic status may contribute to these inconsistencies in coral calcification response to OA (e.g., Cohen & Holcomb 2009, Ries *et al.* 2009, Holcomb *et al.* 2010, Edmunds 2011, Rodolfo-Metalpa *et al.* 2011, Holcomb *et al.* 2012, Drenkard *et al.* 2013). Calcification is generally considered a metabolically costly process, although the cost of calcification as a percent of the coral's energy budget remains unknown. For instance, molecular evidence, which demonstrates the presence of ATPase Ca^{2+}-H^+ pumps within the tissue layer that interfaces with the calcifying space (Zoccola *et al.* 2004), supports the hypothesis that corals actively invest energetic resources to remove protons from the calcifying fluid, effectively raising the pH, Ωar, and increasing aragonite precipitation (McConnaughey & Whelan 1997, Cohen & McConnaughey 2003). Corals obtain the nutrition they would need to fuel this process both by consuming the

photosynthate produced by, and transferred from their algal endosymbionts (i.e., zooxanthellae), and through heterotrophic feeding. Other active mechanisms have also been invoked to explain corals' accelerated $CaCO_3$ precipitation (e.g., discussed in Chalker & Taylor 1975) and numerous studies show that corals can produce more $CaCO_3$ when maintained under elevate nutritional conditions such as sufficient levels of photosynthetically available radiation (PAR) and heterotrophic feeding (e.g., reviewed in Gattuso *et al.* 1999, Ferrier-Pagès *et al.* 2011).

Thus it has been proposed that the elevated nutritional or energetic status of the coral host may mitigate the calcification response to OA (e.g., Atkinson *et al.* 1995; Atkinson & Cuet 2008; Cohen & Holcomb 2009). Several studies employing different forms of nutritional enhancement have been conducted. In general, corals reared under elevated CO_2 combined with elevated levels of inorganic nutrients (Langdon & Atkinson 2005, Holcomb *et al.* 2010) and PAR (Suggett *et al.* 2013, Chan & Connolly 2013) exhibited reduced sensitivity to CO_2. Conversely, in feeding experiments, fed corals produce more $CaCO_3$ than unfed corals but exhibit similar sensitivity to CO_2 (Edmunds 2011, Drenkard *et al.* 2013).

Here we present our results from two experiments in which we manipulated the nutritional status of juvenile zooxanthellate corals reared under ambient and elevated CO_2 conditions. The goal of these experiments was to investigate further the role of nutrition in modulating the calcification response to OA. In these experiments, the nutritional or energetic status of the coral host was manipulated in two ways, by heterotrophic feeding and by elevating light levels in order to stimulate photosynthesis. First, we describe the results of the two experiments conducted in two different years (2011, 2012). We also present new chlorophyll *a* data from the 2010 experiment (Chapter 1) We then combine the results of both experiments with those of the 2010 experiment to investigate the role of light in the coral calcification response to OA.

4.3 Materials and Methods

4.3.1 Experimental setup and conditions

We conducted two experiments at the Bermuda Institute of Ocean Sciences (BIOS) in St. George's, Bermuda during the summers of 2011 and 2012 in which juvenile corals

were reared from settlement (~24 hrs post-release) over a range of CO_2 and light levels. Aquarium maintenance and the methods used to achieve desired CO_2 levels are identical to those reported in Drenkard *et al.* (2013). We regularly monitored the CO_2 concentration of the ambient and CO_2-enriched air that was bubbled into the tanks using a Qubit infrared CO_2 analyzer.

All tanks were maintained on a 12/12 h light-dark cycle using the same low/high output fluorescent aquarium lamps for all three experiments; PAR was measured with a LI-COR probe/meter. In order to maintain consistent aquarium temperatures, all tanks were placed in water baths, which were thermally regulated by in-line chiller/heater systems and individual aquarium temperatures were recorded at 15-minute intervals using HOBO temperature loggers (Onset Corp.); average treatment temperatures are reported in Table 4.1.

Prior to weekly water replacements (performed to prevent excessive accumulation of nitrogenous and other waste products), we collected discrete samples for salinity, alkalinity (Alk), dissolved inorganic carbon (DIC), and dissolved inorganic nitrogen and phosphorous from each aquarium. Salinity samples were analyzed at BIOS (Autosal salinometer) and Alk/DIC samples, which were poisoned with mercuric chloride during collection, were analyzed at WHOI (Marianda VINDTA-3C system); the specific analytical methods to determine these values and calculations for carbonate system parameters ($[HCO_3^-]$, $[CO_3^{2-}]$, and Ωar; reported in Table 4.1) are the same as in Drenkard *et al.* (2013). The nutrient samples for these two experiments and the previous 2010 experiment were analyzed at the WHOI Nutrient Analytical Facility and the results are reported in Table 4.2.

Conditions Specific to 2011 Experiment

The partial pressure (mean ± SD) of the four CO_2 levels bubbled into the experimental tanks were 420 ± 10 ppm, 1060 ± 10 ppm, 1720 ± 90 ppm, and 2660 ± 30 ppm (Table 4.1). Each CO_2-feeding treatment was conducted in triplicate, for a total of 24 aquaria. Crepuscular feeding schedule follows that outlined for our 2010 experiment (Drenkard et al. 2013). Average PAR was 215 ± 21 μmol quanta m^{-2} s^{-1} (mean ± SD); the experiment was conducted for three weeks.

Conditions Specific to 2012 Experiment

The two pCO_2 conditions were 430 ± 20 ppm and 1920 ± 20 ppm for the ambient and high CO_2 treatments respectively (Table 4.1). It is important to note that although the Qubit measurements differed considerably between experiments, these values indicate approximate CO_2 concentration of the gas bubbled through the tanks and often higher than the equilibrated value achieved in treatment tanks. Indeed, the saturation state levels achieved for high and ambient CO_2 tanks were generally comparable across experimental year (Table 4.1). The averaged PAR for the low and higher light conditions were 38 ± 5 and 227 ± 19 μmol quanta m^{-2} s^{-1} (mean ± SD) respectively and there were four replicates for each CO_2-light treatment for a total of 16 aquaria. The experiment was conducted for two weeks.

4.3.2 Coral collection, spawning and larval settlement

Each year, we collected mature colonies of the Atlantic brooding coral, *F. fragum* from the Bailey's Bay patch reefs off the northwest Bermudan coast in early July, approximately one week prior to anticipated peak larval release date (Goodbody-Gringley & de Putron 2009). These colonies were kept in outdoor flow-through seawater aquaria where they were exposed to ambient light and temperature conditions. During larval release, parent colonies were isolated in glass jars in order to keep released planulae contained; all zooxanthellate planulae spawned on a given day where pooled together for settlement.

For both experiments, we followed the settlement and sampling procedures explicitly outlined in Drenkard *et al.* (2013): collected larvae were settled on reef-conditioned terra-cotta tiles in seawater that was at pre-established CO_2 treatment levels. Following a 48-hour settlement period, tiles with metamorphosed larvae (referred to as "spat") were allocated to experimental tanks such that each aquarium contained approximately the same number of juvenile corals.

At the experiments' conclusions, we collected (i.e. removed from the tiles) primary polyps for various soft tissue analyses, including total lipid (10 spat per sample), symbiont density (1 spat per sample), and pigment (5 spat per sample). Samples collected for total lipid and symbiont densities were frozen at -80 °C and -20 °C respectively. The samples used

for pigment (specifically chlorophyll) analysis were originally intended for genetic studies and thus frozen at - 20 °C in RNAlater (QIAGEN). Although this is not the preferred method for storing pigment samples, samples from all years were subjected to the same storage conditions. Therefore, while the exact value for pigment densities may be underestimates, the relative comparisons among treatment conditions are informative. Tiles with corals remaining were placed in 10% bleach/ seawater solution in order to remove the tissue, thus exposing the primary corallite for skeletal analyses.

4.3.3 Quantification and analysis of skeletal size and weight

Skeletal parameters were measured following the methods in Drenkard *et al.* (2013), with corallite size defined as the primary septa (i.e., $CaCO_3$plates extending radial from the coral) diameter, and skeletal weight being the total corallite $CaCO_3$mass. All statistical analyses were performed using MYSTAT® (Systat Software, Inc. Chicago, IL, USA). A t-test was conducted in order to test for the effect due experimental year (i.e., differences in experimental duration; 2wks vs. 3wks) between unfed 2011 and 2012 corals.

In order to compare skeletal weight data within and across experiments, each coral was age-normalized by the number of days it was subjected to experimental conditions. Additionally, given the strong correlation between corallite size and weight ($R^2 = 0.89$; Fig.1), average age-normalized skeletal weight for a given tank was normalized by the average septal diameter for that tank (treatment tank is the lowest common denominator for these data because we were not able to obtain skeletal weight data for every corallite for which we had a size measurement and vice versa). Bonferonni corrected alpha values of 0.0071 and 0.0014 were used to declare F statistic significance with 95% and 99% confidence, respectively (Appendix B.9).

2011 Skeletal Analyses

We conducted two, two-way ANOVAs to test for the effect of CO_2 and feeding on 1) skeletal size and 2) age- and size-normalized skeletal weight.

2012 Skeletal Analyses

We conducted two, two-way ANOVAs to test for the effect of CO_2 and light on 1) skeletal size and 2) age- and size-normalized skeletal weight.

Inter-year Skeletal Analyses

In order to compare experimental results from different experimental years but under similar light regimes, we conducted two, two-way ANOVAs testing for the effect of CO_2 and experimental year on age- and size-normalized skeletal weight. These comparisons considered only unfed corals corals reared under HL (2011/2012) or LL (2010/2012) conditions (Fig. 4-5).

4.3.4 Quantification and analysis of total lipid, symbiont, and chlorophyll density

We use coral total tissue lipid as an indicator of stored energetic reserves available to the organism to withstanding environmental stressors (i.e., OA), and symbiont and chlorophyll density as a measure of the coral host's potential to utilize light as a form of nutrition. As in Drenkard *et al.* (2013), we followed the extraction methods outlined by Folch *et al.* (1957) and Cantin *et al.* (2007) for gravimetric quantification of total lipid content, and extracted coral symbionts via homogenization, centrifugation and re-suspension in order to conduct counts on a known-volume hemocytometer grid. Samples for chlorophyll analysis were homogenized and sonicated in 100% Methanol in order to release pigments. These samples were spiked with canthaxanthin standard in order to track and adjust for pigment decay/loss. These samples were analyzed using HPLC techniques outlined in Wright *et al.* (1991) with results in units of ng of chlorophyll *a*. We assumed that chlorophyll *a* degradation products resulted from the preservation process. This is based on the fact that a set of coral samples from the 2010 experiment were flash frozen and exhibited no detectable amount of pheophytin or chlorophyll *a* degradation products (data not shown). Therefore, we corrected and included these degradation product concentrations in the total reported amount of chlorophyll *a*.

Data for tissue lipid, symbiont counts, and chlorophyll mass were age-adjusted based on

the average number of days each coral in the pooled sample was subjected to experimental conditions, and then normalized to the circular area defined by the average primary septa length (diameter) for a respective tank. It should be noted that tissue date, unlike skeletal weight data, were area-normalized because, unlike the $CaCO_3$ in these juvenile corals' skeletons, which is concentrated in the septa, the coral's tissue is distributed over the entire area of the corallite. Only the 2012 samples were analyzed in the full complement of treatment conditions; a subset of the 2010 and 2011 samples (unfed corals) are presented for comparison to 2012 results.

2012 Tissue Analyses

We conducted three, two-way ANOVAs to test for the effect due to CO_2 and light on area and age-normalized tissue lipid content, zooxanthellae densities and chlorophyll *a* concentrations. Age- and area- normalizes total lipid was transformed to -1/x to homogenize variances.

Inter-year Tissue Analyses

We conducted two, two-way ANOVAs to test for the effect of CO_2 and experimental year on each tissue parameter: Age- and area- normalized tissue lipid, symbiont density and chlorophyll content. Bonferonni corrected alpha values of 0.0083 and 0.0017 were used to declare significance of F-statistics with the 95% and 99% confidence, respectively (Appendix B.9).

To further investigate the role of light-stimulated photosynthesis on the organic host-symbiont holobiont, we conducted inter-year comparisons, similar to those for skeletal weight, for total tissue lipid, and symbiont and chlorophyll densities.

4.4 Results

4.4.1 Skeletal Size and Weight

2011 Results

Fed corals were significantly ($p < 0.01$) larger and produced significantly ($p < 0.05$) more $CaCO_3$ than their unfed counterparts; there was no detectable effect due to CO_2 or

the interaction between CO_2 and feeding on skeletal size or weight (Fig 4-2a & 4-3a).

2012 Results

Among 2012 samples, there was no significant effect due to CO_2 light, or the interaction between these two factors on either skeletal size or weight (Figs.4-2b & 4-3b). Unfed corals from the 2-wk experiment were significantly ($p < 0.01$) smaller in size than unfed corals from the 3-wk experiment conducted in 2011 (Fig. 4-1a & 4-1b).

Inter-year Comparison Results

Age-and size-normalized skeletal weight show a significant effect due to CO_2 ($p < 0.05$)and experimental year ($p < 0.05$) under LL conditions (2010/ 2012 comparison) but not under HL conditions (2011/2012 comparison; Fig. 4-5b & 4-5d).

4.4.2 Lipid, symbiont and pigment density

2012 Results

Corals reared under HL conditions exhibited significantly higher ($p < 0.01$; Fig. 4-4a) age-normalized total tissue lipid densities and significantly less ($p < 0.05$; Fig. 4-4c) chlorophyll *a* than corals under LL conditions, regardless of CO_2 level; We did not detect a significant effect due to light on age-normalized symbiont densities (Fig. 4-4b), nor were there significant effects due to CO_2 or the interaction between light and CO_2 on lipid, symbiont or pigment density (Fig. 4-4).

Inter-year Comparison Results

We did not detect significant effects due to CO_2 or experimental year on age and size-normalized total lipid content, symbiont density or chlorophyll *a* content under LL (2010/ 2012 comparison) or HL (2011/2012 comparison) conditions (Figs. 4-6, 4-7, 4-8).

4.5 Discussion

In this study, we assessed the calcification, stored energetic reserves and the capacity to acquire nutrition via symbiont photosynthesis of recently settled *F. fragum* corals, which we

subjected to various levels of CO_2 and nutritional enhancement via heterotrophic feeding and light. These results, in comparison with those reported in studies such as Langdon & Atkinson (2005), Holcomb *et al.* (2010), and Drenkard *et al.* (2013) help us better understand the mechanism(s) by which nutrition may impact coral calcification response to OA:

Comparable to the septa diameter data reported by Drenkard *et al.* (2013), heterotrophic feeding appears to be the dominant driver of corallite size among 2011 corals, with no significant effect due to CO_2 in either 2011 or 2012 experiments (Fig. 4-3). Therefore, we similarly surmise that OA may have little impact on coral tissue extent, which we assume drives lateral corallite size (i.e., the larger the area covered by calcifying tissue, the larger the diameter of the accreted corallite; Davies 1984. However, unfed HL corals in the 2012 experiment were not significantly larger than LL corals, indicating that nutritional enhancement via light differs metabolically from heterotrophic feeding. This conclusion is consistent with Davies (1984) hypothesis that, although symbiont photosynthesis may provide the coral with considerable metabolic fuel, this carbon-rich "junk food" (Falkowski *et al.* 1984) may not provide sufficient structural materials (i.e., fixed nitrogen) for significantly increasing coral biomass.

With regards to total skeletal weight, Drenkard *et al.* (2013) propose that fed corals produce more $CaCO_3$ due to their larger biomass and larger area over which $CaCO_3$ is accreted. Despite being normalized for lateral size, 2011 fed corals are still significantly heavier than unfed corals, which may indicate a feeding effect on the actual calcification mechanism. However, given the somewhat consistent offset between fed and unfed corals (Fig. 4-2a), it may reflect the discrepancy in vertical size between feeding groups. Unlike fed corals in Drenkard *et al.* (2013) , we were not able to detect a significant effect due to CO_2 among corals in the 2011, HL experiment, which suggests that light availability may influence coral response to OA. However, we were also not able to detect a statistically significant effect due to light or CO_2 in the 2012 LL skeletal weight data (Fig. 4-3b), which contradicts the results in Drenkard *et al.* (2013) and may be due to the shorter experimental duration (i.e., only 2 weeks in 2012 instead of 3 weeks in 2010).

That corals reared under LL conditions (2010/ 2012 comparison, Fig. 4-5a & 4-5c) but not under HL conditions (2011/2012 comparison, Fig 4-5b & 4-5d) exhibit a significant

effect due to CO_2 supports the hypothesis that light can reduce calcification sensitivity to OA. This is similar to the findings presented by Suggett *et al.* (2013) and is consistent with results from Holcomb *et al.* (2010) and Langdon & Atkinson (2005) wherein nutritional enhancement via inorganic nutrients reduces the difference in calcification rate between corals under ambient and high CO_2 conditions. However, as in the nutrient enrichment studies, the reduction in CO_2 sensitivity among 2011 relative to 2010 corals (Fig. 4-5a vs. 4-5b) appears to be due more to a decrease in coral calcification under ambient CO_2 rather than an increase under high CO_2 relative to their LL counterparts. These results may be explained largely by the role of light and its ability to stimulate symbiont photosynthesis: Marubini & Davies (1996) hypothesize that observed reductions in calcification under ambient CO_2 and elevated nutrients may be due to endogenous DIC limitation, wherein nutrient-enhanced photosynthesis consumes intercellular/respiratory CO_2 reducing the amount of carbon available for calcification. OA would thus mitigate this DIC limitation because there would be sufficient carbon available to support both processes (Holcomb *et al.* 2010). Also, Falkowski *et al.* (1993) propose that the addition of inorganic nitrogen disrupts the nutrient limitation imposed by the coral host on its algal symbionts, effectively allowing the zooxanthellae to retain their photosynthate for growth and division and reducing the amount transferred to the host coral that it could metabolize to maintain proton pumping (Muscatine *et al.* 1989).

Smith & Muscatine (1986) and Muscatine *et al.* (1989) demonstrated that ammonium additions significantly increase symbiont densities in *Stylophora pistillata* both in situ and in experimental settings, with an increase in the fixed nitrogen content of symbiont tissue. Additionally, studies assessing the effect due to depth/ light availability generally show coral photoadaptation with higher chlorophyll concentrations (Falkowski & Dubinsky 1981, Porter *et al.* 1984) under low light conditions. Our study is consistent with these latter findings: although we did not observe a significant difference in symbiont densities for different light conditions during the 2012 light experiment (Fig. 4-4b & Fig. 4-7), chlorophyll *a* concentrations were considerably higher under low light conditions (Fig. 4-4c & Fig. 4-8). However, it is difficult to say whether this result, and that LL corals from 2010 appear to exhibit higher symbiont densities than HL 2011 corals (Fig. 4-7a vs. 4-7b), are due to a light-compensation response or to greater DIN availability: In both HL experiments

(2011/2012), there was an apparent drawdown of DIN: nitrate and nitrite concentrations were reduced by an order of magnitude relative to the original fill water conditions, and the lack of ammonium buildup observed in LL tanks did not occur (4.2). This was likely due to considerable algal growth observed in HL tanks, whereas nutritional competition and ammonium recycling by external algal species was probably lower under LL conditions.

Regardless, even with lower photosynthetic capacity (i.e., chlorophyll *a* densities), HL corals still exhibited significantly greater total tissue lipid content (Fig. 4-4a & Fig. 4-6), demonstrating the contrast in holobiont response to different forms of nutritional enhancement. This is likely due to the nature of the nutritional enhancement: elevating light does not increase the availability of photosynthesis substrate (i.e., CO_2) or symbiont structural materials (i.e., DIN), but, until saturating light levels are reached, it does provide additional energy to drive the photosynthesis process. Under continued host-imposed nutrient limitation, symbionts would be unable to utilize and retain this excess, carbon-rich photosynthate for growth and division, thus increasing the transfer to the coral host. Our tissue lipid results (Fig 4-6) are consistent with this hypothesis, suggesting that HL corals are receiving additional carbohydrate resources. However, the fact that these corals are not significantly (2012 comparison) or only marginally (2011/2012 inter-year comparison; Fig. 4-1) larger than corals raised under low light conditions, suggests that this lipid material is not contributing to expanding tissue extent, but rather is being stored by the coral as a metabolic fuel reserve. This is consistent with several previous studies which have found elevated concentration of storage lipid content in corals maintained under elevated light conditions (e.g., Stimson 1987, Oku *et al.* 2003). Further analysis of the lipid composition, specifically quantify structural vs. storage lipid content, would be instrumental in furthering this hypothesis.

Interestingly, though, we do not observe a reduction in lipid reserves under elevated CO_2 conditions (Fig. 4-6) as we might expect if the corals were actively investing metabolic energy to offset OA-driven impacts on calcification (e.g., Ries 2011). Unfed corals, raised under LL conditions may not be able to invest energy in an OA-compensation response because these corals may already posses the minimal tissue lipid content necessary to survive, leaving insufficient excess to spare for countering CO_2-induced reductions in calcification via proton pumping or other active calcification accelerants. However, it is not clear whether

HL corals expend energetic resources to reduced OA sensitivity under high light, as there is no apparent consumption of lipid reserves under either CO_2 condition (Fig. 4-4a & 4-6). It is possible that OA-sensitivity reduction is due instead to CO_2 removal by the symbionts and not increased proton removal by the coral: The high lipid stores (Fig. 4-4 b & 4-4d) suggest that a considerable amount of carbon is being fixed by photosynthesis and with that, DIC limitation may be reducing calcification under ambient CO_2 conditions (Marubini & Davies 1996).

The importance of coral energetic reserves has been emphasized in the literature: corals with higher lipid content and that are metabolically flexible generally have lower mortality risk and are better able to survive stress events such as bleaching (e.g., Anthony *et al.* 2007, Rodrigues & Grottoli 2007, Anthony *et al.* 2009). However, pervious studies have also observed that fed corals do not appear to utilize their stored energetic reserves to offset the impacts of CO_2 on calcification (Drenkard *et al.* 2013, Schoepf *et al.* 2013), suggetsing that maintaining calcification rates may not be a metabolic priority for these scleractinian coral species.

4.6 Conclusions

To the extent that these findings can be extrapolated to larger scale reef ecosystems, our results suggest that coral organisms in regions with higher levels of inorganic nutrients and/or consistent and sufficient light availability will be less adversely affected by OA than corals in regions that are highly oligotrophic and/or prone to extensive cloud cover. However, the mechanism by which this resilience occurs is not clear as the corals do not appear to actively invest metabolic energy reserves in maintaining calcification rates. Furthermore, reductions in sea surface nutrient availability and productivity, projected as a result of CO_2-induced SST rise and increased water column stratification (e.g. Behrenfeld *et al.* 2006, Steinacher *et al.* 2010, Stock et al. in press), may compound the detrimental impacts of elevated CO_2 conditions, thus rendering affected coral systems more vulnerable to OA.

4.7 Acknowledgements

The authors are grateful to Thomas DeCarlo (MIT/WHOI), Claire Ghallager, Kathrine Rose, Ms. Kascia White (BIOS) for assistance with fieldwork and experiment maintenance. This project was funded by NSF OCE-1041106 and NSF OCE-1041052 along with support from the MIT/WHOI Bermuda Biological Station for Research Fund.

4.8 References

Anthony KRN, Connolly SR, Hoegh-Guldberg O (2007) Bleaching, energetics, and coral mortality risk: Effects of temperature, light, and sediment regime. *Limnology and Oceanography* 52

Anthony KRN, Hoogenboom MO, Maynard JA, Grottoli AG, Middlebrook R (2009) Energetics approach to predicting mortality risk from environmental stress: a case study of coral bleaching. *Functional Ecology* 23: 539–550

Atkinson M, Carlson B, Crow G (1995) Coral growth in high-nutrient, low-pH seawater: a case study of corals cultured at the Waikiki Aquarium, Honolulu, Hawaii. *Coral Reefs* 14: 215–223

Atkinson MJ, Cuet P (2008) Possible effects of ocean acidification on coral reef biogeochemistry: topics for research. *Marine Ecology Progress Series* 373: 249–256

Behrenfeld MJ, O/'Malley RT, Siegel DA, McClain CR, Sarmiento JL, Feldman GC, Milligan AJ, Falkowski PG, Letelier RM, Boss ES (2006) Climate-driven trends in contemporary ocean productivity. *Nature* 444: 752–755

Cantin NE, Negri AP, Willis BL (2007) Photoinhibition from chronic herbicide exposure reduces reproductive output of reef-building corals. *Marine Ecology Progress Series* 344: 81–93

Chalker BE, Taylor DL (1975) Light-Enhanced Calcification, and the Role of Oxidative Phosphorylation in Calcification of the Coral Acropora cervicornis. *Proceedings of the Royal Society of London Series B Biological Sciences* 190: 323–331

Chan NCS, Connolly SR (2013) Sensitivity of coral calcification to ocean acidification: a meta-analysis. *Global Change Biology* 19: 282–290

Cohen A, Holcomb M (2009) Why corals care about ocean acidification: Uncovering the mechanism. *Oceanography* 22: 118–127

Cohen AL, McConnaughey TA (2003) Geochemical Perspectives on Coral Mineralization. *Reviews in Mineralogy and Geochemistry* 54: 151–187

Davies PS (1984) The role of zooxanthellae in the nutritional energy requirements of Pocillopora eydouxi. *Coral Reefs* 2: 181–186

Doney SC, Fabry VJ, Feely RA, Kleypas JA (2009) Ocean Acidification: The Other CO_2 Problem. *Annual Review of Marine Science* 1: 169–192, pMID: 21141034

Drenkard E, Cohen A, McCorkle D, de Putron S, Starczak V, Zicht A (2013) Calcification by juvenile corals under heterotrophy and elevated CO_2. *Coral Reefs* 32: 727–735

Edmunds J Peter (2011) Zooplanktivory ameliorates the effects of ocean acidification on the reef coral *Porites spp. Limnology and Oceanography* 56: 2402–2410

Fabricius KE, Langdon C, Uthicke S, Humphrey C, Noonan S, De/'ath G, Okazaki R, Muehllehner N, Glas MS, Lough JM (2011) Losers and winners in coral reefs acclimatized to elevated carbon dioxide concentrations. *Nature Climate Change* 1: 165–169

Fabry VJ, Seibel BA, Feely RA, Orr JC (2008) Impacts of ocean acidification on marine fauna and ecosystem processes. *ICES Journal of Marine Science: Journal du Conseil* 65: 414–432

Falkowski PG, Dubinsky Z (1981) Light-shade adaptation of Stylophora pistillata, a hermatypic coral from the Gulf of Eilat. *Nature* 289: 172–174

Falkowski PG, Dubinsky Z, Muscatine L, Porter JW (1984) Light and the Bioenergetics of a Symbiotic Coral. *BioScience* 34: 705–709

Falkowski PG, Dubinsky Z, Muscatine L, McCloskey L (1993) Population Control in Symbiotic Corals: Ammonium ions and organic materials maintain the density of zooxanthellae. *BioScience* 43: 606–611

Ferrier-Pagès C, Hoogenboom M, Houlbrèque F (2011) The Role of Plankton in Coral Trophodynamics. In: Dubinsky Z, Stambler N (eds.) *Coral Reefs: An Ecosystem in Transition*, 215–229, Springer Netherlands

Folch J, Lees M, Sloane Stanley GH (1957) A simple method for the isolation and purification of total lipides from animal tissues. *Journal of Biological Chemistry* 226: 497–509

Gattuso JP, Frankignoulle M, Bourge I, Romaine S, Buddemeier R (1998) Effect of calcium carbonate saturation of seawater on coral calcification. *Global and Planetary Change* 18: 37–46

Gattuso JP, Allemand D, Frankignoulle M (1999) Photosynthesis and Calcification at Cellular, Organismal and Community Levels in Coral Reefs: A Review on Interactions and Control by Carbonate Chemistry. *American Zoologist* 39: 160–183

Goodbody-Gringley G, de Putron SJ (2009) Planulation patterns of the brooding coral Favia fragum (Esper) in Bermuda. *Coral Reefs* 28: 959–963

Hoegh-Guldberg O, Mumby PJ, Hooten AJ, Steneck RS, Greenfield P, Gomez E, Harvell CD, Sale PF, Edwards AJ, Caldeira K, Knowlton N, Eakin CM, Iglesias-Prieto R, Muthiga N, Bradbury RH, Dubi A, Hatziolos ME (2007) Coral Reefs Under Rapid Climate Change and Ocean Acidification. *Science* 318: 1737–1742

Holcomb M, McCorkle DC, Cohen AL (2010) Long-term effects of nutrient and CO_2 enrichment on the temperate coral Astrangia poculata (Ellis and Solander, 1786). *Journal of Experimental Marine Biology and Ecology* 386: 27–33

Holcomb M, Cohen AL, McCorkle DC (2012) An investigation of the calcification response of the scleractinian coral Astrangia poculata to elevated pCO_2 and the effects of nutrients, zooxanthellae and gender. *Biogeosciences* 9: 29–39

Langdon C, Atkinson MJ (2005) Effect of elevated pCO_2 on photosynthesis and calcification of corals and interactions with seasonal change in temperature/irradiance and nutrient enrichment. *Journal of Geophysical Research: Oceans* 110: C09S07

Langdon C, Takahashi T, Sweeney C, Chipman D, Goddard J, Marubini F, Aceves H, Barnett H, Atkinson MJ (2000) Effect of calcium carbonate saturation state on the calcification rate of an experimental coral reef. *Global Biogeochemical Cycles* 14: 639–654

Marubini F, Davies P (1996) Nitrate increases zooxanthellae population density and reduces skeletogenesis in corals. *Marine Biology* 127: 319–328

McConnaughey T, Whelan J (1997) Calcification generates protons for nutrient and bicarbonate uptake. *Earth-Science Reviews* 42: 95–117

Muscatine L, Falkowski PG, Dubinsky Z, Cook PA, McCloskey LR (1989) The Effect of External Nutrient Resources on the Population Dynamics of Zooxanthellae in a Reef Coral. *Proceedings of the Royal Society of London B Biological Sciences* 236: 311–324

Oku H, Yamashiro H, Onaga K, Sakai K, Iwasaki H (2003) Seasonal changes in the content and composition of lipids in the coral Goniastrea aspera. *Coral Reefs* 22: 83–85

Pandolfi JM, Connolly SR, Marshall DJ, Cohen AL (2011) Projecting Coral Reef Futures Under Global Warming and Ocean Acidification. *Science* 333: 418–422

Porter JW, Muscatine L, Dubinsky Z, Falkowski PG (1984) Primary Production and Photoadaptation in Light- and Shade-Adapted Colonies of the Symbiotic Coral, Stylophora pistillata. *Proceedings of the Royal Society of London Series B Biological Sciences* 222: 161–180

Ries JB (2011) A physicochemical framework for interpreting the biological calcification response to CO_2-induced ocean acidification. *Geochimica et Cosmochimica Acta* 75: 4053 – 4064

Ries JB, Cohen AL, McCorkle DC (2009) Marine calcifiers exhibit mixed responses to CO2-induced ocean acidification. *Geology* 37: 1131–1134

Rodolfo-Metalpa R, Houlbreque F, Tambutte E, Boisson F, Baggini C, Patti FP, Jeffree R, Fine M, Foggo A, Gattuso JP, Hall-Spencer JM (2011) Coral and mollusc resistance to ocean acidification adversely affected by warming. *Nature Climate Change* 1: 308–312

Rodrigues LJ, Grottoli A (2007) Energy reserves and metabolism as indicators of coral recovery from bleaching. *Limnology and Oceanography* 52: 1874–1882

Schoepf V, Grottoli A, Warner ME, Cai WJ, Melman TF, Hoadley KD, Pettay DT, Hu X, Li Q, Xu H, Wang Y, Matsui Y, Baumann JH (2013) Coral Energy Reserves and Calcification in a High-CO2 World at Two Temperatures. *PLoS ONE* 9: e108 082

Shamberger K, Feely R, Sabine C, Atkinson M, DeCarlo E, Mackenzie F, Drupp P, Butterfield D (2011) Calcification and organic production on a Hawaiian coral reef. *Marine Chemistry* 127: 64–75

Shamberger KEF, Cohen AL, Golbuu Y, McCorkle DC, Lentz SJ, Barkley HC (2014) Diverse coral communities in naturally acidified waters of a Western Pacific reef. *Geophysical Research Letters* 41: 499–504

Silverman J, Lazar B, Erez J (2007) Community metabolism of a coral reef exposed to naturally varying dissolved inorganic nutrient loads. *Biogeochemistry* 84: 67–82

Smith G, Muscatine LL (1986) Carbon budget and regulation of the population-density of symbiotic algae. *Endocytobiosis and Cell Research* 3: 213–238

Steinacher M, Joos F, Fröolicher TL, Bopp L, Cadule P, Cocco V, Doney SC, Gehlen M, Lindsay K, Moore JK, Schneider B, Segschneider J (2010) Projected 21st century decrease in marine productivity: a multi-model analysis. *Biogeosciences* 7: 979–1005

Stimson J (1987) Location, quantity and rate of change in quantity of lipids in tissues of Hawaiian hermatypie corals. *Bulletin of Marine Science* 41: 889–904

Suggett D, Dong L, Lawson T, Lawrenz E, Torres L, Smith D (2013) Light availability determines susceptibility of reef building corals to ocean acidification. *Coral Reefs* 32: 327–337

Wright SW, Jeffrey SW, Mantoura RFC, Llewellyn CA, Bjornland T, Repeta D, Welschmeyer N (1991) Improved HPLC method for the analysis of chlorophylls and carotenoids from marine phytoplankton. *Marine Ecology Progress Series* 77: 183–196

Zoccola D, Tambutté E, Kulhanek E, Puverel S, Scimeca JC, Allemand D, Tambutté S (2004) Molecular cloning and localization of a {PMCA} P-type calcium {ATPase} from the coral Stylophora pistillata. *Biochimica et Biophysica Acta (BBA) - Biomembranes* 1663: 117 – 126

Year & Light Condition	Feeding Treatment	CO_2 Treatment (ppm CO_2 ± SD)	Temperature (°C ± SD)	Salinity (psu ± SD)	Alkalinity (μeq kg^{-1} ± SD)	DIC (μmol kg^{-1} ± SD)	$[HCO_3^-]$ (μmol kg^{-1} ± SD)	$[CO_3^{2-}]$ (μmol kg^{-1} ± SD)	Ωar (± SD)
2011 High Light	Fed	420 ± 10	27.4 ± 0.6	36.5 ± 0.9	2,154 ± 110	1,853 ± 70	1,635 ± 68	207 ± 46	3.28 ± 0.71
		1,060 ± 10	27.3 ± 0.5	36.6 ± 1.4	2,200 ± 82	2,054 ± 42	1,907 ± 44	121 ± 33	1.92 ± 0.51
		1,720 ± 90	27.6 ± 0.4	36.1 ± 0.6	2,251 ± 67	2,148 ± 72	2,016 ± 74	95 ± 20	1.52 ± 0.32
		2,660 ± 10	27.2 ± 0.4	36.3 ± 0.9	2,406 ± 45	2,350 ± 53	2,220 ± 52	76 ± 12	1.21 ± 0.19
	Unfed	420 ± 10	27.2 ± 0.4	36.2 ± 0.9	2,160 ± 109	1,852 ± 83	1,629 ± 74	212 ± 31	3.38 ± 0.48
		1,060 ± 10	27.5 ± 0.5	36.3 ± 1.0	2,162 ± 86	2,003 ± 64	1,857 ± 53	123 ± 20	1.95 ± 0.31
		1,720 ± 90	27.3 ± 0.6	36.8 ± 1.4	2,315 ± 123	2,222 ± 72	2,084 ± 62	94 ± 31	1.48 ± 0.47
		2,660 ± 10	27.5 ± 0.5	36.4 ± 1.0	2,370 ± 69	2,314 ± 69	2,186 ± 66	75 ± 13	1.20 ± 0.21
2012 Low Light	Unfed	430 ± 20	27.6 ± 0.3	36.8 ± 0.5	2,352 ± 33	2,018 ± 28	1,772 ± 40	236 ± 11	3.72 ± 0.19
		1,920 ± 20	27.7 ± 0.3	36.8 ± 0.5	2,392 ± 69	2,281 ± 63	2,141 ± 58	103 ± 11	1.62 ± 0.17
2012 High Light	Unfed	430 ± 20	27.6 ± 0.4	36.6 ± 0.2	2,335 ± 27	2,003 ± 17	1,757 ± 11	234 ± 8	3.72 ± 0.12
		1,920 ± 20	27.7 ± 0.4	36.7 ± 0.4	2,357 ± 24	2,254 ± 24	2,119 ± 23	97 ± 8	1.54 ± 0.12

Table 4.1: Measured and calculated carbonate chemistry parameters. Average (± SD) among replicate tanks of a given treatment.

Year	CO_2 Treatment	Ammonium (μM NH_4^+ ± SD)	Phosphate (μM PO_4^{3-} ± SD)	Nitrite & Nitrate (μM $N0_2$ + $N0_3^-$ ± SD)
2010	Fill Water	0.94 ± 0.53	0.11 ± 0.04	0.46 ± 0.23
Low Light	Ambient CO_2	6.31 ± 1.46	0.15 ± 0.10	0.46 ± 0.40
	High CO_2	3.26 ± 2.34	0.10 ± 0.03	0.29 ± 0.28
2011	Fill Water	0.56 ± 0.35	0.09 ± 0.05	0.85 ± 0.20
High Light	Ambient CO_2	0.44 ± 0.13	0.09 ± 0.02	0.08 ± 0.03
	High CO_2	0.33 ± 0.18	0.07 ± 0.01	0.06 ± 0.01
2012	Fill Water	< 0.05	< 0.05	0.71 ± 0.33
Low Light	Ambient CO_2	4.14 ± 0.38	< 0.05	0.45 ± 0.16
	High CO_2	4.81 ± 0.32	< 0.05	0.44 ± 0.15
High Light	Ambient CO_2	0.42 ± 0.54	< 0.05	< 0.05
	High CO_2	0.09 ± 0.09	< 0.05	< 0.05

Table 4.2: Nutrient measurements. Average (± SD) seawater chemistry of replicate aquaria for a given experimental conditions (treatment). Tanks sampled after one week. These values are somewhat approximate; where values were indicated as "ower than a detection limit" the value was replaced with the next 0.005 μM lower for calculation purposes (e.g. ¡0.05 uM became 0.045 μM).

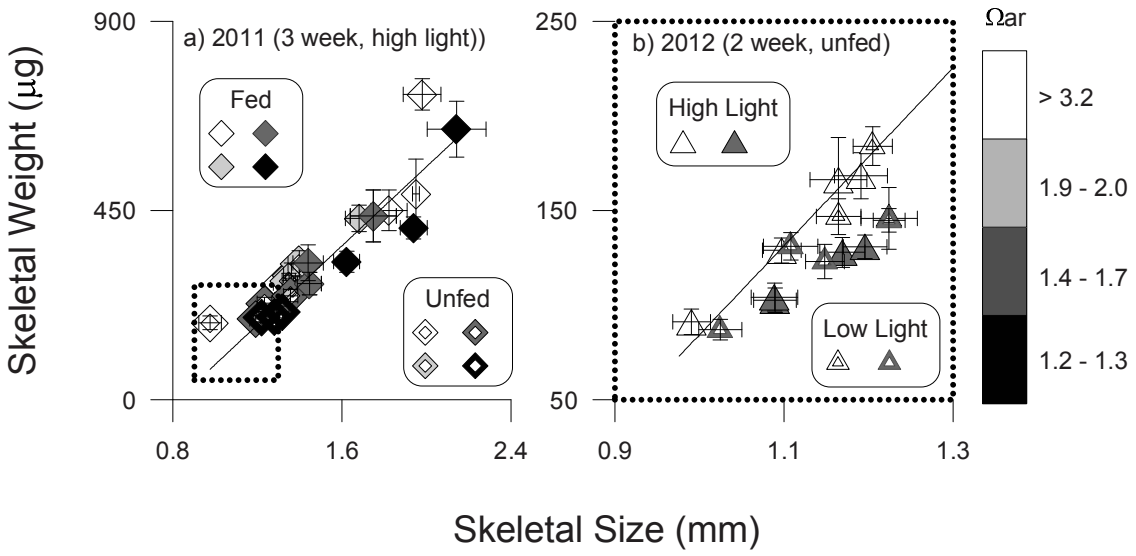

Figure 4-1: Juvenile coral skeletal weight vs. diameter (i.e., size) from a) 2011 and b) 2012. The correlation ($R^2 = 0.89$) between skeletal size and weight is illustrated by the plotted linear regression. Note: the regression was computed using data from both experiments but are separated by year to improve data readability, Each symbol represents the average weight and size for a given treatment tank. Filled symbols indicate elevated nutrition (i.e., fed or high light conditions), hollow symbols indicate limited nutrition (i.e., unfed or low light conditions) and symbol shading represents the saturation state range. Error bars indicate $\pm$ 1 standard error.

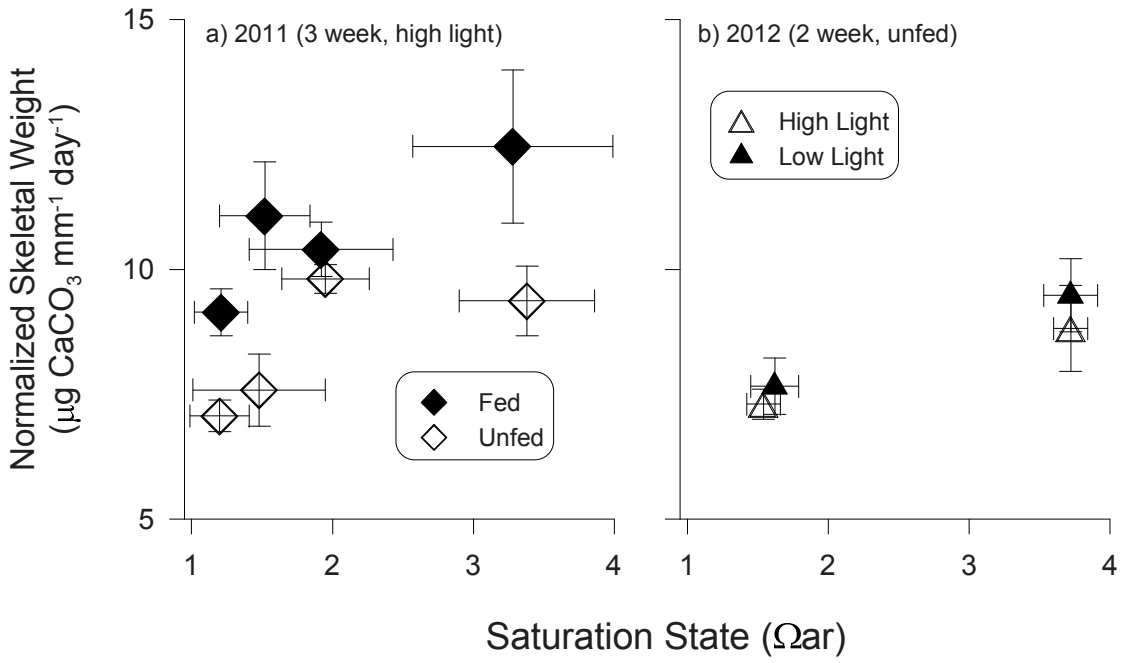

Figure 4-2: Juvenile coral age- and size-normalized skeletal weight from a) 2011 and b) 2012 experiments plotted against the average aragonite saturation state of their respective treatment conditions. Vertical error bars indicate ± 1 standard error and horizontal error bars indicate ± the average standard deviation among treatment tanks.

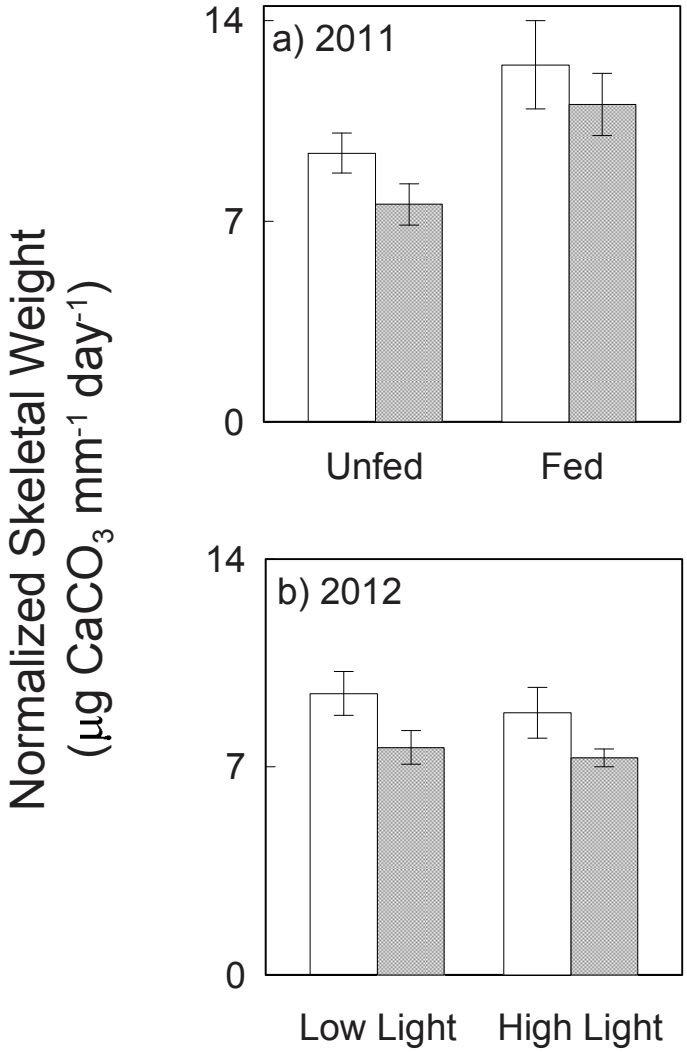

Figure 4-3: Juvenile coral age- and size-normalized skeletal weight from the a) 2011 and b) 2012 experiments. White (shaded) bars represent ambient (elevated) CO_2 conditions; Error bars indicate $\pm$ 1 standard error

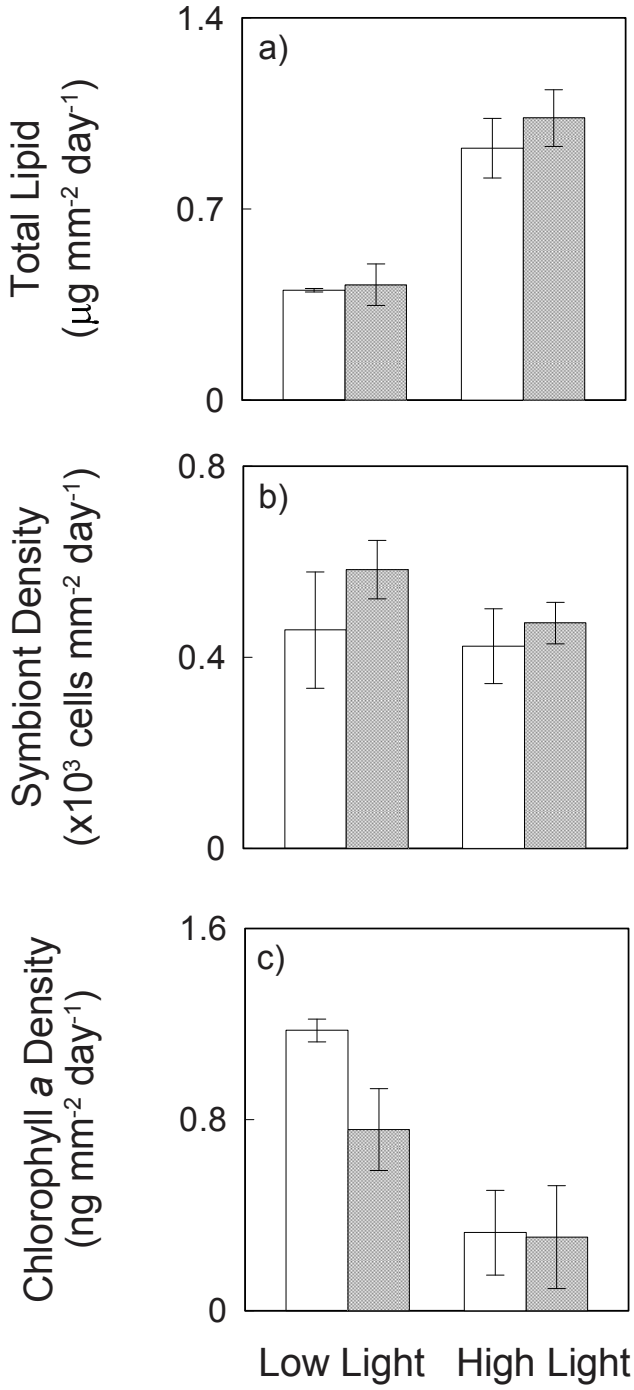

Figure 4-4: Age-and area- normalized a) total tissue lipid content, b) symbiont density, and c) chlorophyll *a* density from the 2012, light and CO_2 experiment. White (shaded) bars represent ambient (elevated) CO_2 conditions; Error bars indicate ± 1 standard error

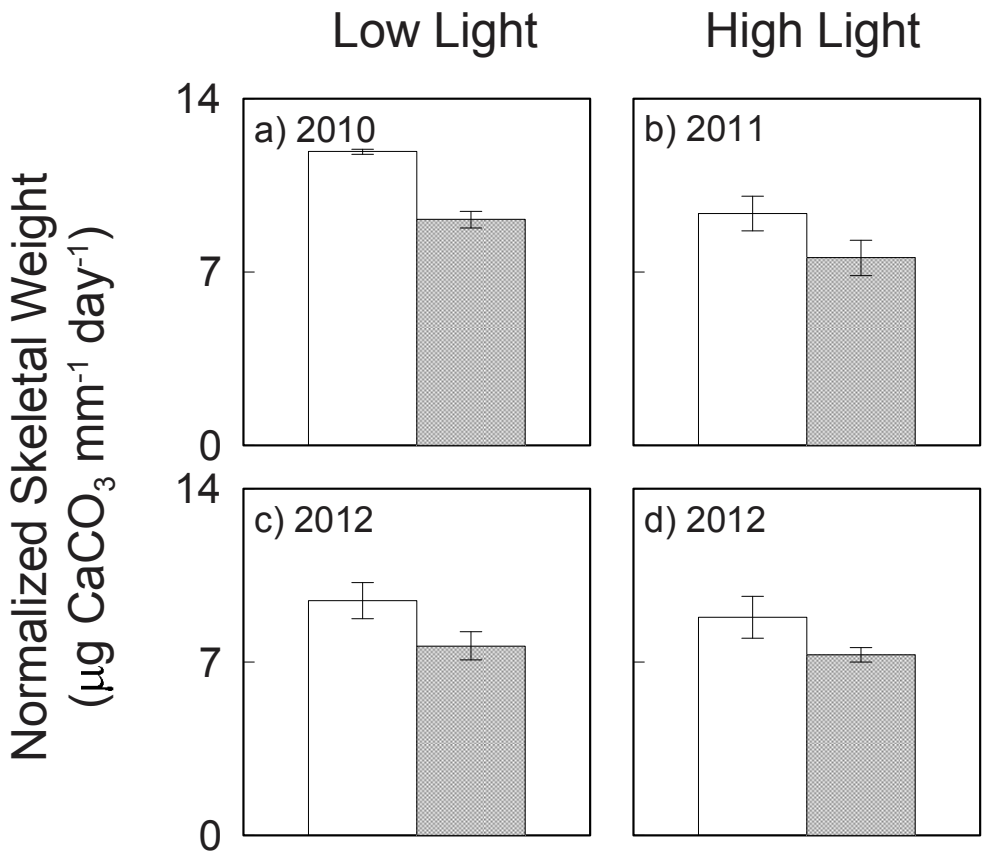

Figure 4-5: Juvenile coral age- and area-normalized skeletal weight from the a) 2010, b) 2011, c & d) 2012 experiments. White (shaded) bars represent ambient (elevated) CO_2 conditions; Error bars indicate ± 1 standard error

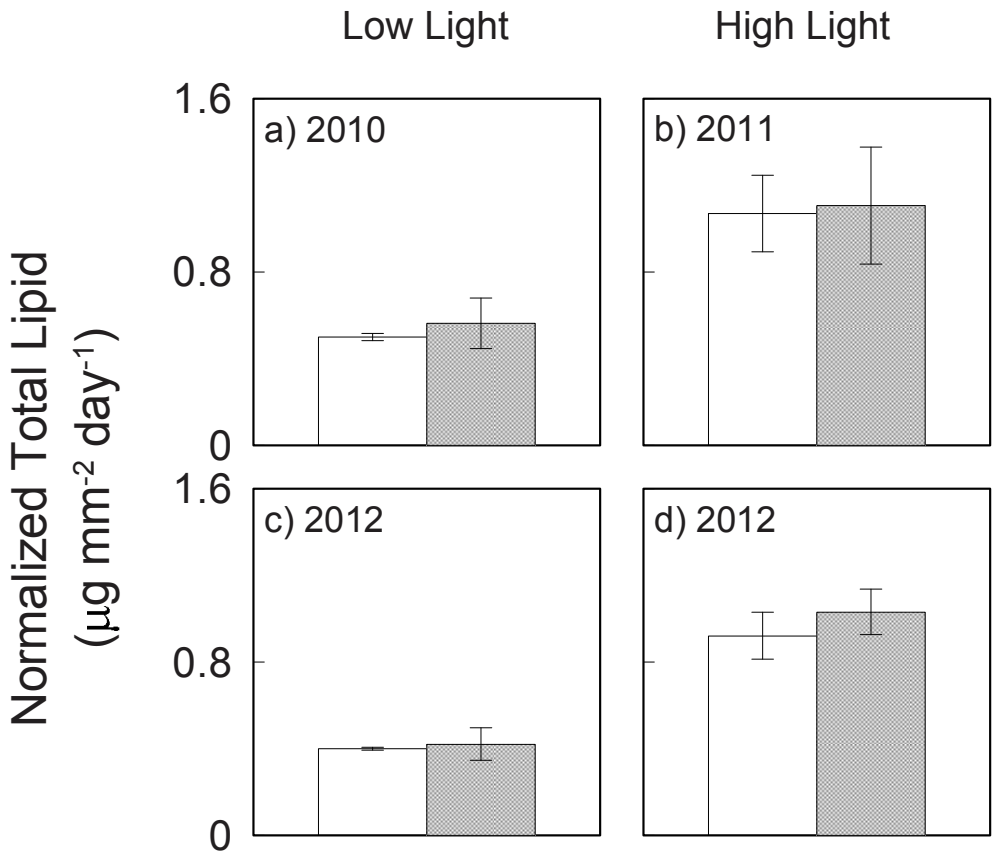

Figure 4-6: Juvenile coral age- and area-normalized total lipid content from the a) 2010, b) 2011, c & d) 2012 experiments. White (shaded) bars represent ambient (elevated) CO_2 conditions; Error bars indicate ± 1 standard error

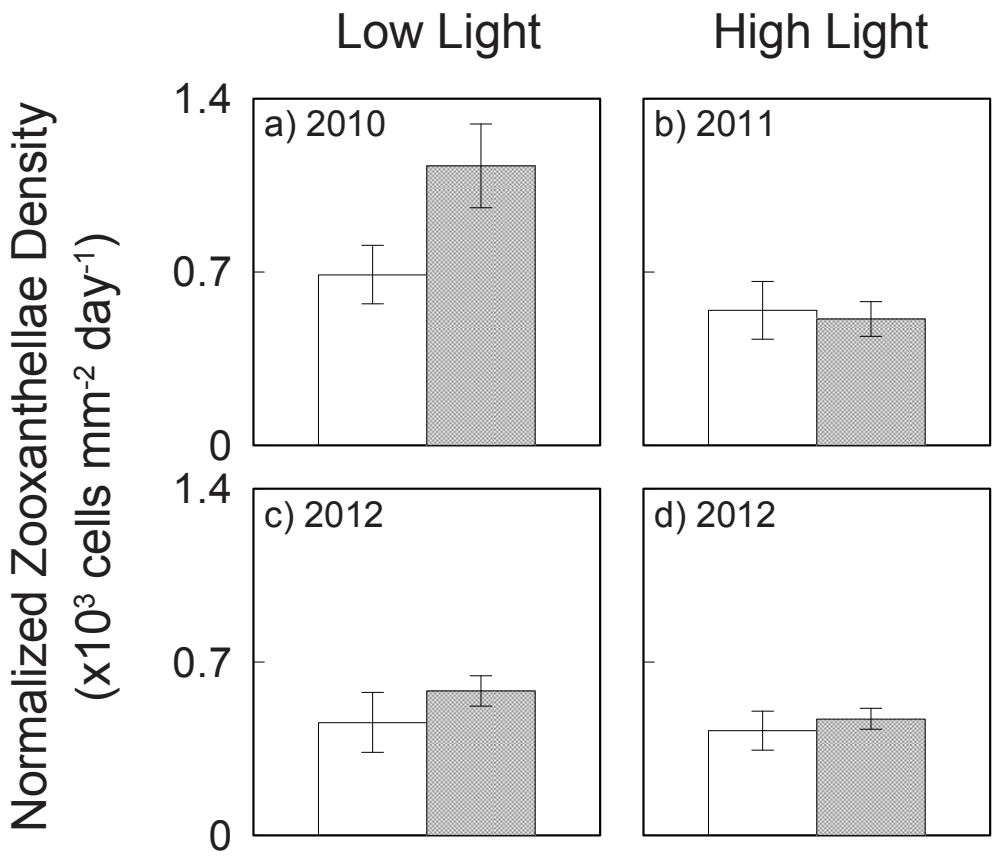

Figure 4-7: Juvenile coral age- and area-normalized symbiont densities from the a) 2010, b) 2011, c & d) 2012 experiments. White (shaded) bars represent ambient (elevated) CO_2 conditions; Error bars indicate ± 1 standard error

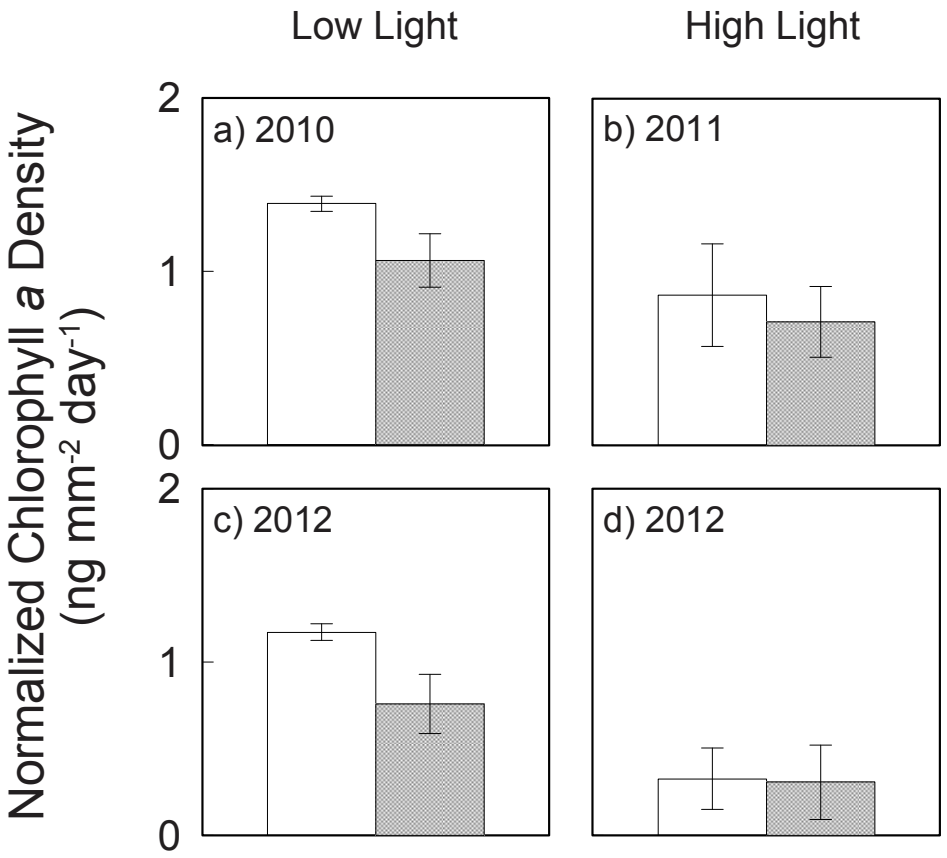

Figure 4-8: Juvenile coral age- and area-normalized chlorophyll *a* concentrations from the a) 2010, b) 2011, c & d) 2012 experiments. White (shaded) bars represent ambient (elevated) CO_2 conditions; Error bars indicate ± 1 standard error

Chapter 5

Conclusions

If anthropogenic CO_2 emissions continue unabated, it is likely that once pristine and diverse coral reef ecosystems will degrade beyond the point of recovery (Veron *et al.* 2009) Focusing conservation efforts on environmental refugia where oceanographic conditions naturally mitigate CO_2-driven stressors may increase the probability of conservation success (West & Salm 2003; Riegl & Piller 2003). However, rising levels of atmospheric CO_2 drive changes in multiple ocean properties (e.g., temperature, pH) and these in turn drive other changes that also affect coral reef ecosystems (e.g., stratification and productivity). Understanding and predicting the nature, magnitude, and interaction of these changes for specific coral reef ecosystems and the potential range of responses of coral reef organisms is necessary for the development of appropriate and effective conservation strategies.

For coral reef islands in the central equatorial Pacific, my research has shown that: 1) the EUC has intensified over the last ~140 years. This finding bolsters the hypothesis that future EUC intensification may strengthen upwelling around equatorial Pacific islands, thus reducing the impact of rising SST on these reefs (Karnauskas & Cohen 2012); and 2) although corals on these reef systems will be exposed to elevated levels of CO_2, which can be detrimental to skeletal growth, this response may be offset, at least partially, by the nutritional enhancement conferred by nutrient-rich EUC water. We observe two distinct patterns of OA-nutrition interactions: i) heterotrophic feeding results in larger corals that produce more calcium carbonate but remain sensitive to elevated CO_2 levels and ii) elevated light levels does not affect corallite size but reduce coral calcification sensitivity to CO_2.

Our assessment of the Simple Ocean Data Assimilation (SODA) reanalysis suggests that there is robust evidence of EUC intensification since the late 1800s (Chapter 2). This historical precedent lends indirect support to model projections of future EUC intensification (e.g., Luo *et al.* 2009, Sen Gupta *et al.* 2012, Karnauskas & Cohen 2012). If the projected EUC intensification occurs, increased topographic upwelling of EUC waters on equatorial Pacific islands will reduce projected warming of the sea surface around these islands (Karnauskas & Cohen 2012). The historical intensification signal is dominated by two dynamically distinct

seasonal mechanisms, which we have characterized through decomposition and diagnosis of equatorial Pacific zonal momentum budget. The first mechanism entails strengthening of the pressure gradient force, which occurs due to strengthening of the trade winds and sea surface height gradient in the western Pacific during boreal spring. The second, which occurs in boreal summer, is characterized by a reduction in vertical shear stress caused by weakening of the eastern Pacific trade winds and surface current, resulting in local shoaling and acceleration of the EUC.

Interannual variability of EUC intensity, especially as it relates to the El Niño Southern Oscillation (ENSO), may limit the ability of equatorial Pacific islands to act as refugia. Although we demonstrate historical strengthening of the EUC throughout the annual cycle (Fig. 2-5e), the EUC will weaken during strong El Niño events (e.g., Firing *et al.* 1983), causing warming that could render equatorial Pacific islands vulnerable (e.g., D'Croz *et al.* 2001). However, to counter this concern, one study of the response of Gilbert Islands corals to thermal stress suggests that corals naturally exposed to higher amplitude thermal variability, as are the equatorial communities, are less susceptible to heat stress which may enable them to withstand temporary reductions in EUC intensity (Carilli *et al.* 2012).

The nutritional benefit to corals conferred by nutrients and productivity associated with EUC upwelling may further mitigate thermal stress from El Niño events. Energetic (e.g., lipid) reserves and biomass accumulated by corals prior to thermal stress events are likely crucial to their survival (e.g., Rodrigues & Grottoli 2007, Anthony *et al.* 2007, Anthony *et al.* 2009, Thornhill *et al.* 2011). In Chapter 3, we demonstrate that fed corals have greater total lipid content and biomass. Also, massive *Porites sp.* from equatorial Pacific islands exhibit a longitudinal gradient in tissue thickness that correlates with EUC (and upwelling) strength (Fig. 5-1). Since coral tissue thickness is often used as a bio-indicator of coral resilience to stress (e.g., Thornhill *et al.* 2011), such observations imply that stronger upwelling is beneficial to *Porites* health and that corals on these highly productive reef systems may be able to withstand the stress of strong El Niño events.

Additionally, our experiments demonstrate that fed corals produce $CaCO_3$ more rapidly than unfed corals even under elevated CO_2 conditions (Chapter 3) and that elevated light appears to reduce calcification sensitivity to CO_2 (Chapter 4). Holcomb *et al.* (2010) showed that even modest nutrient enrichments, similar in magnitude to that caused by EUC up-

welling (*Gove, unpublished data*) are also capable of reducing calcification sensitivity to elevated CO_2 conditions. In both cases (under elevated light or nutrients), the mechanism for CO_2-sensitivity reduction appears to be closely linked, and likely attributable to enhanced symbiont photosynthesis (Langdon & Atkinson 2005, Chapter 4). Yet the question remains, how will these different forms of nutrition interact and which will dominate in determining coral calcification response to changes in EUC upwelling? Enhanced symbiont photosynthesis due to the availability of inorganic nutrition may reduce the decline in calcification caused by CO_2-rich water by as much as 100% (i.e., Langdon & Atkinson 2005, Holcomb *et al.* 2010). Also, increased productivity and availability of planktonic food for coral heterotrophy could increase the baseline calcification that is otherwise lower due to high levels of inorganic nutrients. In our experiments, fed corals produced approximately 40% more $CaCO_3$ than unfed corals under elevated CO_2 conditions. Of course the balance of these contributing factors may be highly variable. For instance, if corals were to bleach, then the mechanism of reduced CO_2-sensitivity conferred by symbiont photosynthesis would be lost.

This thesis presents new evidence for the historical, mechanistic drivers of EUC intensification and for the role of coral nutrition in determining calcification response under elevated CO_2 conditions. My results support the overarching hypothesis that the EUC's impact on equatorial Pacific island SST and biogeochemistry will play an important role in determining the potential of these islands as climate change refugia for coral reef communities.

5.1 References

Anthony KRN, Connolly SR, Hoegh-Guldberg O (2007) Bleaching, energetics, and coral mortality risk: Effects of temperature, light, and sediment regime. *Limnology and Oceanography* 52

Anthony KRN, Hoogenboom MO, Maynard JA, Grottoli AG, Middlebrook R (2009) Energetics approach to predicting mortality risk from environmental stress: a case study of coral bleaching. *Functional Ecology* 23: 539–550

Carilli J, Donner SD, Hatmann AC (2012) Historical Temperature Variability Affects Coral Response to Heat Stress. *PLoS ONE* 7: e34 418

D'Croz L, Mate J, Oke J (2001) Responses to elevated sea water temperature and UV radiation in the coral Porites lobata from upwelling and non-upwelling environments on the Pacific coast of Panama. *Bulletin of Marine Science* 69: 203–214

Firing E, Lukas R, Sadler J, Wyrtki K (1983) Equatorial Undercurrent Disappears During 1982-1983 El Niño. *Science* 222: 1121–1123

Holcomb M, McCorkle DC, Cohen AL (2010) Long-term effects of nutrient and CO_2 enrichment on the temperate coral Astrangia poculata (Ellis and Solander, 1786). *Journal of Experimental Marine Biology and Ecology* 386: 27–33

Karnauskas KB, Cohen AL (2012) Equatorial refuge amid tropical warming. *Nature Climate Change* 2: 530–534

Langdon C, Atkinson MJ (2005) Effect of elevated pCO_2 on photosynthesis and calcification of corals and interactions with seasonal change in temperature/irradiance and nutrient enrichment. *Journal of Geophysical Research: Oceans* 110: C09S07

Luo Y, Rothstein LM, Zhang RH (2009) Response of Pacific subtropical-tropical thermocline water pathways and transports to global warming. *Geophysical Research Letters* 36: L04 601

Riegl B, Piller W (2003) Possible refugia for reefs in times of environmental stress. *International Journal of Earth Sciences* 92: 520–531

Rodrigues LJ, Grottoli A (2007) Energy reserves and metabolism as indicators of coral recovery from bleaching. *Limnology and Oceanography* 52: 1874–1882

Sen Gupta A, Ganachaud A, McGregor S, Brown JN, Muir L (2012) Drivers of the projected changes to the Pacific Ocean equatorial circulation. *Geophysical Research Letters* 39: L09 605

Thornhill D, Rotjan RD, Todd BD, Chilcoat GC, Iglesias-Prieto R, Kemp D, LaJeunesse T, McCabe Reynolds J, Schmidt G, Shannon T, Warner ME, Fitt WK (2011) A Connection between Colony Biomass and Death in Caribbean Reef-Building Corals. *PLoS ONE* 6: e29 535

Veron J, Hoegh-Guldberg O, Lenton T, Lough J, Obura D, Pearce-Kelly P, Sheppard C, Spalding M, Stafford-Smith M, Rogers A (2009) The coral reef crisis: The critical importance of <350 ppm CO_2. *Marine Pollution Bulletin* 58: 1428–1436

West JM, Salm RV (2003) Resistance and Resilience to Coral Bleaching: Implications for Coral Reef Conservation and Management. *Conservation Biology* 17: 956–967

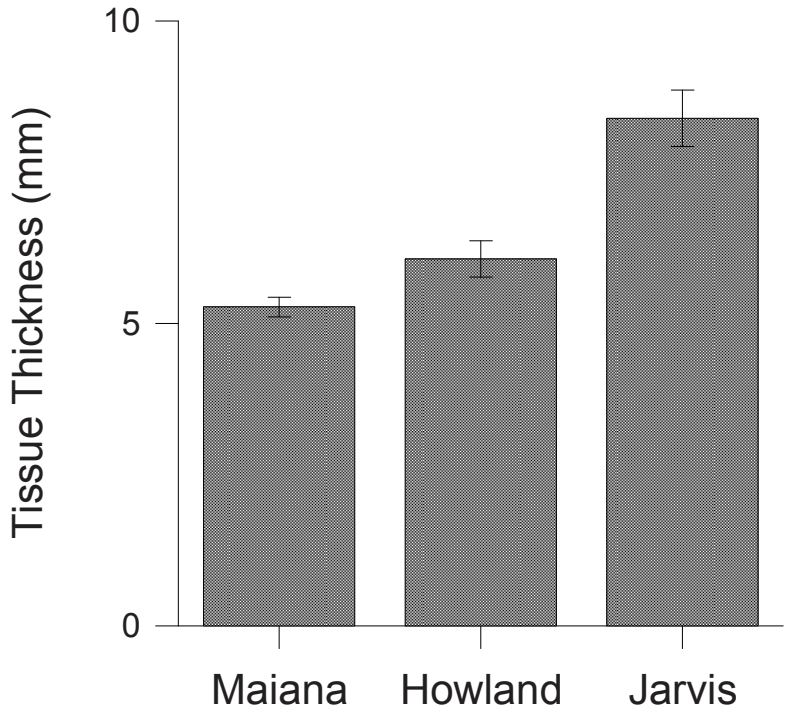

Figure 5-1: Average tissue thickness of *Porites sp.* collected from the equatorial Pacific islands: Maiana (Republic of Kiribati), Howland and Jarvis (both U.S. National Wildlife Refuges). All three islands are located within 2° latitude of the equator and are situated along a longitudinal gradient of increasing mean-state EUC intensity: 173°E, 176.5°W, and 160°W respectively. Coral samples were pneumatically cored and collected from both east and west sides of these islands (except for the eastern side of Howland where there were no Porites available for sampling). Cross-sections perpendicular to the core tops were made in order to expose the full tissue extent. These cross-sections were digitally photographed and analyzed using SPOT™ software to measure the tissue thickness. All coral samples were collected during September 2012 when EUC intensity is at a seasonal low (Johnson et al. 2012) and therefore the contrast in environmental conditions between west (i.e., upwelling) and east (i.e., non-upwelling) sides of islands due to topographic upwelling would be weakest, with both sides likely reflecting the influence of wind-driven equatorial upwelling.

Appendix A

Data for Chapter 3

A.1 2010 Skeletal Size and Weight Data

Tank Treatment	Tile ID	Tile Age (days)	Coralite ID	Size (μm)	Weight (μg)	ASN Weight (μg mm^{-1}day^{-1})
1	4	20	N	1274		
1670 ppm CO_2			O	1708	437	16.05
Unfed			T	1253	159	5.84
			W	1321	169	6.21
			Y	1714	422	15.50
	5	20	A	1316	216	7.93
			B	1440	296	10.87
			C	1224	187	6.87
			D	1094	146	5.36
			E	1493	329	12.08
			F	1150	161	5.91
			H	1357	226	8.30
			J	1474	308	11.31
			K	1340	259	9.51
			L	1322	187	6.87
			M	1533	301	11.05
			N	1331	189	6.94
			O	1545	280	10.28
			P	1340	245	9.00
			Q	1699	451	16.56
			R	1254	198	7.27
	6B	21	A	1337	298	10.42
			B	1118	158	5.53
			C	1345	276	9.65
			F	1073	306	10.70
			I	1278		
			J		201	7.03
			K	1374	267	9.34
			L	1447	319	11.16
	7	21	A	1401	262	9.16
			B		261	9.13
			C	1452	330	11.54
			D	1171		
			E	1496		
			G	1349	264	9.23

2010 skeletal size and weight data, continued

Tank Treatment	**Tile ID**	**Tile Age (days)**	**Coralite ID**	**Size (μm)**	**Weight (μg)**	**ASN Weight (μg mm^{-1}day^{-1})**
			H	1424	376	13.15
			I	1210	192	6.72
			J	1591	337	11.79
			K	1256	238	8.32
			L	1385	257	8.99
			M	1207	212	7.42
Tank 1 Average				1361	263	9.43
2	4	21	H	2351	614	14.07
420 ppm CO_2			P	1491	256	5.87
Fed			Q/U	2116	546	12.51
			R	2070	498	11.41
			S	2070	475	10.88
			V	2050	565	12.94
	5	22	B	2275	632	13.82
			C	2070	474	10.37
			D	2487	642	14.04
			E	2502	730	15.96
			F	2153	647	14.15
			H	2218	665	14.54
			I	2281	631	13.80
			M	1945	503	11.00
			N	2676	762	16.66
			O	2424	738	16.14
			P	1989	490	10.72
			Y	2392	771	16.86
			AB	2253	696	15.22
			AE	2375	732	16.01
			AL		387	8.46
			AM	2323	702	15.35
			AN	1745	344	7.52
			AQ	2398	718	15.70
			AU	2183	627	13.71
			AV	1729	394	8.62
			AW	2469		
			AX	2040	538	11.77
			AZ	2314	655	14.32
			BA	2254	506	11.07
	7	21	A	1786	340	7.79
			B	1543	222	5.09
			I	1962	356	8.16

2010 skeletal size and weight data, continued

Tank Treatment	**Tile ID**	**Tile Age (days)**	**Coralite ID**	**Size (μm)**	**Weight (μg)**	**ASN Weight (μg mm^{-1}day^{-1})**
			K	1742		
			L	1978	213	4.88
			M	2503	665	15.24
			N	1762		
			O	2150	499	11.43
			P	1866	448	10.26
			Q	2331	636	14.57
			R	2088	409	9.37
			S	1869	185	4.24
			T	1600	336	7.70
			U	1144	178	4.08
			V	1487	299	6.85
Tank 2 Average				2078	517	11.50
3	4	20	A	1442	384	13.37
420 ppm CO_2			I	1377	368	12.81
Unfed			K	1387	431	15.00
	5	22	E	1118	221	6.99
			F	1595	449	14.21
			G	1018	184	5.82
			H	1641		
			P	1592	503	15.92
			Q	1568	477	15.09
			R	1426	318	10.06
			X	1416	358	11.33
			AB	1455	337	10.66
			AD		244	7.72
			AF	1494	405	12.82
			AH		270	8.54
			AI	1571	473	14.97
			AA	1631	509	16.11
			U	1504	395	12.50
			W	1759	552	17.47
			AJ	1712	604	19.11
			AM	1823	630	19.94
			AK	1309	312	9.87
			AP	1385	306	9.68
			AQ	1663	514	16.27
			AR	1246	311	9.84
			AS	1133	226	7.15
			AU	1334	322	10.19

2010 skeletal size and weight data, continued

Tank Treatment	Tile ID	Tile Age (days)	Coralite ID	Size (μm)	Weight (μg)	ASN Weight ($\mu g\ mm^{-1} day^{-1}$)
			AW	1498	432	13.67
			AY	1411	387	12.25
			BA	1565	419	13.26
			BC	1537	446	14.11
			BB	1541	440	13.92
			BD	1476	324	10.25
	8	21	A	1406	362	12.00
			B	999	173	5.74
			D	1602	474	15.71
			H	1370		
			I	1555		
			J	1334		
			K		283	9.38
			L	1153	214	7.09
			M	1453	365	12.10
			N	1458	379	12.56
			O	1508	418	13.86
			P	1860	545	18.07
			Q	1525	464	15.38
			R	1524		
			S	1458	317	10.51
			T		318	10.54
			V	1286	336	11.14
			W	1462	395	13.10
			X	1569		
			Y	1392	373	12.37
			Z	1430		
			AA	978	138	4.58
			AB	1543		
			AC	1427		
			AD	1509	477	15.81
			AE	1425	363	12.03
			AF	1249	250	8.29
			AG	1427	372	12.33
			AH	1314	325	10.77
			AI	1523	424	14.06
			AJ	819	111	3.68
Tank 3 Average				1436	371	12.04
4	3	21	B	1280		
1670 ppm CO_2			C	1263		

2010 skeletal size and weight data, continued

Tank Treatment	Tile ID	Tile Age (days)	Coralite ID	Size (μm)	Weight (μg)	ASN Weight (μg mm^{-1}day^{-1})
Unfed			D	1156		
			E	1308	232	8.31
			F	1379	181	6.48
			G	1120	178	6.38
			H		162	5.80
			I	1215	182	6.52
			K	1308	186	6.66
			L	1561	159	5.70
			M	1332	221	7.92
			N	1424	331	11.86
			O	1245	207	7.42
			P	1292	228	8.17
			Q	1404	294	10.53
			R	1281	217	7.77
	5	22	E	1482		
			F	1413	230	7.86
			G	1515	297	10.16
			H	1443	306	10.46
			K		178	6.09
			L	1456	292	9.99
			M	1410		
			O	1103	152	5.20
			Q	1407	286	9.78
			R	1265	251	8.58
	7	20	B	1254	191	7.18
			C	1404	343	12.90
			D	1343	291	10.95
			E	1195	194	7.30
			G	1503	338	12.71
	8	21	A	1305	266	9.53
			B	1143		
Tank 4 Average				1329	237	8.45
5	4	21	I	2535		
1670 ppm CO_2			J	1846	318	7.52
Fed			L	2476	552	13.05
	5	21	E	2319	422	9.98
	8	23	A	2031	394	8.51
			B	2073	497	10.73
			D	2110	401	8.66
	10	21	A	1684	245	5.79

2010 skeletal size and weight data, continued

Tank Treatment	**Tile ID**	**Tile Age (days)**	**Coralite ID**	**Size (μm)**	**Weight (μg)**	**ASN Weight (μg mm^{-1}day^{-1})**
			B	2081	442	10.45
			C	1745	259	6.12
			D	1718	269	6.36
			E	1550	218	5.15
Tank 5 Average				2014	365	8.39
6	6	22	A	1397	308	10.27
420 ppm CO_2			AB	1331	276	9.20
Unfed			B	1808	573	19.10
			D	1575	460	15.33
			E	1425	377	12.57
			F	1382	365	12.17
			H	1333	326	10.87
			K	1394	365	12.17
			L	1490		
			O	1413	427	14.23
			S	1369	348	11.60
			U	949	210	7.00
			V	1460	428	14.27
			C	1200	240	8.00
			AC	1250	292	9.73
			AH	1467	438	14.60
			AL	1229		
			AE	1428	275	9.17
			AF	1266	375	12.50
	7	20	A	1573	379	13.90
			B	1372	269	9.86
			C	1457		
			D	1538	305	11.18
			F	1509	350	12.83
			J	1566	374	13.71
			K	1056		
			L	1133		
			N	1166		
			O	1268		
			Q	1261	288	10.56
			R		252	9.24
			AA	1545	464	17.01
			AC	1297	293	10.74
			AD		252	9.24
			AE	1221		

2010 skeletal size and weight data, continued

Tank Treatment	Tile ID	Tile Age (days)	Coralite ID	Size (μm)	Weight (μg)	ASN Weight (μg mm^{-1}day^{-1})
			AF	1239		
Tank 6 Average				1364	345	11.89
7	3	20	K	1440	425	15.52
420 ppm CO_2			O	1263	257	9.38
Unfed			P	1577	451	16.47
			T	1599	386	14.09
			U	1160	193	7.05
			V	1376	340	12.41
			Y	1554	432	15.77
			Z	1495	449	16.39
			AB	1164	253	9.24
	6	22	A	1415	440	14.60
			AA	1286	311	10.32
			B	1533	446	14.80
			F	1497	465	15.43
			G	1381	287	9.53
			H	1548		
			J	1461	407	13.51
			K	1423	400	13.28
			L	1345	309	10.26
			M	1200	295	9.79
			N	1583		
			P	1171	252	8.36
			S	1350	339	11.25
			U	1195	268	8.90
			X	1241	295	9.79
			Z	1460	464	15.40
			D	1536	393	13.04
	7	21	A	1396	309	10.74
			B	1489	456	15.86
			C	1361	312	10.85
			D	1601	464	16.13
			E	1285	240	8.35
			F	1145	210	7.30
			G		272	9.46
			H	1250	274	9.53
			I	1385	321	11.16
			J	1214	233	8.10
			K	1479	383	13.32
			L		263	9.15

2010 skeletal size and weight data, continued

Tank Treatment	Tile ID	Tile Age (days)	Coralite ID	Size (μm)	Weight (μg)	ASN Weight (μg mm^{-1}day^{-1})
			M	1249	247	8.59
			N		283	9.84
			O	1390		
			P	1060	461	16.03
			Q	1579	391	13.60
	10	22	C	1323	326	10.82
			D	1061	224	7.43
Tank 7 Average				1369	339	11.69
8	4	21	K	1230		
1670 ppm CO_2			L	1425	327	12.19
Unfed			P	1289		
			Q	1631	402	14.99
			R	1383	300	11.18
			S	1534	357	13.31
	5	21	A	1396	237	8.83
			D	1147	206	7.68
			F		224	8.35
			I	1084	165	6.15
			M	1087	207	7.72
			N	1268		
			O	1526	328	12.23
			P	1289	298	11.11
	6	20	E	1448	386	15.11
			F	1456	289	11.31
			G	1304	172	6.73
			H	1464	293	11.47
			I	1165	197	7.71
			K	1405	243	9.51
			L	1135	200	7.83
			O	1247	197	7.71
	7	22	A	1303	224	7.97
			B	1401	291	10.35
			C	850	109	3.88
			D	1113	166	5.91
	9	21	C	1148	217	8.09
			D	988	150	5.59
			UNNAMED	977		
	12	20	A	1508	343	13.43
			B	1123		
Tank 8 Average				1277	251	9.47

2010 skeletal size and weight data, continued

Tank Treatment	Tile ID	Tile Age (days)	Coralite ID	Size (μm)	Weight (μg)	ASN Weight (μg mm^{-1}day^{-1})
9	4	21	A	2324		
1670 ppm CO_2			D	2887	786	18.07
Fed			F	1728	263	6.05
			K	1898		
	6	21	B	2773	622	14.30
			C	2010	452	10.39
			D		202	4.64
			F	2032	439	10.09
	9	23	A	1706	296	6.21
			B	2181	559	11.73
			C	1421	191	4.01
	10	21	A	1743		
			B	2197	525	12.07
			C	2027	444	10.21
Tank 9 Average				2071	434	9.80
10	3	21	A	2666	746	16.73
420 ppm CO_2			B	2685	643	14.42
Fed			C		575	12.90
			D	2319	578	12.96
	10	21	A	2131	524	11.75
			B	1675	358	8.03
			D	1731	348	7.81
			E	1866	491	11.01
			F	2312	781	17.52
			H	1510	329	7.38
			I	2336	617	13.84
Tank 10 Average				2123	545	12.21
11	3	20	H	2327	617	14.04
420 ppm CO_2			K		694	15.79
Fed			L	2672	830	18.89
			P	2882	806	18.34
			Q	2497	747	17.00
			R	2079		
			U	2085	492	11.20
			AP	2434	696	15.84
			AQ	1735	412	9.38
			AR		474	10.79
			E	1607	313	7.12
	7	21	I	1652	280	6.07
Tank 11 Average				2197	578	13.13

2010 skeletal size and weight data, continued

Tank Treatment	Tile ID	Tile Age (days)	Coralite ID	Size (μm)	Weight (μg)	ASN Weight (μg mm^{-1}day^{-1})
12	4	22	I	2301	595	12.87
1670 ppm CO_2			J	1819	341	7.38
Fed			O	2413	509	11.01
			P	2297	484	10.47
			Q	1847	360	7.79
			R	1662	207	4.48
			U		765	16.55
	5	22	E	2523	654	14.15
			G	2519	565	12.23
			I	2171	340	7.36
	8	20	A	1689	330	7.85
			B	1868	417	9.93
Tank 12 Average				2101	464	10.17

Table A.1: Skeletal size (i.e., septa diameter), Weight (i.e., mass $CaCO_3$), and Age-and Size-Normalized (ASN) weight of juvenile *Favia fragum* from the 2010 CO_2 x Feeding experiment. ASN Weight is the total mass of $CaCO_3$ for the sample divided by the average skeletal size for the tank and the average age of the sample.

A.2 2010 Coral Tissue Lipid Data

Tank Treatment	Sample ID	Average Age (days)	Total Lipid (μg)	AN Lipid (μg mm^{-2}spat^{-1})	AAN Lipid (μg mm^{-2}day^{-1}spat^{-1})
1	LIP 59	21	92	6.29	0.30
1670 ppm CO_2	LIP 60	21	88	6.05	0.29
Unfed	LIP 61	20	118	8.11	0.41
	LIP 96	21.3	145	9.96	0.47
Tank 1 Average			111	7.60	0.37
2	LIP 74	22	416	12.26	0.56
420 ppm CO_2	LIP76	21	389	11.45	0.55
Fed	LIP 98	21.4	392	11.54	0.54
Tank 2 Average			399	11.75	0.55
3	LIP 62	21	178	10.95	0.52
420 ppm CO_2	LIP 64	20	151	9.32	0.47
Unfed	LIP 95	21	159	9.78	0.47
Tank 3 Average			162	10.02	0.48
4	LIP 78	22	138	9.94	0.45
1670 ppm CO_2	LIP 79	21	243	17.51	0.83
Unfed	LIP 77	22	115	8.29	0.38
Tank 4 Average			165	11.91	0.55
5	LIP 80	21.7	420	13.17	0.61
1670 ppm CO_2					
Fed					
Tank 5 Average			420	13.17	0.61
6	LIP 91	20.5	137	9.38	0.46
420 ppm CO_2	LIP 92	21.5	154	10.54	0.49
Unfed	LIP 65	21	176	12.05	0.57
	LIP 66	20	178	12.19	0.61
Tank 6 Average			161	11.04	0.53
7	LIP 72	21	152	10.29	0.49
420 ppm CO_2	LIP 73	20.3	203	13.78	0.68
Unfed	LIP 93	21	105	7.13	0.34
	LIP 94	22	133	9.03	0.41
Tank 7 Average			148	10.06	0.48
8	LIP 84	21	263	20.48	0.98
1670 ppm CO_2	LIP 85	21	150	11.70	0.56
Unfed					
Tank 8 Average			206	16.09	0.77
9	LIP 86	22	426	12.64	0.57
1670 ppm CO_2	LIP 87	21	377	11.19	0.53
Fed	LIP 100	21.1	295	8.74	0.41
Tank 9 Average			366	10.86	0.51

2010 lipid data, continued

Tank Treatment	**Sample ID**	**Average Age (days)**	**Total Lipid (μg)**	**AN Lipid (μg mm^{-2}spat^{-1})**	**AAN Lipid (μg mm^{-2}day^{-1}spat^{-1})**
10	LIP 99	21.9	466	13.15	0.60
420 ppm CO_2	LIP 88	22	450	12.70	0.58
Fed					
Tank 10 Average			458	12.92	0.59
11	LIP 68	20	499	13.15	0.66
420 ppm CO_2	LIP 97	22	478	12.61	0.57
Fed					
Tank 11 Average			488	12.88	0.62
12	LIP 69	21	336	9.68	0.46
1670 ppm CO_2	LIP 70	21	413	11.90	0.57
Fed	LIP 71	20	335	9.67	0.48
Tank 12 Average			361	10.42	0.50

Table A.2: Total lipid weight, Area-Normalized (AN) lipid weight and Age- and Area-Normalized (AAN) lipid weight. AN Lipid is the total mass of lipid measured for a given sample divided by the number of specimens in that sample (10) and the circular area defined by the average skeletal size (i.e., septa diameter) for the tank (derived from Appendix A.1). AAN Lipid is AN Lipid divided by the average age of the sample.

A.3 2010 Symbiont Density Data

Tank Treatment	Sample ID	Average Age (days)	Symbionts (cells)	AN Symbionts ($x10^3$cells $mm^{-2}spat^{-1}$)	AAN Symbionts ($x10^3$cells $mm^{-2}day^{-1}spat^{-1}$)
1	ZOOX 11	21.0	71.5	24.54	1.17
1670 ppm CO_2	ZOOX 12	20.0	42.5	14.58	0.73
Unfed	ZOOX 13	20.0	45.5	15.61	0.78
Tank 1 Average			53.1	18.25	0.89
2	ZOOX 25	21	128.5	18.93	0.90
420 ppm CO_2	ZOOX 26	20	115.1	16.97	0.85
Fed	ZOOX 27	20	87.9	12.96	0.65
	ZOOX 47	21	167.8	24.72	1.18
Tank 2 Average			124.8	18.39	0.89
3	ZOOX 14	21	48.0	14.80	0.70
420 ppm CO_2	ZOOX 15	20	33.3	10.27	0.51
Unfed	ZOOX 44	21	27.4	8.46	0.40
	ZOOX 45	21	25.2	7.78	0.37
Tank 3 Average			33.5	10.33	0.50
4	ZOOX 28	21	79.6	28.69	1.37
1670 ppm CO_2	ZOOX 29	20	62.3	22.45	1.12
Unfed	ZOOX 30	20	34.0	12.27	0.61
Tank 4 Average			58.7	21.14	1.03
5	ZOOX 31	21.0	110.4	17.32	0.82
1670 ppm CO_2	ZOOX 32	21.0	106.4	16.69	0.79
Fed	ZOOX 36	21.4	168.2	26.40	1.23
Tank 5 Average			128.3	20.14	0.95
6	ZOOX 16	21	51.5	17.65	0.84
420 ppm CO_2	ZOOX 17	21	27.1	9.29	0.44
Unfed	ZOOX 40b	20	26.5	9.09	0.45
	ZOOX 41	21	56.3	19.29	0.92
Tank 6 Average			40.4	13.83	0.66
7	ZOOX 23	21	72.3	24.53	1.17
420 ppm CO_2	ZOOX 24	20	46.2	15.67	0.78
Unfed	ZOOX 42	20	53.6	18.19	0.91
	ZOOX 43	21	47.3	16.07	0.77
Tank 7 Average			54.8	18.61	0.91
8	ZOOX 33	22	66.8	26.08	1.19
1670 ppm CO_2	ZOOX 34	21	93.4	36.43	1.73
Unfed	ZOOX 35	21	78.3	30.55	1.45

2010 symbiont data, continued

Tank Treatment	**Sample ID**	**Average Age (days)**	**Symbionts (cells)**	**AN Symbionts ($x10^3$cells $mm^{-2}spat^{-1}$)**	**AAN Symbionts ($x10^3$cells $mm^{-2}day^{-1}spat^{-1}$)**
Tank 8 Average			79.5	31.02	1.46
9	ZOOX 37	21	153.3	22.75	1.08
1670 ppm CO_2					
Fed					
Tank 9 Average			153.3	22.75	1.08
10	ZOOX 38	21	173.1	24.45	1.16
420 ppm CO_2	ZOOX 39	21	173.5	24.51	1.17
Fed	ZOOX 40a	21	120.4	17.01	0.81
Tank 10 Average			155.7	21.99	1.05
11	ZOOX 18	20	105.2	13.87	0.69
420 ppm CO_2	ZOOX 19	20	97.6	12.87	0.64
Fed	ZOOX 46	20.8	66.6	8.79	0.42
Tank 11 Average			89.8	11.84	0.59
12	ZOOX 20	21	99.8	14.40	0.69
1670 ppm CO_2	ZOOX 21	20	95.5	13.78	0.69
Fed	ZOOX 22	20	78.2	11.28	0.56
Tank 12 Average			91.2	13.15	0.65

Table A.3: Symbiont count, Area-Normalized (AN) Symbiont density, and Area- and Age-Normalized (AAN) Symbiont density for the 2010 CO_2 x Feeding experiment. Symbionts is the average number of zooxanthellae cells counted in the hemacytometer grid, AN Symbionts is the total symbiont density for the sample divided by the number of specimens in that sample (5) and the circular area defined by the average skeletal size (i.e., septa diameter) for the tank (derived from Appendix A.1), and AAN Symbionts is AN Symbionts divided by the average age of the sample.

A.4 2010 Pigment Data

Tank Treatment	Sample ID	Average Age (days)	Pigment (ng *chl a*)	AN Pigment (ng *chl a* $mm^{-2}spat^{-1}$)	AANPigment (ng *chl a* $mm^{-2}day^{-1}spat^{-1}$)
1	RNA 22	20.0	114.71	15.76	0.79
1670 ppm CO_2	RNA 23	21.6	210.38	28.90	1.34
Unfed	RNA 24	22.0	214.20	29.43	1.34
Tank 1 Average			179.76	24.70	1.15
3	RNA 19	22.0	208.26	25.70	1.17
420 ppm CO_2	RNA 20	22.0	268.78	33.17	1.51
Unfed					
Tank 3 Average			238.52	29.44	1.34
4	RNA 5	22.0	221.48	31.92	1.45
1670 ppm CO_2	RNA 6	20.0	151.63	21.85	1.09
Unfed					
Tank 4 Average			186.56	26.89	1.27
6	RNA 11	22.0	117.28	16.06	0.73
420 ppm CO_2	RNA 12	22.0	162.57	22.26	1.01
Unfed	RNA 13	22.0	431.09	59.03	2.68
Tank 6 Average			236.98	32.45	1.48
7	RNA 14	21.8	218.06	29.61	1.36
420 ppm CO_2					
Unfed					
Tank 7 Average			218.06	29.61	1.36
8	RNA 8	21.0	86.51	13.50	0.64
1670 ppm CO_2	RNA 9	21.0	106.81	16.67	0.79
Unfed	RNA 10	20.0	109.20	17.04	0.85
Tank 8 Average			100.84	15.74	0.76

Table A.4: Pigment mass, Area-Normalized (AN) Pigment density, and Area- and Age-Normalized (AAN) Pigment density for the 2010 CO_2 x Feeding experiment. Pigment is the total mass *chl a* in the sample, AN Pigment is the total pigment mass for the sample divided by the number of specimens in that sample (5) and the circular area defined by the average skeletal size (i.e., septa diameter) for the tank (derived from Appendix A.1), and AAN Pigment is AN Pigment divided by the average age of the sample.

A.5 2010 Statistical Analyses

A.5.1

Source	**df**	**MS**	***F***	***p***
Feeding	1	2.108	126.876	<0.001
CO_2	1	0.01	0.579	0.469
CO_2 x Feeding	1	0.000	0.004	0.949
Error	8	0.017		

Results from two-way ANOVA for skeletal development (% spat). Data were arc sin square root transformed in order to homogenize variances prior to analyses. Table reports df (degrees of freedom), and MS (mean sum of squares), F (F statistic) and p (significance level) for indicated sources.

A.5.2

Source	**df**	λ	***F***	***p***
Feeding	2, 7	0.010	337.628	<0.001
CO_2	2, 7	0.064	50.924	<0.001
CO_2 x Feeding	2, 7	0.630	2.055	0.199
Tank (CO_2x Feeding)	16, 558	0.953	0.858	0.619

Results from two-way, nested MANOVA of mean corallite diameter and weight. Dependent variables were weight and diameter, tank effect was nested within CO_2 and feeding interaction. Prior to analysis, corallite weight was natural log transformed and diameter was square root transformed. Table reports df (degrees of freedom), λ (Wilk's lambda), F (F statistic) and p (significance level) for indicated sources.

A.5.3

		Weight			Diameter		
Source	**df**	**MS**	***F***	***p***	**MS**	***F***	***p***
Feeding	1	10.002	136.696	<0.001	3893.983	589.073	<0.001
CO_2	1	4.766	65.135	<0.001	35.606	5.386	0.049
CO_2 x Feeding	1	0.097	1.326	0.283	0.144	0.022	0.886
Tank (CO_2 x Feeding)	8	0.073	0.688	0.702	6.610	0.741	0.655
Error	280	0.107			8.923		

Univariate results on each dependent variable used in the MANOVA F-tests were declared significant at alpha = 0.0062 determined for a Bonferroni correction on a total of eight F-tests. Table reports df (degrees of freedom), λ (Wilk's lambda), F (F statistic) and p (significance level) for indicated sources.

A.5.4

		Tissue Lipid Conent			Symbiont Density		
Source	**df**	**MS**	***F***	***p***	**MS**	***F***	***p***
Feeding	1	2.817E-03	2.279	0.170	1.201E+07	0.136	0.722
CO_2	1	1.150E-04	0.093	0.768	2.164E+08	2.456	0.156
CO_2 x Feeding	1	1.170E-04	0.095	0.766	1.670E+08	1.895	0.206
Tank (CO_2 x Feeding)	8	1.236E-03	2.870	0.022	8.811E+07	4.158	0.003
Error	24	4.310E-04			2.119E+07		

Results from two-way, nested ANOVAs for mean, area-normalized tissue lipid content and symbiont density. Lipid data were -1/x transformed to homogenize the variances prior to analysis. Table reports df (degrees of freedom), MS (mean sum of squares), F (F statistic) and p (significance level) for indicated sources.

A.5.5

Treatment	Skeletal Development	Skeletal Diameter ANOVA (MANOVA)	Skeletal Weight ANOVA (MANOVA)	Symbiont Density	Lipid Weight
Ambient CO_2 Fed	11, 12, 45	10, 10, 44 (10, 10, 41)	11, 11, 42 (10, 10, 41)	4, 3, 3	2, 3, 3
Ambient CO_2 Unfed	39, 36, 54	42, 34, 60 (39, 26, 51)	41, 27, 55 (39, 26, 51)	4, 4, 4	4, 4, 3
High CO_2 Fed	14, 17, 17	11, 13, 12 (11, 10, 11)	12, 11, 11 (11, 10, 11)	2, 2, 3	3, 3, 2
High CO_2 Unfed	33, 35, 44	30, 31, 39 (25, 25, 35)	26, 27, 37 (25, 25, 35)	3, 3, 3	2, 3, 4

Sample size (n) for each statistical assessment reported in order of tank replicate (1, 2, 3) for a given condition

Appendix B

Data for Chapter 4

B.1 2011 Skeletal Size and Weight Data

Tank Treatment	Tile ID	Tile Age (days)	Coralite ID	Size (μm)	Weight (μg)	ASN Weight ($\mu g\ mm^{-1} day^{-1}$)
1	1	21	A	1008		
1670 ppm CO_2			B	1264	219	8.46
Unfed			C	1105	210	8.11
			D	1308	233	9.00
			F	1185	251	9.69
			E	1197	176	6.80
			H	1430	300	11.59
			J	1287	217	8.38
			L	1193		
			M	1303		
	2	21	B	1283		
Tank 1 Average				1233	229	8.86
2	3	24	B	1840	461	10.54
420 ppm CO_2			E	1414	316	7.23
Fed			G	2147	739	16.90
			I	1720	348	7.96
			K	1466	304	6.95
	10	23	A	2074		
			C	1277	316	7.54
			H	1760	434	10.36
			I	1229	248	5.92
			J	1970	588	14.03
	15	23	F	1285	256	6.11
			G	2125	574	13.70
			P	2114	589	14.06
			Q	2236	603	14.39
			T	1640	443	10.57
	16	23	A	2255		
			B	2472	600	14.32
			D	1769	390	9.31
Tank 2 Average				1822	451	10.62
3	1	21	B	1483	350	12.25
1200 ppm CO_2			C	1269	258	9.03
Unfed			J	1350	340	11.90
	2	21	B	1264	129	4.52

2011 skeletal size and weight data, continued

Tank Treatment	Tile ID	Tile Age (days)	Coralite ID	Size (μm)	Weight (μg)	ASN Weight (μg mm^{-1}day^{-1})
			E	1246	227	7.95
	4	24	B	1436	368	11.27
	5	24	A	1537	452	13.85
	9	23	A	1428	307	9.81
			B	1351		
			C	1457	336	10.74
	19	22	C	1138	187	6.25
Tank 3 Average				1360	295	9.76
4	2	21	A	1506	270	10.53
2700 ppm CO_2	13	23	C	1312	212	7.55
Unfed			D	1331	242	8.62
	17	22	A	1393	257	9.57
			B	913	117	4.36
			C	1268	162	6.03
			D	1175	261	9.72
			E	1175	170	6.33
			F	1054		
			G	1017	131	4.88
			H	1078	138	5.14
			I	1296	213	7.93
			J	1250	176	6.55
			K	1319	237	8.83
			L	1325	194	7.22
			M	1117	177	6.59
Tank 4 Average				1221	197	7.32
5	1	21	A	1831	473	13.40
1200 ppm CO_2	2	21	A	1255	286	8.10
Fed	6	24	B	1527	413	10.24
			C	1505	414	10.26
			D	1792		
			E	1801	518	12.84
	15	23	H	1914	432	11.17
			M	1837	434	11.23
			L	1407	289	7.48
			N	2020	615	15.91
			O	1628	331	8.56
			C	1655	541	13.99
Tank 5 Average				1681	431	11.20
6	4	26	A	1155	185	5.97
1670 ppm CO_2			B	1198	203	6.55

2011 skeletal size and weight data, continued

Tank Treatment	**Tile ID**	**Tile Age (days)**	**Coralite ID**	**Size (μm)**	**Weight (μg)**	**ASN Weight (μg mm^{-1}day^{-1})**
Unfed			C	1151	211	6.81
			D	1211	211	6.81
			E	1247	190	6.13
			F	1152	164	5.29
			G	1164	157	5.07
			H	1471		
			I	1194		
			J	1167	177	5.71
			K	868		
			L	1149		
			M	1100	198	6.39
			N	1171		
			O	1205		
			P	1242		
			Q	1068		
			R	1041		
	5	24	A	1441	250	8.74
			B	1190	156	5.45
			C	1450	216	7.55
Tank 6 Average				1192	193	6.37
7	2	21	E	1546	249	6.78
1200 ppm CO_2			I	1274	251	6.84
Fed			J	1849	513	13.98
			K	1767		
	3	21	H	1231		
			D	1758	285	7.76
	6	25	H	1764	474	10.85
			I	2297	744	17.03
			J	2212	633	14.49
			G	1419	260	5.95
	8	25	B	2110	525	12.01
Tank 7 Average				1748	437	10.63
8	11	25	A	1227	188	5.88
2700 ppm CO_2			B	1476	264	8.25
Fed	13	24	Q	1453	252	8.21
			R	1104	169	5.50
			S	1270		
			T	1446	241	7.85
			U	1242	144	4.69
			V	1296	196	6.38

2011 skeletal size and weight data, continued

Tank Treatment	Tile ID	Tile Age (days)	Coralite ID	Size (μm)	Weight (μg)	ASN Weight ($\mu g\ mm^{-1} day^{-1}$)
	17	24	A	1216	217	7.07
			B	1201	192	6.25
			C	1019	115	3.75
			D	1107	126	4.10
			E	1679	365	11.89
			F	1359	237	7.72
			G	1223	181	5.89
			H	1385	260	8.47
			I	1331	203	6.61
			J	1252	196	6.38
			K	1292	177	5.76
			L	1211	171	5.57
			M	1234	205	6.68
			N	1289	192	6.25
			O	1408	223	7.26
			P	1053	111	3.61
			R	1306	239	7.78
			Q	1374	179	5.83
			S	1047	125	4.07
			T	1460	289	9.41
			U	1243	192	6.25
			V	1203	196	6.38
			W	1231	154	5.02
			X	1348	194	6.32
			Y	1095	158	5.15
			Z	1632	247	8.04
			AA	1456	262	8.53
			AB	1479	260	8.47
			AC	1151	157	5.11
			AD	1330	192	6.25
			AE	1089	112	3.65
			AF	1095	161	5.24
			AG	1259	215	7.00
			AH	908	74	2.41
			AI	1469		
			AJ	1076	157	5.11
			AK	1561	317	10.32
			AL	1273	213	6.94
Tank 8 Average				1279	198	6.44
9	9	25	F	1693		

2011 skeletal size and weight data, continued

Tank Treatment	Tile ID	Tile Age (days)	Coralite ID	Size (μm)	Weight (μg)	ASN Weight (μg mm^{-1}day^{-1})
420 ppm CO_2			G	1581	508	10.27
Fed	10	25	J	1770	671	13.56
			K	1488	471	9.52
			L	1884	663	13.40
	14	23	C	1432	390	8.57
			D	2545	1022	22.46
			E	2032	776	17.05
	16	23	A	2747	1062	23.34
			B	2613	970	21.31
Tank 9 Average				1979	726	15.50
10	12	25	M	1560	350	10.32
1670 ppm CO_2			N	1175	185	5.46
Unfed			O	1355	279	8.23
	13	24	A	1407	228	7.00
			K	1307	228	7.00
			L	1457	315	9.68
			M	1251	200	6.14
	14	24	N	1298	236	7.25
			O	1477	260	7.99
	16	24	F	1420	240	7.37
			G	1196	186	5.71
			H	1370	264	8.11
Tank 10 Average				1356	248	7.52
11	5	26	A	2129	342	6.79
2700 ppm CO_2			G	1916	500	9.92
Fed	6	26	A	1742	527	10.46
			D	1889	309	6.13
	7	26	H	1628	378	7.50
			L	1564	259	5.14
	8	26	A	1759	394	7.82
			B	1896		
			C	1941	566	11.23
			D	1993		
			E	1837	339	6.73
			G	1836	433	8.59
	13	25	A	2133	437	9.02
	16	24	A	2475		
			D	2331	425	9.14
Tank 11 Average				1938	409	8.21
12	2	22	D	1450	380	12.37

2011 skeletal size and weight data, continued

Tank Treatment	Tile ID	Tile Age (days)	Coralite ID	Size (μm)	Weight (μg)	ASN Weight (μg mm^{-1}day^{-1})
1200 ppm CO_2			E	1409	399	12.99
Unfed	3	21	C	1574	384	13.09
	6	21	E	1085	187	6.38
	7	21	A	1281	260	8.86
			B	1419	356	12.14
	12	25	F	1451	378	10.83
	14	24	A	1627	456	13.60
	17	24	N	1189	170	5.07
			O	1481	267	7.97
Tank 12 Average				1397	324	10.33
13	3	21	A	1404	332	12.03
420 ppm CO_2	6	21	A	1293		
Unfed			F	1235	260	9.42
			G	1361	297	10.76
			H (I)	1074	159	5.76
			K	1403	325	11.77
			L	1148	191	6.92
			N	1154	199	7.21
	9	21	A	1433	333	12.06
			L	1589	431	15.61
			F	1253	259	9.38
			G	1407	282	10.22
			E	1337	260	9.42
Tank 13 Average				1314	277	10.05
14	2	22	B	1462	279	9.62
2700 ppm CO_2			C	1254		
Unfed			D	1321		
	7	21	F	1207	161	5.82
			G	1198	180	6.50
			K	1340	224	8.09
			L	1305	204	7.37
			H (I)	1248	196	7.08
	8	21	E	1062	130	4.70
			F	1490	290	10.48
			G	1373		
			H	1457	230	8.31
			J	1322		
			K	1407	202	7.30
	15	24	F	1328	207	6.54
Tank 14 Average				1318	209	7.44

2011 skeletal size and weight data, continued

Tank Treatment	**Tile ID**	**Tile Age (days)**	**Coralite ID**	**Size (μm)**	**Weight (μg)**	**ASN Weight (μg mm^{-1}day^{-1})**
15	4	21	A	1328	235	7.77
1670 ppm CO_2			B	1496		
Unfed			F	1343	267	8.83
			L	1338	240	7.94
			M	1579	437	14.46
			J	1923	547	18.10
			K	1454	311	10.29
	6	21	A	1587	376	12.44
			B			
			C	1252		
			D	1095	193	6.38
Tank 15 Average				1439	326	10.78
16	1	22	A	1519	358	12.07
1200 ppm CO_2			B (C)	1404	279	9.41
Unfed			D	1436	338	11.40
			H	1216	200	6.74
			I	1255	230	7.76
			O	1279	204	6.88
			P	1494	355	11.97
			L	1266		
			S	1180	219	7.39
			G	1457	325	10.96
	10	24	G	1235	289	8.93
			D	1437	353	10.91
			C	1345	248	7.67
Tank 16 Average				1348	283	9.34
17	?	23	H	1540	665	13.50
1200 ppm CO_2			I	1870		
Unfed			J	1717		
			K	1643	412	8.36
	17	23	E	1873	477	9.68
			F	2782	809	16.42
			G	2375	487	9.89
			H	2993	1032	20.95
			I	2313	698	14.17
			J	2119	636	12.91
			K	1817	382	7.76
			L	2658	839	17.03
Tank 17 Average				2142	644	13.07
18	4	24	?	1241	195	4.17

2011 skeletal size and weight data, continued

Tank Treatment	Tile ID	Tile Age (days)	Coralite ID	Size (μm)	Weight (μg)	ASN Weight (μg mm^{-1}day^{-1})
420 ppm CO_2			C	1962	465	9.94
Fed			D	1528	352	7.52
			E	1403		
			F	1129	186	3.98
	13	22	B	2264	560	13.06
			C	1825	367	8.56
			F	2008		
			G	1919	455	10.61
			H	1829	458	10.68
			I	2051	598	13.94
			J	2112	709	16.53
			K	1815		
			L	2534		
			M	1841	416	9.70
			U	1976	522	12.17
	14	22	B	2087		
			C	2759	932	21.73
			F	2023		
			G	2369	576	13.43
			H	2261	549	12.80
Tank 18 Average				1949	489	11.26
19	10	22	A	1373	299	9.93
420 ppm CO_2			B	1033	160	5.31
Unfed			J	1471	496	16.47
	15	21	A(F)	1352	269	9.36
			E	1384	301	10.47
			D	1512	318	11.06
			J	1476	347	12.07
			M	1241	273	9.50
	17	20	A	1395	220	8.04
			D	1386	229	8.36
	18	20	A	1398	304	11.10
			C	1406	256	9.35
Tank 19 Average				1369	289	10.08
20	11	21	A	1827	411	11.77
2700 ppm CO_2			B	1482	305	8.74
Fed			C	1410	264	7.56
			G	1903	350	10.02
	12	21	A	1807	417	11.94
			B	1212	204	5.84

2011 skeletal size and weight data, continued

Tank Treatment	Tile ID	Tile Age (days)	Coralite ID	Size (μm)	Weight (μg)	ASN Weight (μg mm^{-1}day^{-1})
			G	1785	385	11.03
			I	1668	416	11.91
			J	1605	301	8.62
			H	1338	211	6.04
	15	21	B	1801		
			E	1968	420	12.03
			I	1707	301	8.62
			J	1763		
Tank 20 Average				1663	332	9.51
21	13	21	A	1789	423	13.93
1200 ppm CO_2			B	1690	427	14.07
Fed			L	1313	193	6.36
			M	1548	288	9.49
	15	20	C	1333	222	7.68
			D	1282	211	7.30
			G	1224	193	6.68
			H	1311	233	8.06
			I	1412	225	7.78
			J	1635	370	12.80
			K	1364	257	8.89
Tank 21 Average				1446	277	9.37
22	2	23	E	1692		
1670 ppm CO_2	10	21	A	1384	271	7.96
Fed	11	21	C	1887	370	10.87
			E	1829	447	13.13
	13	24	A	1801	243	6.24
			B	1587	368	9.46
	14	21	D	1445	251	7.37
			F	1510	343	10.07
			G	1456	336	9.87
Tank 22 Average				1621	329	9.37
23	5	23	A	1547		
2700 ppm CO_2	11	22	B	1476	271	7.86
Fed			C	898	305	8.84
			D	1736	327	9.48
			E	1417		
	18	21	A	1656	330	10.02
			B	1504	287	8.72
			D	1368	243	7.38
			F	1666	406	12.33

2011 skeletal size and weight data, continued

Tank Treatment	**Tile ID**	**Tile Age (days)**	**Coralite ID**	**Size (μm)**	**Weight (μg)**	**ASN Weight (μg mm^{-1}day^{-1})**
			G	1921	348	10.57
			H	1699	339	10.30
			I	1535	302	9.17
			L	1766	399	12.12
			N	1762		
Tank 23 Average				1568	323	9.71
24	4	24	G	911	185	7.90
420 ppm CO_2			H		165	7.04
Unfed	5	24	A	1007		
			E	800	117	5.00
			F	701	131	5.59
			G	1137	218	9.31
	13	23	A	919	204	9.09
	10	23	A	1001	195	8.69
			E	1170		
			F	1138	252	11.23
Tank 24 Average				976	183	7.98

Table B.1: Skeletal size (i.e., septa diameter), Weight (i.e., mass $CaCO_3$), and Age-and Size-Normalized (ASN) weight of juvenile *Favia fragum* from the 2011 CO_2 x Feeding experiment. ASN Weight is the total mass of $CaCO_3$ for the sample divided by the average skeletal size for the tank and the average age of the sample.

B.2 2011 Coral Tissue Lipid Data

Specimen	Sample ID	Total Lipid (μg)	N Lipid (μg larvae^{-1})
Larvae	LIP 1	695	34.73
	LIP 2	630	31.50
	LIP 3	649	32.43
	LIP 4	588	29.38
	LIP 5	585	29.23
	LIP 6	634	31.70
	LIP 7	675	33.73
	LIP 8	550	27.50
	LIP 9	594	29.70
	LIP 10	612	30.60
	LIP 11	670	33.48
	LIP 12	602	30.08
	LIP 13	595	29.73
	LIP 14	621	31.03
	LIP 15	606	30.28
Larval Average		620	31.00

Tank Treatment	Sample ID	Average Age (days)	Total Lipid (μg)	AN Lipid (μg mm^{-2}spat^{-1})	AAN Lipid (μg mm^{-2}day^{-1}spat^{-1})
1	LIP 70	22.5	235	19.64	0.87
1670 ppm CO_2	LIP 71	22.6	383	32.03	1.42
Unfed	LIP 72	22	288	24.08	1.09
	LIP 73	22.1	321	26.84	1.21
Tank 1 Average			306	25.65	1.15
6	LIP 91	24	214	19.13	0.80
1670 ppm CO_2	LIP 92	23.6	291	26.07	1.10
Unfed	LIP 93	23	228	20.43	0.89
		21	322	72.12	3.43
Tank 6 Average			264	34.44	1.56
10	LIP 25	21	252	24.92	1.19
1670 ppm CO_2	LIP 109	24.2	180	12.43	0.51
Unfed	LIP 115	24.5	159	10.97	0.45
	LIP 116	25.1	149	10.28	0.41
	LIP 117	25.3	195	13.46	0.53
Tank 10 Average			187	14.41	0.62
13	LIP 30	21.4	246	18.09	0.85
420 ppm CO_2	LIP 31	21.2	270	19.90	0.94
Unfed	LIP 32	21	248	18.28	0.87
	LIP 33	21	284	20.93	1.00
	LIP 34	21	316	23.29	1.11

2011 lipid data, continued

Tank Treatment	**Sample ID**	**Average Age (days)**	**Total Lipid (μg)**	**AN Lipid (μg mm^{-2}spat^{-1})**	**AAN Lipid (μg mm^{-2}day^{-1}spat^{-1})**
Tank 13 Average			273	20.10	0.95
19	LIP 45	20.3	279	18.96	0.93
420 ppm CO_2	LIP 46	21	270	18.31	0.87
Unfed	LIP 47	20	189	14.23	0.71
	LIP 48	19.9	250	16.98	0.85
Tank 19 Average			247	17.12	0.84
24	LIP 16	21.5	229	30.54	1.42
420 ppm CO_2					
Unfed					
Tank 24 Average			229	30.54	1.42

Table B.2: Total lipid weight, Area-Normalized (AN) lipid weight and Age- and Area-Normalized (AAN) lipid weight. AN Lipid is the total mass of lipid measured for a given sample divided by the number of specimens in that sample and the circular area defined by the average skeletal size (i.e., septa diameter) for the tank (derived from Appendix B.1). AAN Lipid is AN Lipid divided by the average age of the sample. Lipid samples typically contain 10 corallites (20 larvae) with the exception of samples LIP 20, 25, and 47 which contained 4, 7, and 9 corallites respectively. Note: only a subset of samples collected were processed, specifically unfed corals at 420 and 1670 ppm CO_2 for comparison with 2012 results.

B.3 2011 Symbiont Density Data

Tank Treatment	Sample ID	Average Age (days)	Symbionts (cells)	AN Symbionts ($x10^3$cells $mm^{-2}spat^{-1}$)	AAN Symbionts ($x10^3$cells $mm^{-2}day^{-1}spat^{-1}$)
1	ZOOX 59	22	22.3	9.32	0.42
1670 ppm CO_2	ZOOX 60	22	25.6	10.70	0.49
Unfed	ZOOX 61	22	31.4	13.14	0.60
	ZOOX 62	22	35.8	14.99	0.68
	ZOOX 63	23	41.4	17.35	0.75
Tank 1 Average			31.3	13.10	0.59
6	ZOOX 89	24	16.3	7.28	0.30
1670 ppm CO_2	ZOOX 90	23	36.9	16.55	0.72
Unfed	ZOOX 91	23	21.8	9.74	0.42
	ZOOX 92	23	28.7	12.85	0.56
	ZOOX 93	23	44.8	20.05	0.87
Tank 6 Average			29.7	13.29	0.58
10	ZOOX 136	25	51.0	17.65	0.71
1670 ppm CO_2	ZOOX 137	25	17.8	6.17	0.25
Unfed	ZOOX 138	24	20.4	7.07	0.29
	ZOOX 139	25	37.2	12.87	0.51
	ZOOX 140	25	6.8	2.36	0.09
Tank 10 Average			26.7	9.22	0.37
13	ZOOX 15	21	58.4	21.51	1.02
420 ppm CO_2	ZOOX 16	21	33.4	12.32	0.59
Unfed	ZOOX 17	22	25.4	9.35	0.42
	ZOOX 18	22	20.3	7.48	0.34
	ZOOX 19	22	60.6	22.31	1.01
Tank 13 Average			39.6	14.60	0.68
19	ZOOX 32	22	35.8	12.17	0.55
420 ppm CO_2	ZOOX 33	22	25.6	8.68	0.39
Unfed	ZOOX 34	22	14.7	4.99	0.23
	ZOOX 35	20	11.1	3.76	0.19
	ZOOX 36	20	12.8	4.33	0.22
Tank 19 Average			20.0	6.79	0.32
24	ZOOX 69	24	23.8	15.92	0.66
420 ppm CO_2	ZOOX 70	23	26.8	17.88	0.78
Unfed	ZOOX 71	23	17.0	11.36	0.49
Tank 24 Average			22.5	15.05	0.64

Table B.3: Symbiont count, Area-Normalized (AN) Symbiont density, and Area- and Age-Normalized (AAN) Symbiont density for the 2011 CO_2 x Feeding experiment. Symbionts is the average number of zooxanthellae cells counted in the hemacytometer grid, AN Symbionts Lipid is the total symbiont density for the sample divided by the number of specimens in that sample (1) and the circular area defined by the average skeletal size (i.e., septa diameter) for the tank (derived from Appendix B.1), and AAN Symbionts is AN Symbionts divided by the average age of the sample.

B.4 2011 Pigment Data

Tank Treatment	Sample ID	Average Age (days)	Pigment (ng *chl a*)	AN Pigment (ng *chl a* $mm^{-2}spat^{-1}$)	AANPigment (ng *chl a* $mm^{-2}day^{-1}spat^{-1}$)
1	RNA 1	21.0	111.62	18.69	0.89
1670 ppm CO_2	RNA 40	22.4	61.06	10.23	0.46
Unfed	RNA 41	22.2	170.59	28.57	1.29
Tank 1 Average			114.42	19.16	0.88
6	RNA 56	24.0	128.59	23.04	0.96
1670 ppm CO_2	RNA 57	24.0	118.68	21.27	0.89
Unfed	RNA 58	23.0	129.68	23.24	1.01
Tank 6 Average			125.65	22.51	0.95
10	RNA 7	21.0	45.68	6.32	0.30
1670 ppm CO_2	RNA 75	24.6	57.24	7.92	0.32
Unfed					
Tank 10 Average			51.46	7.12	0.31
13	RNA 11	21.4	121.21	17.86	0.83
420 ppm CO_2	RNA 12	21.0	85.35	12.58	0.60
Unfed	RNA 13	21.0	101.22	14.92	0.71
Tank 13 Average			102.59	15.12	0.71
19	RNA 23	21.0	81.22	11.04	0.53
420 ppm CO_2	RNA 24	21.2	65.96	8.96	0.42
Unfed	RNA 25	21.0	61.14	8.31	0.40
Tank 19 Average			69.44	9.44	0.45
24	RNA 45	23.0	104.91	28.05	1.22
420 ppm CO_2	RNA 46	23.6	170.81	45.67	1.94
Unfed	RNA 47	23.0	100.12	26.77	1.16
Tank 24 Average			125.28	33.49	1.44

Table B.4: Pigment mass, Area-Normalized (AN) Pigment density, and Area- and Age-Normalized (AAN) Pigment density for the 2011 CO_2 x Feeding experiment. Pigment is the total mass *chl a* in the sample, AN Pigment is the total pigment mass for the sample divided by the number of specimens in that sample (5) and the circular area defined by the average skeletal size (i.e., septa diameter) for the tank (derived from Appendix B.1), and AAN Pigment is AN Pigment divided by the average age of the sample.

B.5 2012 Skeletal Size and Weight Data

Tank Treatment	Tile ID	Tile Age (days)	Coralite ID	Size (μm)	Weight (μg)	ASN Weight ($\mu g\ mm^{-1} day^{-1}$)
1	2	14	A	1215	133	8.66
420 ppm CO_2	6	14	A	1150	124	8.07
High Light			B	1008		
			C	1016		
			D	1017		
	9	14	A	1009	140	9.11
			B	1152	150	9.77
			C	1209		
			D	1104		
			E	1114		
	13	14	A	1062	123	8.01
			B	1272		
			C	1006	132	8.59
			D	947	101	6.58
	14	14	A	1140	102	6.64
			B	1210	179	11.65
			C	967		
			D	1228		
			E	1019	104	6.77
Tank 1 Average				1097	129	8.39
2	2	14	A	1130		
1670 ppm CO_2	3	14	A	1128	96	6.30
High Light	4	14	A	1098		
	5	14	A	1135		
	6	14	A	1333	165	10.82
	7	14	A	1271	172	11.28
			B	1371	136	8.92
	8	14	A	1009	84	5.51
			B	1252	132	8.66
	9	14	A	896	61	4.00
			B	1068	101	6.62
	10	14	A	1049	93	6.10
			B	1280	167	10.95
	11	14	A	963	76	4.98
			B	1146	100	6.56
			C	858	46	3.02
			D	984	85	5.57
			E	1183		
			F	842	67	4.39
			G	1122	110	7.21

2012 skeletal size and weight data, continued

Tank Treatment	Tile ID	Tile Age (days)	Coralite ID	Size (μm)	Weight (μg)	ASN Weight (μg mm^{-1}day^{-1})
			H	1023	108	7.08
	12	14	A	1232		
			B	1143		
			C	1114	115	7.54
	13	14	A	1061		
			B		82	5.38
			C	914	105	6.89
			D	1173	122	8.00
			E	807	64	4.20
			F	919		
			G	1211		
	14	14	A	1296	127	8.33
			B	953	72	4.72
			C	989	82	5.38
			D	1081	99	6.49
Tank 2 Average				1089	103	6.73
3	3	14	A	1226	135	8.25
1670 ppm CO_2	4	14	A	1229		
High Light			B	1050	105	6.42
			C	1239		
	9	14	A	1281		
			B			
			C	1408		
			D	1209	120	7.33
			E	1390	190	11.61
			F	1323	192	11.73
	10	14	A	1062	70	4.28
			B	926	65	3.97
			C	1320	144	8.80
			D	1212	105	6.42
	12	14	A		124	7.58
			B	1213		
			C	1073	102	6.23
			D	1387	160	9.78
	14	14	A	924	84	5.13
			B	1291	180	11.00
			C	1062	120	7.33
	15	14	A	1157	133	8.13
			B	1225		
			C	1106	156	9.53

2012 skeletal size and weight data, continued

Tank Treatment	Tile ID	Tile Age (days)	Coralite ID	Size (μm)	Weight (μg)	ASN Weight (μg mm^{-1}day^{-1})
			D	1021	111	6.78
			E	1101	116	7.09
			F			
			G	849		
			H	1034		
			I	1116		
			J	1302	168	10.27
			K	1164	106	6.48
Tank 3 Average				1169	128	7.82
4	2	14	A	958		
420 ppm CO_2	3	14	A	963		
High Light			B	1018	96	6.92
	4	14	A	1229		
	7	14	A	914	69	4.98
			B	970		
			C	1199	92	6.63
	8	14	A	1127	113	8.15
			B	1014	86	6.20
			C	1092	118	8.51
			D	1134	165	11.90
			E	1053	99	7.14
	9	14	A	1167	111	8.01
			B	928		
	10	14	A	839		
	11	14	A	921	43	3.10
	12	14	A	922		
	14	14	A	883	78	5.63
			B	892		
			C	776	64	4.62
			D	990	76	5.48
			E	917	89	6.42
			F	1050	105	7.57
			G	867	65	4.69
			H	930	82	5.91
			I	999		
Tank 4 Average				990	91	6.58
5	1	14	A	1341	225	13.80
420 ppm CO_2	2	14	A	1387	281	17.24
High Light	4	14	A	1213	175	10.74
	8	14	A	1480	326	20.00

2012 skeletal size and weight data, continued

Tank Treatment	Tile ID	Tile Age (days)	Coralite ID	Size (μm)	Weight (μg)	ASN Weight ($\mu g\ mm^{-1} day^{-1}$)
			B	1221	215	13.19
			C	1243	240	14.72
			x		331	20.31
	10	14	A	1197	181	11.10
			B	1363	259	15.89
			C	1275		
	11	14	A	1024	71	4.36
			B	818		
			C	1045	70	4.29
			D	1013	51	3.13
			E	1169	90	5.52
			F	1060	86	5.28
	12	14	A	896	62	3.80
			B	1189	144	8.83
			C	1114	110	6.75
	14	14	A	1197		
			B	1106		
			C	1073	77	4.72
			D	1194		
Tank 5 Average				1164	166	10.20
6	3	14	A	1053	97	5.79
1670 ppm CO_2	6	14	A	1262	115	6.87
High Light			B	1119	116	6.93
	8	14	A	1081	84	5.02
			B	1262	124	7.41
	9	14	A	1202	146	8.72
			B	1044	107	6.39
	10	14	A	1239	131	7.83
			B	1266	156	9.32
			C	1367	163	9.74
	11	14	A	1203	166	9.92
			B	1218	142	8.48
	12	14	A	932	85	5.08
			B	1091	118	7.05
	13	14	A	1359		
			B	1154	141	8.42
	14	14	A	1229		
			B	1230	151	9.02
	15	14	A	1245	160	9.56
			B	1360	155	9.26

2012 skeletal size and weight data, continued

Tank Treatment	Tile ID	Tile Age (days)	Coralite ID	Size (μm)	Weight (μg)	ASN Weight ($\mu g\ mm^{-1} day^{-1}$)
Tank 6 Average				1196	131	7.82
7	3	14	A	1341		
1670 ppm CO_2	6	14	A	1052	110	7.22
High Light			B	953		
	7	14	A	1345	119	7.81
			B	1214	86	5.64
			C	910	56	3.67
			D	1186	177	11.61
			E	1050	72	4.72
			F	1121	93	6.10
			G	1196	84	5.51
			H	909	104	6.82
			I	1206	109	7.15
			J	1132		
	8	14	A	1274	136	8.92
			B			
			C	818	57	3.74
			D	1126	122	8.00
			E	1168	118	7.74
	12	14	A	1125		
			B	1039	84	5.51
			C	1056	122	8.00
			D	1052		
	13	14	A	1092		
			B	869	71	4.66
			C	1162	90	5.91
			D	947	73	4.79
			E	1125	120	7.87
			F	991	89	5.84
			G	1183	148	9.71
			H	715	61	4.00
	14	14	A	1303	203	13.32
Tank 7 Average				1089	104	6.85
8	1	14	A	870	111	6.66
420 ppm CO_2	3	14	A	1173	108	6.48
High Light			B	1103		
	5	14	A	1237	221	13.25
			B	1335	221	13.25
			C	1344	218	13.07
	6	14	A	1257	185	11.10

2012 skeletal size and weight data, continued

Tank Treatment	Tile ID	Tile Age (days)	Coralite ID	Size (μm)	Weight (μg)	ASN Weight ($\mu g\ mm^{-1} day^{-1}$)
	8	14	A	1163	174	10.44
			B	1039	88	5.28
			C	1307	228	13.67
	9	14	A	1361	218	13.07
			B	1499	275	16.49
			C	1344		
			D	1365	189	11.34
	10	14	A	1169	180	10.80
			B	1205	167	10.02
	11	14	A	1119	161	9.66
			B	989	139	8.34
			C	1252	217	13.01
			D	1051	141	8.46
			E	1086	152	9.12
	12	14	A	1011	65	3.90
			B	1114	81	4.86
Tank 8 Average				1191	169	10.11
9	1	14	A	1204	128	7.96
1670 ppm CO_2			B	1107		
Low Light	2	14	A	1249	143	8.90
	3	14	A	1260	126	7.84
			B	1047	77	4.79
	7	14	A	1102	109	6.78
			B	1227	112	6.97
	8	14	A	940	15	0.93
			B	976		
	11	14	A	1206	153	9.52
			B	1308	136	8.46
			C	1221	127	7.90
			D	1348	173	10.76
			E	1172	146	9.08
			F	1284	143	8.90
	12	14	A	1090	96	5.97
			B	1119	127	7.90
			C	1142		
			D	1171		
	13	14	A	1024		
			B	906		
			C	1073	102	6.35
			D	1344	210	13.06

2012 skeletal size and weight data, continued

Tank Treatment	**Tile ID**	**Tile Age (days)**	**Coralite ID**	**Size (μm)**	**Weight (μg)**	**ASN Weight (μg mm^{-1}day^{-1})**
			E	941	58	3.61
			F	1180	136	8.46
			G	1267		
	14	14	A	1108	107	6.66
			B	1057	75	4.67
			C		122	7.59
	15	14	A	1039		
			B	1337	211	13.13
Tank 9 Average				1148	123	7.66
11	2	14	A	1014	241	14.29
420 ppm CO_2			B	744	111	6.58
Low Light			C	1107		
	3	14	A	1158	177	10.49
	4	14	A	1242	191	11.32
	5	14	A	1374	265	15.71
			B	1149		
	8	14	A	1385	243	14.41
			B	1327	243	14.41
			C	1276		
	10	14	A	1139	152	9.01
			B	1261	181	10.73
			C	1226	187	11.09
			D	1219	178	10.55
	13	14	A	1291	136	8.06
			B	1217	195	11.56
	15	14	A	1199	184	10.91
			B	1263	180	10.67
			C	1127	109	6.46
			D	1349	243	14.41
			E	1362	252	14.94
			F	1165	146	8.66
			G	1150	149	8.83
			H	1149		
			I	1200		
			J	1226	178	10.55
			K	1118	108	6.40
			L	1231		
			M	1269		
Tank 11 Average				1205	184	10.91
12	2	14	A	1284	158	9.22

2012 skeletal size and weight data, continued

Tank Treatment	Tile ID	Tile Age (days)	Coralite ID	Size (μm)	Weight (μg)	ASN Weight (μg mm^{-1}day^{-1})
1670 ppm CO_2	3	14	A	1260	130	7.59
Low Light	4	14	A	1180	162	9.45
			B	1113	86	5.02
			C	1216	151	8.81
	7	14	A	1179	138	8.05
			B	1421		
	9	14	A	1144	129	7.53
			B	1132	116	6.77
	10	14	A	1129	115	6.71
			B	1269	163	9.51
	11	14	A	1337		
			B	1360	186	10.85
	12	14	A	1307	177	10.33
			B	1061	104	6.07
	13	14	A	1042	78	4.55
			B	1204	138	8.05
			C	1155		
			D	1255	143	8.34
	14	14	A	1213	166	9.69
			B	1163	137	7.99
			C	1343	180	10.50
	15	14	A	1374	180	10.50
			B	1210	168	9.80
	16	14	A	1224	167	9.75
			B	1252	160	9.34
Tank 12 Average				1224	145	8.45
13	1	14	A	1085		
1670 ppm CO_2			B	751		
Low Light	6	14	A	1172	129	8.99
			B	1164	106	7.39
			C	1248		
	9	14	A	998	65	4.53
			B	1192	82	5.72
			C	1087	83	5.79
	11	14	A	934	62	4.32
			B		42	2.93
			C	905	63	4.39
	13	14	A	814	58	4.04
			B	974		
			C	885		

2012 skeletal size and weight data, continued

Tank Treatment	Tile ID	Tile Age (days)	Coralite ID	Size (μm)	Weight (μg)	ASN Weight (μg mm^{-1}day^{-1})
			D	1061		
			E	1139	107	7.46
			F	1182	100	6.97
			G	1087	95	6.62
			H	850	75	5.23
			I	944		
			J	1125	117	8.16
	14	14	A	1029	90	6.27
			B	1182	133	9.27
			C	861	46	3.21
			D	1049	85	5.93
			E	1197	108	7.53
			F	788	58	4.04
			H	925	73	5.09
			I	1086	114	7.95
			J	1157	112	7.81
			G	865		
Tank 13 Average				1025	87	6.07
14	2	14	A	1172	161	9.39
420 ppm CO_2			B	1176	161	9.39
Low Light			C	1354	223	13.01
			D	1119	155	9.04
			E	1346	239	13.95
	8	14	A	1155	171	9.98
			B	1267	176	10.27
			C	1242	171	9.98
			D	1577		
			E	1309		
	10	14	A	1099	109	6.36
			B	834	44	2.57
			C	1211		
	11	14	A	1238	217	12.66
			B	1206	181	10.56
			C	1259	173	10.09
			D	1379	277	16.16
	12	14	A	1262	76	4.43
			C	1184	79	4.61
			D	1242	48	2.80
			E	849	27	1.58
			F	1286	84	4.90

2012 skeletal size and weight data, continued

Tank Treatment	Tile ID	Tile Age (days)	Coralite ID	Size (μm)	Weight (μg)	ASN Weight ($\mu g\ mm^{-1} day^{-1}$)
			G	1392		
Tank 14 Average				1224	146	8.51
15	1	14	A	1174	162	9.94
420 ppm CO_2			B	1148	132	8.10
Low Light			C	1170	158	9.69
	2	14	A	1326	183	11.23
	3	14	A	1176	173	10.61
	4	14	A	1490		
			B	1361	226	13.86
	5	14	A	1174	183	11.23
			B	908		
	6	14	A	1223	138	8.46
			B	1022		
	8	14	A	1250	173	10.61
			B	1269	172	10.55
	9	14	A	1259	198	12.15
			B	1314	221	13.56
	11	14	A	1055	63	3.86
			B	1082	87	5.34
			C	929	95	5.83
			D	1107	67	4.11
			E	1262	120	7.36
	13	14	A	1138	140	8.59
			B	1046	109	6.69
			C	1118	148	9.08
			D	982	95	5.83
			E	1113	152	9.32
			F	1182	183	11.23
Tank 15 Average				1164	147	9.01
16	2	14	A	1233	169	10.90
1670 ppm CO_2	3	14	A	1166		
Low Light	4	14	A	984		
	5	14	A	1249	104	6.71
			B	1244	142	9.16
			C	1127	112	7.22
	7	14	A	1049	86	5.54
			B	1405	174	11.22
			C	1312	152	9.80
	10	14	A	1098	104	6.71
			B	1314	165	10.64

2012 skeletal size and weight data, continued

Tank Treatment	Tile ID	Tile Age (days)	Coralite ID	Size (μm)	Weight (μg)	ASN Weight ($\mu g\ mm^{-1} day^{-1}$)
			C	1052		
			D	1239	134	8.64
			E	1290	152	9.80
			F	1080	91	5.87
			G	1266	150	9.67
	12	14	A	904	156	10.06
			B	889	107	6.90
			C	883	140	9.03
			D	964		
			E	861	145	9.35
			F	854	109	7.03
			G	1067	202	13.02
	13	14	A	967	85	5.48
			B	1037	66	4.26
			C	1274	141	9.09
Tank 16 Average				1108	131	8.46

Table B.5: Skeletal size (i.e., septa diameter), Weight (i.e., mass $CaCO_3$), and Age-and Size-Normalized (ASN) weight of juvenile *Favia fragum* from the 2012 CO_2 x Light experiment. ASN Weight is the total mass of $CaCO_3$ for the sample divided by the average skeletal size for the tank and the average age of the sample.

B.6 2012 Coral Tissue Lipid Data

Specimen	Sample ID	Total Lipid (μg)	N Lipid (μg larvae^{-1})
Larvae	LIP 1	449	22.45
	LIP 2	428	21.38
	LIP 3	424	21.18
	LIP 5	327	16.35
	LIP 6	390	19.48
	LIP 7	538	26.90
	LIP 8	382	19.10
	LIP 9	451	22.53
	LIP 11	493	24.63
	LIP 12	487	24.33
	LIP 13	412	20.58
	LIP 14	375	18.75
	LIP 15	320	15.98
	LIP 16	418	20.90
	LIP 17	427	21.33
	LIP 18	590	29.48
	LIP 19	448	22.40
	LIP 20	442	22.10
Larval Average		433	21.66

Tank Treatment	Sample ID	Average Age (days)	Total Lipid (μg)	AN Lipid (μg mm^{-2}spat^{-1})	AAN Lipid (μg mm^{-2}day^{-1}spat^{-1})
1	LIP 21	14	81	8.57	0.61
420 ppm CO_2	LIP 62	14	144	15.18	1.08
High Light	LIP 63	14	202	21.32	1.52
Tank 1 Average			142	15.02	1.07
2	LIP 22	14	141	15.13	1.08
1670 ppm CO_2	LIP 65	14	146	15.62	1.12
High Light	LIP 66	14	276	29.62	2.12
	LIP 67	14	131	14.06	1.00
Tank 2 Average			173	18.61	1.33
3	LIP 60	14	93	8.67	0.62
1670 ppm CO_2	LIP 61	14	160	14.86	1.06
High Light	LIP 68	14	146	13.60	0.97
	LIP 69	14	135	12.53	0.90
Tank 3 Average			133	12.42	0.89
4	LIP 57	14	73	9.47	0.68
420 ppm CO_2	LIP 58	14	114	14.80	1.06
High Light	LIP 59	14	52	6.75	0.48

2012 lipid data, continued

Tank Treatment	Sample ID	Average Age (days)	Total Lipid (μg)	AN Lipid (μg mm^{-2}spat^{-1})	AAN Lipid (μg mm^{-2}day^{-1}spat^{-1})
	LIP 70	14	154	19.99	1.43
Tank 4 Average			98	12.75	0.91
5	LIP 23	14	179	16.76	1.20
420 ppm CO_2	LIP 54	14	166	15.59	1.11
High Light	LIP 55	14	157	14.70	1.05
	LIP 56	14	147	13.76	0.98
Tank 5 Average			162	15.20	1.09
6	LIP 52	14	119	10.60	0.76
1670 ppm CO_2	LIP 53	14	169	15.05	1.07
High Light	LIP 71	14	131	11.66	0.83
Tank 6 Average			140	12.44	0.89
7	LIP 50	14	143	15.36	1.10
1670 ppm CO_2	LIP 72	14	125	13.38	0.96
High Light					
Tank 7 Average			134	14.37	1.03
8	LIP 24	14	83	7.45	0.53
420 ppm CO_2	LIP 44	14	81	7.27	0.52
High Light	LIP 48	14	126	11.27	0.80
Tank 8 Average			97	8.66	0.62
9	LIP 33	14	31	2.99	0.21
1670 ppm CO_2	LIP 45	14	20	1.93	0.14
Low Light	LIP 46	14	62	5.99	0.43
Tank 9 Average			38	3.64	0.26
11	LIP 38	14	48	4.17	0.30
420 ppm CO_2	LIP 39	14	85	7.41	0.53
Low Light	LIP 40	14	86	7.50	0.54
	LIP 73	14	32	2.76	0.20
Tank 11 Average			62	5.46	0.39
12	LIP 31	14	33	2.76	0.20
1670 ppm CO_2	LIP 32	14	110	9.35	0.67
Low Light	LIP 37	14	56	4.72	0.34
	LIP 75	14	36	3.06	0.22
Tank 12 Average			59	4.97	0.36
13	LIP 35	14	41	4.97	0.36
1670 ppm CO_2	LIP 36	14	41	4.91	0.35
Low Light	LIP 74	14	79	9.58	0.68
Tank 13 Average			54	6.49	0.46
14	LIP 28	14	71	5.99	0.43
420 ppm CO_2	LIP 29	14	78	6.63	0.47
Low Light	LIP 30	14	39	3.31	0.24

2012 lipid data, continued

Tank Treatment	**Sample ID**	**Average Age (days)**	**Total Lipid (μg)**	**AN Lipid (μg mm^{-2}spat^{-1})**	**AAN Lipid (μg mm^{-2}day^{-1}spat^{-1})**
	LIP 41	14	86	7.26	0.52
Tank 14 Average			68	5.80	0.41
15 420 ppm CO_2 Low Light	LIP 43	14	60	5.63	0.40
Tank 15 Average			60	5.63	0.40
16	LIP 25	14	83	8.56	0.61
1670 ppm CO_2	LIP 26	14	86	8.92	0.64
Low Light	LIP 27	14	79	8.19	0.59
Tank 16 Average			83	8.56	0.61

Table B.6: Reporting total lipid weight, Area-Normalized (AN) lipid weight and Age- and Area- Normalized (AAN) lipid weight. AN Lipid is the total mass of lipid measured for a given sample divided by the number of specimens in that sample and the circular area defined by the average skeletal size (i.e., septa diameter) for the sampled tank (derived from Appendix B.5). AAN Lipid is AN Lipid divided by the average age of the sample. Lipid samples typically contain 10 corallites (20 larvae).

B.7 2012 Symbiont Density Data

Tank Treatment	Sample ID	Average Age (days)	Symbionts (cells)	AN Symbionts ($x10^3$cells $mm^{-2}spat^{-1}$)	AAN Symbionts ($x10^3$cells $mm^{-2}day^{-1}spat^{-1}$)
1	ZOOX 49	14	5.0	2.64	0.19
420 ppm CO_2	ZOOX 50	14	8.2	4.34	0.31
High Light	ZOOX 51	14	5.3	2.80	0.20
	ZOOX 53	14	3.7	1.96	0.14
	ZOOX 72	14	8.1	4.26	0.30
Tank 1 Average			6.1	3.20	0.23
2	ZOOX 52	14	14.7	7.88	0.56
1670 ppm CO_2	ZOOX 55	14	13.9	7.48	0.53
High Light	ZOOX 56	14	23.4	12.54	0.90
	ZOOX 57	14	4.0	2.15	0.15
	ZOOX 73	14	18.6	9.99	0.71
Tank 2 Average			14.9	8.01	0.57
3	ZOOX 1	14	13.6	6.35	0.45
1670 ppm CO_2	ZOOX 44	14	12.3	5.73	0.41
High Light	ZOOX 45	14	11.4	5.33	0.38
	ZOOX 46	14	9.7	4.50	0.32
	ZOOX 54	15	12.0	5.59	0.37
Tank 3 Average			11.8	5.50	0.39
4	ZOOX 2	14	7.3	4.74	0.34
420 ppm CO_2	ZOOX 3	14	10.7	6.91	0.49
High Light	ZOOX 43	14	22.8	14.80	1.06
	ZOOX 47	14	9.8	6.33	0.45
	ZOOX 48	14	9.3	6.04	0.43
Tank 4 Average			12.0	7.76	0.55
5	ZOOX 37	14	11.7	5.47	0.39
420 ppm CO_2	ZOOX 38	14	10.9	5.10	0.36
	ZOOX 39	14	9.2	4.30	0.31
High Light	ZOOX 40	14	9.8	4.58	0.33
	ZOOX 41	14	12.8	6.01	0.43
Tank 5 Average			10.8	5.09	0.36
6	ZOOX 4	14	1.3	0.56	0.04
1670 ppm CO_2	ZOOX 5	14	16.8	7.46	0.53
High Light	ZOOX 6	14	14.4	6.41	0.46

2012 symbiont data, continued

Tank Treatment	Sample ID	Average Age (days)	Symbionts (cells)	AN Symbionts ($x10^3$cells $mm^{-2}spat^{-1}$)	AAN Symbionts ($x10^3$cells $mm^{-2}day^{-1}spat^{-1}$)
	ZOOX 42	14	10.8	4.81	0.34
	ZOOX 74	14	22.0	9.80	0.70
Tank 6 Average			13.0	5.81	0.41
7	ZOOX 27	14	22.1	11.85	0.85
1670 ppm CO_2	ZOOX 35	14	12.5	6.71	0.48
High Light	ZOOX 36	14	11.0	5.91	0.42
	ZOOX 58	14	14.2	7.60	0.54
	ZOOX 59	14	7.2	3.86	0.28
Tank 7 Average			13.4	7.19	0.51
8	ZOOX 8	14	33.4	14.99	1.07
420 ppm CO_2	ZOOX 33	14	10.8	4.83	0.34
High Light	ZOOX 62	14	19.1	8.58	0.61
	ZOOX 63	14	11.2	5.00	0.36
	ZOOX 64	14	10.8	4.83	0.34
Tank 8 Average			17.0	7.65	0.55
9	ZOOX 7	14	4.9	2.34	0.17
1670 ppm CO_2	ZOOX 31	14	24.6	11.86	0.85
Low Light	ZOOX 34	14	5.4	2.61	0.19
	ZOOX 60	14	28.0	13.52	0.97
	ZOOX 61	14	5.0	2.39	0.17
Tank 9 Average			13.6	6.54	0.47
11	ZOOX 24	14	32.5	14.26	1.02
420 ppm CO_2	ZOOX 25	14	23.6	10.36	0.74
Low Light	ZOOX 26	14	15.5	6.78	0.48
	ZOOX 32	14	16.1	7.05	0.50
Tank 11 Average			21.9	9.61	0.69
12	ZOOX 10	14	17.1	7.24	0.52
1670 ppm CO_2	ZOOX 13	14	23.6	10.01	0.71
Low Light	ZOOX 21	14	17.9	7.58	0.54
	ZOOX 22	14	16.4	6.97	0.50
	ZOOX 23	14	6.1	2.57	0.18
Tank 12 Average			16.2	6.88	0.49
13	ZOOX 9	14	18.1	10.95	0.78
1670 ppm CO_2	ZOOX 12	14	30.4	18.44	1.32
Low Light	ZOOX 28	14	21.9	13.25	0.95
	ZOOX 29	14	15.5	9.37	0.67
	ZOOX 30	14	17.7	10.71	0.76
	ZOOX 65	14	4.4	2.65	0.19
	ZOOX 75	14	5.9	3.55	0.25
Tank 13 Average			16.2	9.85	0.70

2012 symbiont data, continued

Tank Treatment	**Sample ID**	**Average Age (days)**	**Symbionts (cells)**	**AN Symbionts ($x10^3$cells $mm^{-2}spat^{-1}$)**	**AAN Symbionts ($x10^3$cells $mm^{-2}day^{-1}spat^{-1}$)**
14	ZOOX 11	14	4.9	2.08	0.15
420 ppm CO_2	ZOOX 18	14	3.6	1.51	0.11
Low Light	ZOOX 19	14	4.3	1.82	0.13
	ZOOX 20	14	13.5	5.73	0.41
	ZOOX 69	14	8.3	3.53	0.25
	ZOOX 70	14	18.9	8.03	0.57
Tank 14 Average			8.9	3.78	0.27
15	ZOOX 14	14	32.3	15.14	1.08
420 ppm CO_2	ZOOX 15	14	9.7	4.53	0.32
Low Light	ZOOX 16	14	3.1	1.46	0.10
	ZOOX 76	14	10.5	4.91	0.35
	ZOOX 77	14	6.5	3.05	0.22
Tank 15 Average			12.4	5.82	0.42
16	ZOOX 17	14	28.4	14.70	1.05
1670 ppm CO_2	ZOOX 66	14	19.3	9.98	0.71
Low Light	ZOOX 67	14	26.1	13.51	0.97
	ZOOX 68	14	5.3	2.72	0.19
	ZOOX 78	14	12.3	6.35	0.45
Tank 16 Average			18.2	9.46	0.68

Table B.7: Symbiont count, Area-Normalized (AN) Symbiont density, and Area- and Age-Normalized (AAN) Symbiont density for the 2012 CO_2 x Light experiment. Symbionts is the average number of zooxanthellae cells counted in the hemacytometer grid, AN Symbiont Lipid is the total symbiont density for the sample divided by the number of specimens in that sample (1) and the circular area defined by the average skeletal size (i.e., septa diameter) for the tank (derived from Appendix B.5), and AAN Symbionts is AN Symbionts divided by the average age of the sample.

B.8 2012 Pigment Data

Tank Treatment	Sample ID	Average Age (days)	Pigment (ng *chl a*)	AN Pigment (ng *chl a* $mm^{-2}spat^{-1}$)	AANPigment (ng *chl a* $mm^{-2}day^{-1}spat^{-1}$)
1	RNA 29	14	65.14	13.78	0.98
420 ppm CO_2	RNA 45	14	0.00	0.00	0.00
High Light		14			
Tank 1 Average			32.57	6.89	0.49
2	RNA 28	14	52.65	11.30	0.81
1670 ppm CO_2	RNA 30	14	0.00	0.00	0.00
High Light	RNA 31	14	0.00	0.00	0.00
Tank 2 Average			17.55	3.77	0.27
3	RNA 25	14	0.00	0.00	0.00
1670 ppm CO_2	RNA 41	14	0.00	0.00	0.00
High Light					
Tank 3 Average			0.00	0.00	0.00
4	RNA 42	14	0.00	0.00	0.00
420 ppm CO_2					
High Light					
Tank 4 Average			0.00	0.00	0.00
5	RNA 23	14	73.74	13.85	0.99
420 ppm CO_2	RNA 24	14	0.00	0.00	0.00
	RNA 33	14	0.00	0.00	0.00
High Light	RNA 33	14	148.75	27.94	2.00
Tank 5 Average			55.62	10.45	0.75
6	RNA 22	14	8.27	1.47	0.11
1670 ppm CO_2	RNA 32	14	0.00	0.00	0.00
High Light	RNA 43	14	0.00	0.00	0.00
Tank 6 Average			2.76	0.49	0.04
7	RNA 18	14	121.31	26.06	1.86
1670 ppm CO_2	RNA 20	14	0.00	0.00	0.00
High Light	RNA 21	14	60.01	12.89	0.92
Tank 7 Average			60.44	12.99	0.93
8	RNA 19	14	16.55	2.97	0.21
420 ppm CO_2	RNA 35	14	0.00	0.00	0.00
High Light	RNA 36	14	0.00	0.00	0.00
Tank 8 Average			5.52	0.99	0.07

2012 pigment data, continued

Tank Treatment	**Sample ID**	**Average Age (days)**	**Pigment (ng *chl a*)**	**AN Pigment (ng *chl a* $mm^{-2}spat^{-1}$)**	**AANPigment (ng *chl a* $mm^{-2}day^{-1}spat^{-1}$)**
9	RNA 16	14	89.45	17.28	1.23
1670 ppm CO_2	RNA 17	14	29.20	5.64	0.40
Low Light	RNA 34	14	0.00	0.00	0.00
Tank 9 Average			39.55	7.64	0.55
11	RNA 3	14	94.13	16.51	1.18
420 ppm CO_2	RNA 13	14	80.44	14.11	1.01
Low Light	RNA 15	14	108.16	18.98	1.36
Tank 11 Average			94.24	16.53	1.18
12	RNA 7	14	165.45	28.12	2.01
1670 ppm CO_2	RNA 37	14	64.56	10.97	0.78
Low Light	RNA 44	14	72.79	12.37	0.88
Tank 12 Average			100.93	17.16	1.23
13	RNA 12	14	68.21	16.55	1.18
1670 ppm CO_2	RNA 14	14	41.91	10.17	0.73
Low Light	RNA 46	14	28.92	7.02	0.50
Tank 13 Average			46.35	11.24	0.80
14	RNA 4	14	158.11	26.86	1.92
420 ppm CO_2	RNA 9	14	83.26	14.15	1.01
Low Light	RNA 11	14	68.48	11.64	0.83
Tank 14 Average			103.28	17.55	1.25
15	RNA 5	14	129.87	24.39	1.74
420 ppm CO_2	RNA 6	14	77.03	14.47	1.03
Low Light	RNA 38	14	36.31	6.82	0.49
Tank 15 Average			81.07	15.22	1.09
16	RNA 8	14	50.35	10.45	0.75
1670 ppm CO_2	RNA 39	14	43.70	9.07	0.65
Low Light	RNA 40	14	0.00	0.00	0.00
Tank 16 Average			31.35	6.50	0.46

Table B.8: Pigment mass, Area-Normalized (AN) Pigment density, and Area- and Age-Normalized (AAN) Pigment density for the 2012 CO_2 x Light experiment. Pigment is the total mass *chl a* in the sample, AN Pigment is the total pigment mass for the sample divided by the number of specimens in that sample (5) and the circular area defined by the average skeletal size (i.e., septa diameter) for the tank (derived from Appendix B.5), and AAN Pigment is AN Pigment divided by the average age of the sample.

B.9 Chapter 4 Statistical Analyses

B.9.1 Skeletal Size Comparison of 2011/2012 Unfed Corals

				t-test	
Group	**N**	**Mean**	**Standard Deviation**	**df**	***p***
2011	12	1.280	0.116	25	<0.001
2012	15	1.139	0.071		

Results from t-test comparing skeletal size of 2011/2012 unfed corals. Table reports N (sample size), standard deviation of each group, df (degrees of freedom), and MS (mean sum of squares), F (F statistic) and p (significance level) for indicated sources.

B.9.2 2011 Skeletal Size Analysis

Source	**df**	**MS**	***F***	***p***
Feeding	1	1.321	41.032	<0.001
CO_2	3	0.008	0.235	0.871
CO_2 x Feeding	3	0.049	1.511	0.250
Error	16	0.032		

Two-way ANOVA results for for 2011 skeletal size. Table reports df (degrees of freedom), and MS (mean sum of squares), F (F statistic) and p (significance level) for indicated sources.

B.9.3 2011 Skeletal Weight Analysis

Source	**df**	**MS**	***F***	***p***
Feeding	1	31.808	16.265	<0.001
CO_2	3	8.498	4.346	0.020
CO_2 x Feeding	3	2.510	1.283	0.314
Error	16	1.956		

Two-way ANOVA results for 2011 age- and size-normalized skeletal weight. Table reports df (degrees of freedom), and MS (mean sum of squares), F (F statistic) and p (significance level) for indicated sources.

B.9.4 2012 Skeletal Size Analysis

Source	df	MS	*F*	*p*
Light	1	5.560E-3	1.099	0.317
CO_2	1	2.013E-3	0.398	0.541
CO_2 x Light	1	8.611E-3	1.702	0.219
Error	11	5.059E-3		

Two-way ANOVA results for 2012 skeletal size. Table reports df (degrees of freedom), and MS (mean sum of squares), F (F statistic) and p (significance level) for indicated sources.

B.9.5 2012 Skeletal Weight Analysis

Source	df	MS	*F*	*p*
Light	1	0.955	0.623	0.447
CO_2	1	10.260	6.697	0.025
CO_2 x Light	1	0.083	0.054	0.820
Error	11	1.532		

Two-way ANOVA results for 2012 age- and size-normalized skeletal weight. Table reports df (degrees of freedom), and MS (mean sum of squares), F (F statistic) and p (significance level) for indicated sources.

B.9.6 Inter-year, (Low Light) Skeletal Weight Comparison

Source	df	MS	*F*	*p*
Year	1	11.876	13.829	0.005
CO_2	1	16.699	19.445	0.002
CO_2 x Year	1	0.699	0.814	0.391
Error	9	0.859		

Two-way ANOVA results for 2010/2012 skeletal weight. Table reports df (degrees of freedom), and MS (mean sum of squares), F (F statistic) and p (significance level) for indicated sources.

B.9.7 Inter-year, (High Light) Skeletal Weight Comparison

Source	df	MS	*F*	*p*
Year	1	0.596	0.376	0.554
CO_2	1	9.348	5.895	0.036
CO_2 x Year	1	0.062	0.039	0.847
Error	10	1.586		

Two-way ANOVA results for 2011/2012 age- and size-normalized skeletal weight. Table reports df (degrees of freedom), and MS (mean sum of squares), F (F statistic) and p (significance level) for indicated sources.

B.9.8 2012 Total Lipid Comparison

Source	df	MS	*F*	*p*
Light	1	8.118	28.296	<0.001
CO_2	1	3.67E-4	1.279E-3	0.972
CO_2 x Light	1	0.069	0.241	0.633
Error	11	0.287		

Two-way ANOVA results for 2012 age- and area-normalized total lipid. Data were -1/x transformed in order to homogenize variances prior to analyses. Table reports df (degrees of freedom), and MS (mean sum of squares), F (F statistic) and p (significance level) for indicated sources.

B.9.9 2012 Symbiont Density Comparison

Source	df	MS	*F*	*p*
Light	1	19.820E3	0.948	0.351
CO_2	1	28.450E3	1.361	0.268
CO_2 x Light	1	5.638E3	0.270	0.614
Error	11	20.899E3		

Two-way ANOVA results for 2012 age- and area-normalized symbiont density. Table reports df (degrees of freedom), and MS (mean sum of squares), F (F statistic) and p (significance level) for indicated sources.

B.9.10 2012 Pigment Comparison

Source	df	MS	*F*	*p*
Light	1	1.556	13.211	0.004
CO_2	1	0.174	1.474	0.250
CO_2 x Light	1	0.144	1.222	0.293
Error	11	0.118		

Two-way ANOVA results for 2012 age- and area-normalized pigment density. Table reports df (degrees of freedom), and MS (mean sum of squares), F (F statistic) and p (significance level) for indicated sources.

B.9.11 Inter-year, (Low Light) Total Lipid Comparison

Source	df	MS	*F*	*p*
Year	1	1.841	5.842	0.039
CO_2	1	0.062	0.196	0.668
CO_2 x Year	1	4.82E-4	1.531E-3	0.970
Error	9	0.315		

Two-way ANOVA results for 2010/2012 age- and area-normalized total lipid. Data were -1/x transformed in order to homogenize variances prior to analyses. Table reports df (degrees of freedom), and MS (mean sum of squares), F (F statistic) and p (significance level) for indicated sources.

B.9.12 Inter-year, (High Light) Total Lipid Comparison

Source	df	MS	*F*	*p*
Year	1	0.011	0.103	0.755
CO_2	1	0.006	0.056	0.817
CO_2 x Year	1	0.038	0.357	0.564
Error	10	0.106		

Two-way ANOVA results for 2011/2012 age- and area-normalized total lipid. Data were -1/x transformed in order to homogenize variances prior to analyses. Table reports df (degrees of freedom), and MS (mean sum of squares), F (F statistic) and p (significance level) for indicated sources

B.9.13 Inter-year, (Low Light) Symbiont Density Comparison

Source	df	MS	*F*	*p*
Year	1	4.818E5	11.074	0.009
CO_2	1	2.561E5	5.886	0.038
CO_2 x Year	1	7.792E4	1.791	0.214
Error	9	4.351E4		

Two-way ANOVA results for 2010/2012 age- and area-normalized symbiont density. Table reports df (degrees of freedom), and MS (mean sum of squares), F (F statistic) and p (significance level) for indicated sources.

B.9.14 Inter-year, (High Light) Symbiont Density Comparison

Source	df	MS	*F*	*p*
Year	1	2.272E4	1.104	0.318
CO_2	1	1.735E2	8.430E3	0.929
CO_2 x Year	1	5.931E3	0.288	0.603
Error	10	2.058E4		

Two-way ANOVA results for 2011/2012 age- and area-normalized symbiont density. Table reports df (degrees of freedom), and MS (mean sum of squares), F (F statistic) and p (significance level) for indicated sources.

B.9.15 Inter-year, (Low Light) Pigment Comparison

Source	df	MS	*F*	*p*
Year	1	0.216	3.753	0.085
CO_2	1	0.440	7.639	0.022
CO_2 x Year	1	0.006	0.105	0.753
Error	9	0.058		

Two-way ANOVA results for 2010/2012 age- and area-normalized pigment density. Table reports df (degrees of freedom), and MS (mean sum of squares), F (F statistic) and p (significance level) for indicated sources.

B.9.16 Inter-year, (High Light) Pigment Comparison

Source	**df**	**MS**	***F***	***p***
Year	1	0.767	4.506	0.060
CO_2	1	0.026	0.150	0.706
CO_2 x Year	1	0.015	0.090	0.770
Error	10	0.170		

Two-way ANOVA results for 2011/2012 age- and area-normalized pigment density. Table reports df (degrees of freedom), and MS (mean sum of squares), F (F statistic) and p (significance level) for indicated sources.

Appendix C

Data for Chapter 5

C.1 Tissue Thickness of Equatorial Pacific Coral Core Samples

Coral ID	Tissue Thicnkness (mm)	Coral ID	Tissue Thicnkness (mm)
West Jarvis		East Jarvis	
Short Core A1	6.87	Short Core A	7.96
Short Core A2	8.08	Short Core B	6.13
Short Core B	9.28	Short Core C	6.29
Short Core C	8.00	Short Core D	8.83
Short Core E	8.00	Short Core E	6.30
Long Core B	13.20	Long Core A	7.96
Long Core C	9.42	Long Core B	9.21
Long Core D	7.39	Long Core C	11.28
West Howland			
Short Core A	5.24		
Short Core B	7.47		
Short Core C	5.83		
Short Core D	5.72		
Short Core E	5.71		
Long Core A	7.24		
Long Core B	5.18		
Long Core F	6.14		
West Maiana		East Maiana	
Short Core C	5.22	Short Core B	7.00
Short Core D	4.63	Short Core C	5.66
Short Core E	4.93	Short Core D	5.27
Short Core F	5.01	Short Core E	5.51
Short Core G	4.35	Short Core F	4.75
Long Core A	4.94	Long Core A	5.23
Long Core B	5.89		
Long Core H	5.06		
Long Core I	6.04		
Long Core J	4.80		

Table C.1: Tissue thickness measurements from coral core samples collected from west and east sides of central equatorial Pacific islands in September 2012.

C.2 Water Chemistry Samples from 2012 Equatorial Pacific Sea Dragon Expedition

Date Sampled	Depth (meters)	GPS (latitude)	GPS (longitude)	Temp. (°C)	Sal. (psu)	Alk. (μeq kg^{-1})	DIC (μmol kg^{-1})	$[NH_4^+]$ (μM)	$[SiO_4]$ (μM)	$[PO_4^{3-}]$ (μM)	$[NO_2^{1-} + NO_3^{2-}]$ (μM)
Transit Hydrocasts											
Sept-7	0	2 °00.36 N	157°43.82 W	28.3	35.3	2321.8	2021.5	4.0	2.3	0.3	3.8
	150	2°00.36 N	157°43.82 W	14.2	34.7	2294.3	2142.0	2.7	18.9	1.3	18.4
	50	2°00.36 N	157°43.82 W	28.2	35.3	2327.0	2017.2	0.1	2.7	0.1	2.9
	100	2°00.38 N	157°43.83 W	28.0	35.3	2323.2	2019.0	3.5	2.6	0.1	3.4
Sept-8	0	1°00.16 S	157°45.02 W	28.0	35.5	2339.9	2037.3	2.3	2.4	0.3	4.0
	50	1°00.16 S	157°45.02 W	28.0	35.5	2340.6	2025.4	1.7	3.4	0.2	4.0
	100	1°00.16 S	157°45.02 W	27.8	35.5	2331.0	2047.3	1.3	2.4	0.3	4.3
	150	1°00.16 S	157°45.02 W	25.5	35.9	2354.7	2114.6	1.5	3.4	0.7	8.6
Sept-9	150	0°00.14 N	157°45.16 W	25.1	35.5	2328.0	2056.0	1.5	3.2	0.2	5.9
	0	0°00.03 S	157°45.75 W	27.4	35.5	2328.5	2036.7	2.4	2.2	0.1	4.0
	100	0°00.14 N	157°45.16 W	27.2	35.4	2323.1	2043.0	3.8	3.0	0.9	5.7
	50	0°00.14 N	157°45.16 W	27.5	35.5	2316.6	2042.5	1.2	2.7	0.1	4.5
Sept-9	0	1°00.33 N	157°44.97 W	27.7	35.3	2311.7	2050.7	0.8	2.6	0.2	3.9
	50	1°00.33 N	157°44.97 W	27.5	35.3	2313.4	2031.3	1.1	3.0	0.2	3.9
	100	1°00.33 N	157°44.97 W	27.0	35.1	2303.1	2054.3	<0.05	4.1	0.4	6.7
	150	1°00.33 N	157°44.97 W	22.7	34.8	2298.3	2097.4	0.4	9.8	0.7	11.4
Sept-18	0	1°33.00 N	165°00.11 W	28.9	35.2	2307.4	2004.4	6.0	2.1	0.2	2.4
	50	1°33.00 N	165°00.11 W	28.7	35.2	2299.8	2005.6	2.5	1.9	<0.05	2.0
	100	1°33.00 N	165°00.11 W	27.6	35.3	2307.2	2036.8	0.2	2.9	0.2	5.0
	150	1°33.00 N	165°00.11 W	25.1	35.0	2304.9	2072.1	1.4	5.4	0.4	7.9

2012 Sea Dragon water chemistry, continued

Date Sampled	Depth (meters)	GPS (latitude)	GPS (longitude)	Temp. (°C)	Sal. (psu)	Alk. (μeq kg^{-1})	DIC (μmol kg^{-1})	$[NH_4^+]$ (μM)	$[SiO_4]$ (μM)	$[PO_4^{3-}]$ (μM)	$[NO_2^{1-} + NO_3^{2-}]$ (μM)
Sept-20	0	0°59.96 N	169°59.47 W	28.1	35.2	2305.8	2025.5	0.9	2.7	0.1	3.0
	50	0°59.96 N	169°59.47 W	28.1	35.2	2300.3	2015.0	0.3	2.5	0.1	3.2
	100	0°59.96 N	169°59.47 W	27.0	35.2	2302.6	2035.8	1.2	3.1	0.2	5.4
	150	0°59.96 N	169°59.47 W	22.3	35.1	2312.8	2084.1	0.1	6.4	0.5	8.6
Sept-25	0	0°59.84 N	178°33.64 W		35.2	2308.6	1999.0	3.6	1.8	<0.05	1.5
	50	0°59.84 N	178°33.64 W		35.2	2310.2	1998.3	1.3	2.0	0.2	2.0
	100	0°59.84 N	178°33.64 W		35.4	2312.7	2026.7	0.8	2.9	<0.05	4.3
	150	0°59.84 N	178°33.64 W		35.3	2316.4	2074.4	0.6	4.6	0.2	7.7
Oct-2	0	1°00.7601 N	172°46.4032 E	27.5	35.4	2321.9	2054.2	<0.05	3.1	0.1	6.6
	50	1°00.7601 N	172°46.4032 E	29.9	35.3	2311.2	1996.2	<0.05	1.8	<0.05	0.1
	100	1°00.7601 N	172°46.4032 E	30.0	34.8	2276.1	1960.6	<0.05	5.9	0.3	9.1
	150	1°00.7601 N	172°46.4032 E	23.9	35.3	2318.2	2089.7	0.4	1.7	<0.05	<0.05
East Jarvis											
Sept-13	0	0°22.27 S	159°56.22 W	27.7	35.5	2335.5	2035.3	2.7	2.7	0.2	4.4
	50	0°22.27 S	159°56.22 W	27.6	35.5	2325.0	2041.4	5.7	2.6	1.4	4.8
	100	0°22.27 S	159°56.22 W	29.2	35.5	2325.1	2063.8	2.0	2.7	0.3	5.2
	150	0°22.27 S	159°56.22 W	18.4	35.3	2325.8	2151.0	0.9	9.1	0.9	14.2
Sept-14	17 (ft)	0°22.287 S	159°58.935 W	28.4	35.5	2319.1	2031.3	5.1	2.6	0.6	5.8
	15 (ft)	0°22.436 S	159°59.004 W	28.0	35.5	2316.7	2024.4	1.1	2.6	0.2	4.9
West Jarvis											
Sept-15	61 (ft)	0°22.134 S	160°00.487 W	27.8	35.6	2314.6	2043.0	1.1	7.9	0.3	5.0
	39 (ft)	0°22.149 S	160°00.500 W	27.6	35.6	2327.0	2043.5	2.2	3.6	0.1	5.0

2012 Sea Dragon water chemistry, continued

Date Sampled	Depth (meters)	GPS (latitude)	GPS (longitude)	Temp. (°C)	Sal. (psu)	Alk. (μeq kg^{-1})	DIC (μmol kg^{-1})	$[NH_4^+]$ (μM)	$[SiO_4]$ (μM)	$[PO_4^{3-}]$ (μM)	$[NO_2^{1-} + NO_3^{2-}]$ (μM)
Sept-16	0	0°22.03 S	160°00.85 W	28.5	35.5	2328.0	2049.5	0.3	2.7	0.3	4.6
	50	0°22.03 S	160°00.85 W	26.5	35.7	2340.8	2075.3	5.7	3.1	2.8	7.5
	100	0°22.03 S	160°00.85 W	24.5	35.7	2342.8	2097.9	<0.05	3.5	0.5	8.8
	150	0°22.03 S	160°00.85 W	21.1	35.3	2328.4	2119.6	1.3	7.1	0.7	12.1
Sept-16	24 (ft)	0°22.176 S	160°00.498 W	27.3	35.5	2330.5	2038.5	1.4	2.6	0.3	5.2
West Howland											
Sept-22	0	0°48.35 N	176°37.63 W	29.2	35.3	2313.8	2012.3	1.8	2.5	0.1	2.2
	50	0°48.35 N	176°37.63 W	28.1	35.5	2326.9	2053.2	2.1	3.0	0.3	6.4
	100	0°48.35 N	176°37.63 W	27.4	35.4	2318.6	2047.4	1.0	3.1	0.3	6.0
	150	0°48.35 N	176°37.63 W	22.4	34.9	2296.3	2088.5	0.2	8.4	0.6	9.8
Sept-22	27 (ft)	0°48.627 N	176°37.347 W	28.8	35.3	2312.8	2013.0	0.2	2.2	0.1	2.8
	18 (ft)	0°48.539 N	176°37.320 W	28.8	35.3	2310.5	2016.9	<0.05	2.4	0.1	2.8
East Howland											
Sept-24	0	0°49.04 N	176°34.78 W	29.0	35.3	2313.8	2025.8	<0.05	2.1	0.1	2.0
	50	0°49.04 N	176°34.78 W	28.8	35.3	2313.4	2020.9	1.1	2.1	0.1	2.0
	100	0°49.04 N	176°34.78 W	28.5	35.4	2316.0	2027.2	0.9	2.4	0.1	2.9
	150	0°49.04 N	176°34.78 W	20.8	35.1	2308.4	2107.0	<0.05	9.3	0.8	11.3
Sept-24	15 (ft)	0°49.066 N	176°36.933 W	29.5	35.3	2306.3	1988.8	0.7	2.2	0.1	2.5
	10 (ft)	0°48.563 N	176°36.673 W	29.1	35.3	2305.0	2012.0	0.4	2.1	0.2	2.4
	15 (ft)	0°48.055 N	176°36.618 W	29.1	35.3	2300.8	1988.9	0.2	2.1	0.1	2.7
	20-30 (ft)	0°48.019 N	176°37.247 W	28.8	35.3	2311.6	2007.1	1.0	2.4	0.2	2.8

2012 Sea Dragon water chemistry, continued

Date Sampled	Depth (meters)	GPS (latitude)	GPS (longitude)	Temp. (°C)	Sal. (psu)	Alk. (μeq kg^{-1})	DIC (μmol kg^{-1})	$[NH_4^+]$ (μM)	$[SiO_4]$ (μM)	$[PO_4^{3-}]$ (μM)	$[NO_2^{1-} + NO_3^{2-}]$ (μM)
East Maiana											
Sept-29	0	0°57.1104 N	173°06.6104 E	30.3	34.7	2272.7	1955.1	0.2	1.8	0.2	<0.05
	50	0°57.1104 N	173°06.6104 E	29.9	35.4	2316.9	1983.3	3.3	1.6	0.2	1.0
	100	0°57.1104 N	173°06.6104 E	28.6	35.4	2315.6	2027.0	2.7	1.7	0.2	0.9
	150	0°57.1104 N	173°06.6104 E	22.7	35.3	2318.6	2094.5	2.5	1.6	0.2	0.2
Oct-1	20-30 (ft)	0°57.981 N	173°04.449 E	30.4	34.9	2259.6	1945.0	0.2	1.8	0.2	<0.05
	20-30 (ft)	0°55.990 N	173°02.371 E	30.5	34.8	2255.9	1944.8	3.3	1.6	0.2	1.0
	20-30 (ft)	0°53.991 N	173°01.436 E	30.2	35.4	2267.0	1964.1	2.7	1.7	0.2	0.9
	20-30 (ft)	0°51.995 N	173°00.674 E	30.2	34.8	2279.0	1947.7	2.5	1.6	0.2	0.2
West Maiana											
Sept-29	13 (ft)	1°00.428 N	172°58.962 E	30.1	35.0	2271.1	1952.0	<0.05	2.0	0.1	0.3
Sept-30	6 (ft)	1°00.413 N	172°58.976 E		34.7	2055.4	1766.5	2.1	3.1	0.1	1.0
	14 (ft)	1°00.443 N	172°58.952 E		34.7	2043.7	1792.5	<0.05	3.1	<0.05	0.5
Sept-30	0	0°59.5656 N	172°66.5345 E	30.6	35.0	2293.5	1963.7	<0.05	2.6	0.2	<0.05
	50	0°59.5656 N	172°66.5345 E	29.9	35.4	2311.2	1988.6	0.6	1.9	0.1	<0.05
	100	0°59.5656 N	172°66.5345 E	29.3	35.4	2314.7	2010.3	4.0	3.1	1.0	2.6
	150	0°59.5656 N	172°66.5345 E	25.8	35.6	2328.1	2070.2	0.3	3.3	0.4	7.2
Sept-30	23.9 (ft)	0°57.856 N	172°57.705 E	30.2	35.1	2239.3	1936.5	0.2	2.1	0.1	0.3
	18 (ft)	0°56.748 N	172°56.841 E	29.8	35.3	2272.7	1983.1	0.2	2.1	0.1	0.4
Oct-1	28 (ft)	0°59.121 N	172°57.970 E	29.7	35.1	2206.7	1957.3	<0.05	2.0	0.2	0.5
	7 (ft)	0°57.209 N	172°57.309 E	30.2	35.0	2118.6	1877.8	1.1	2.2	0.1	1.1

Table C.2: Results from chemical analyses of seawater samples collected from and around central equatorial Pacific islands. The collection date, depth and GPS location (latitude and longitude) are given for each sample, in addition to *in situ* temperature, measured salinity (Sal.), Alkaliniy (Alk.), dissolved inorganic carbon (DIC) and nutrient concentrations. Water samples were collected using Niskin bottles and temperatures measured using Onset Hobo® Loggeres that were either tethered to a line or sitting in close proximity to coral sampling sites